Measurements of Mixed-Gas Heat Transfer Coefficients

by
Frederick J. Schwartz

A thesis submitted in partial fulfillment of
the requirements for the degree of

Master of Science
(Mechanical Engineering)

at the
UNIVERSITY OF WISCONSIN – MADISON
2015

_____ _____

Professor Franklin K. Miller, Assistant Professor of ME **Date**

_____ _____

Professor Gregory F. Nellis, Professor of ME **Date**

Abstract

This work describes an experimental facility designed and constructed to measure the heat transfer coefficients and frictional pressure drop in a small diameter, horizontal test section with two-phase, multi-component zeotropic mixtures at moderate cryogenic temperatures. The aim of this test facility is to enable the collection of data with high accuracy to being filling the void of heat transfer and pressure drop data for zeotropic mixtures undergoing a phase change (boiling). These data can then be used to support model development efforts to characterize the pressure drop and heat transfer process in horizontal tubes.

The test facility is intended to provide measurements for a range of test conditions including varying mixture components and concentrations, heat fluxes, mass fluxes, pressures, and tube diameters ranging from 0.5 mm to 3 mm. The temperature range associated with the mixture measurements varies from 100 K to room temperature. The data provided to calculate the heat transfer coefficients have been shown to be repeatable and accurate, producing results with an uncertainty of less than 10%, which was the goal of this research. The pressure drop measurements have been utilized to develop relationships; the facility is capable of measuring the frictional pressure drop under both adiabatic and non-adiabatic conditions.

Acknowledgements

I would first and foremost like to thank my advisors, Greg Nellis and Franklin Miller, for their help and support. This is an opportunity that I will never forget and be forever grateful to each of them. Admittedly, it was very difficult to return to academia in pursuit of this degree, but both Greg and Franklin were always patient and understanding throughout the process of becoming acclimated at the university. It was such a pleasure to witness the wealth of knowledge shared between the two. Though I will likely never come close to operating at their level, both men are an inspiration to me, and I will do my best to show my appreciation by conducting myself in the field as each would expect me to.

Of course I am equally grateful to Sandy Klein; had I not taken his Thermodynamics course, I would not have been introduced to him and the Solar Energy Lab. I am very grateful to him for this opportunity as well. Also very noteworthy and deserving of my thanks is Thatcher Root from the Chemical Engineering department. His assistance in helping me to understand the functionality of the gas chromatograph as it could be used for this project was greatly appreciated. I'd like to acknowledge ASHRAE for funding this research endeavor, as it provided me a more comfortable experience during my time in the lab and school.

I would be remiss to claim full credit for the work as described in this thesis, as I received great help and insight from my colleagues in the Solar Energy Lab. Some of you were beyond helpful in guiding me during various phases of the project. It will be interesting to see what amazing accomplishments these individuals in the group achieve outside of the lab in the future.

Finally, I would like to thank my family for their continued love and support. I'll never forget how much of a privilege it is to be a part of this family. The opportunities I've been afforded I attribute to them. The best feeling in the world is knowing someone will support your goals and

dreams, and I know my family always will be supportive of mine. I'm looking forward to progressing in my career, which I'm sure is greatly improved by my accomplishments here at UW. It's interesting to look back and remember that I am here because I thought I wanted to be a dentist…

Table of Contents

Table of Figures

List of Tables

1 Introduction

Low temperature coolers are often divided into two general categories of regenerative and recuperative systems. The recuperative systems have the advantage of providing steady flow in one direction analogous to DC systems, whereas regenerative systems provide oscillatory flow, analogous to AC systems. Thus, recuperative systems have the advantage of being simple in design compared to their counterpart. One commonly used recuperative system is the Joule-Thomson (JT). These systems have many unique applications, such as use in cryosurgeries, sensor cooling, liquefaction processes, current lead cooling, and cryopreservation. Research on the use of mixed-gas refrigerants as the working fluid for this type cooler has been rapidly increasing over the past several decades. As will be discussed in subsequent sections, it is preferable to use zeotropic mixtures for reasons that include higher heat exchanger effectiveness and subsequently higher system efficiency. The objective of this chapter is to introduce concepts that are useful in measuring the heat transfer coefficient of these zeotropic mixtures discussed throughout this work.

1.1 Overview of cryocooler technology

Like traditional refrigeration systems, cooling systems need to remove thermal energy from a source operating at an ultimate low temperature at the cold side and reject this thermal energy to a thermal reservoir at a higher temperature, often the surrounding ambient conditions. The temperature and power requirement for the cold side highly depends on the specific application. Of the many applications requiring cooling systems, it has been noted that certain coolers are more suitable for particular applications, for example, fluid based or solid-state systems. Among the applications mentioned is cryosurgery, where the size of the instrument is of greatest importance. Among other applications are liquefaction of natural gases, separation, cryo-pumping, superconductors, and low temperature detectors.

Various refrigeration techniques exist for these moderate cryogenic temperature applications, ranging from 100 to 300 Kelvin. When designing these types of cooling systems, it is important to consider the effects of parameters such as mass flow rate, pressure, geometry, and heat transfer coefficients, on the system performance in order to utilize optimal cooling techniques for the various temperature ranges. Again, these techniques are mainly divided into two sub-categories: recuperative and regenerative cooling systems as shown in Figure 1. In industry, these systems are collectively referred to as cryocooler's where the working fluid temperatures spans from near room temperature down to very low temperatures.

1.1.1 Regenerative Cycles

Regenerative cooling systems, such as Gifford-McMahon, Stirling, and pulse-tube, are currently the most commonly used cooling systems operating in the moderate to low cryogenic temperature range mentioned above. Regenerative cooling is accomplished by expanding compressed gas, resulting in a temperature reduction, thereby removing thermal energy from the cold end of the cooling device. This cold, expanded gas then passes through a heat exchanger, where it is used to remove thermal energy from the high temperature, high pressure incoming gas. The flow through this heat exchanger occurs in an oscillatory fashion where hot fluid flows through the regenerator (heat exchanger) depositing thermal energy into the regenerator bed before heat being picked up from the regenerator bed by flowing cold fluid through such bed. From this operational description, it can be deduced that the heat exchanger is of particular importance in the design of this type of system. An optimal design requires a practical balance of several parameters: high heat capacity of the solid material in the regenerator bed and working fluid, flow resistance and porosity, and low axial conduction.

1.1.2 Recuperative Cycles

Conversely, recuperative cooling systems such as the Brayton and Joule-Thomson (J-T), are steady flow systems. Low pressure gas enters the compressor near room temperature and is compressed to a higher pressure, thereby raising the temperature of the fluid significantly. An aftercooler is used to remove this thermal energy from the fluid, typically returning the fluids temperature to nearly ambient conditions. The fluid continues flowing through a recuperator, which results in a temperature reduction of the incoming fluid before being expanded in one of two ways, such as a piston-cylinder or turbine in a turbo-Brayton cycle or a restrictive valve in a Joule Thomson cycle (needle valve, capillary). Heat is removed from the specimen using a heat exchanger. The cold exhaust fluid is used in the recuperator to cool the incoming hot fluid, reducing the cooling load required to cool the incoming gas. This completes the cycle in a recuperative cooler.

These type coolers are beginning to gain more significant presence in cryocooling applications due to their simple and compact design requirements. The focus of the remainder of this chapter is to explain the relevance of the measurements presented in this work with the Joule-Thomson cycle and its applications.

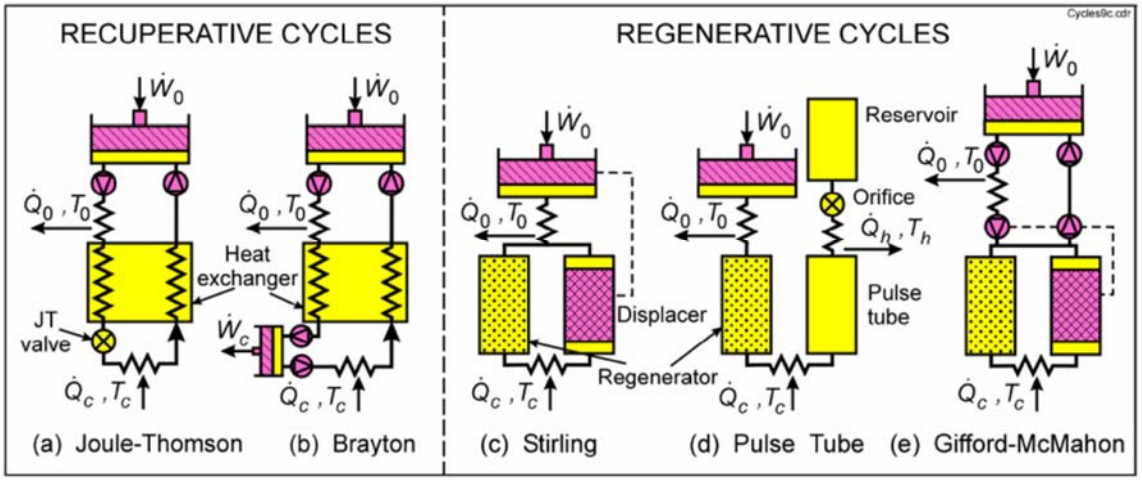

Figure 1. Schematics of common cryocooler refrigeration cycles (Radebaugh 2009)

1.2 Overview Mixed gas joule Thomson cooling systems

The goal of this section is to present a technical description of one cycle operation of a typical Joule-Thomson cooling system, and compare it with zeotropic refrigerants as the working fluid in such systems. Figure 2 show a diagram of a typical Joule-Thomson system. It consists of a compressor, an aftercooler, a recuperative heat exchanger, an expansion device, and an evaporator. The expansion device is commonly referred to as a throttling device.

The process begins with near room temperature fluid entering the compressor inlet (state 1). Work is done on the fluid through the compressor to compress the fluid to high pressure (state 2). The energy input to this process raises the temperature of the fluid; therefore, the refrigerant must be cooled down to near room temperature for apparent reasons that include higher system efficiency. Typically, this is done by exchanging heat with the ambient through a heat exchanger referred to as the aftercooler. The reduced temperature, high pressure fluid leaves the aftercooler (state 3) and begins exchanging heat with the exhaust cold fluid in the recuperator until it exits (state 4). The high pressure, low temperature fluid is then expanded through a needle valve in an isenthalpic process, as no energy is transferred to or from the fluid within the valve. This process results in a significant pressure drop of the refrigerant across the valve causing the fluid temperature to substantially drop before entering the evaporative heat exchanger (state 5). Heat from the source being cooled is absorbed by the fluid within the heat exchanger, raising the temperature of the refrigerant before exiting the evaporative heat exchanger (state 6). As stated earlier, the cold exhaust is used to cool the hot incoming fluid within the recuperator, raising its temperature (state 1). The refrigerant has gone through one cycle of the Joule-Thomson system.

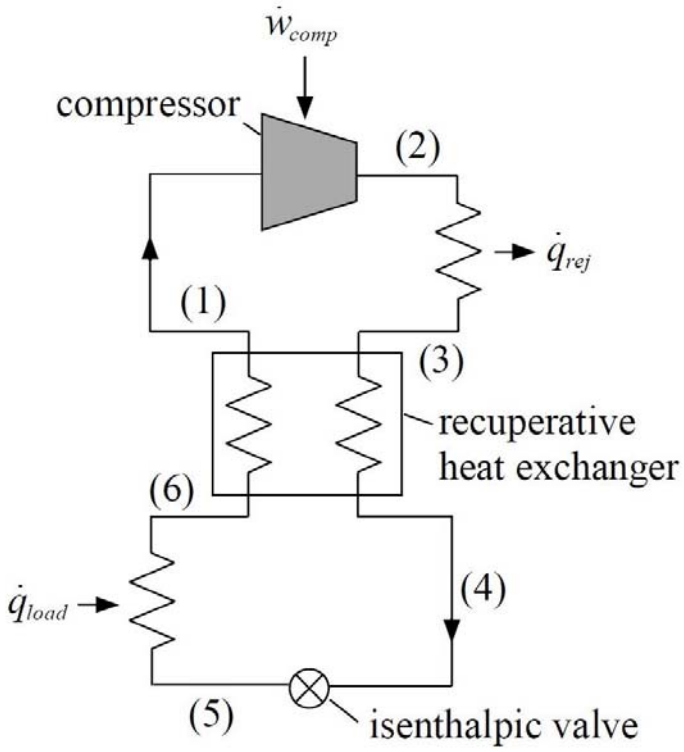

Figure 2. A diagram of a typical Joule-Thomson system (Klein/Nellis 2012).

In the typical Joule-Thomson cycle with a pure refrigerant as the working fluid, high pressure gas expands into a vapor-liquid state. The liquid evaporates in the evaporative heat exchanger by absorbing energy from the source being cooled. In contrast to the pure refrigerant Joule-Thomson cycle, a zeotropic refrigerant Joule-Thomson cycle works almost completely in the vapor-liquid region. Typically, condensation occurs relatively close to ambient temperatures. The incoming high pressure hot stream of mixture is cooled down in the recuperator and further condensed at a sliding temperature, so that the refrigerant is completely in the liquid phase before entering the throttle valve. The refrigerant only partially evaporates in the evaporator. The low pressure stream continues to boil in the recuperator at continually rising temperatures as shown on the temperature-entropy diagram in Figure 3.

An energy balance that encompasses the recuperator, the expansion device and the evaporator reveals that the refrigeration power ($\dot{q}_{ref}$) is determined by the enthalpy difference between the incoming hot stream and outgoing cold stream of the recuperator as:

$$\dot{q}_{ref} = \dot{m} \left(h\left(P_{low}, T\right) - h\left(P_{high}, T + \Delta T\right) \right) \tag{0.1}$$

where P_{low} and P_{high} are the exiting low pressure and entering high pressure stream respectively. The variable T is the local temperature of the low pressure stream, and ΔT is the temperature difference between the low and high pressure streams. This equation implies that the refrigeration load is maximized when the enthalpy difference between the low and high pressure stream is minimized over the temperature spanned by the recuperator. Therefore the refrigeration capacity is highly dependent on the thermodynamic properties of the fluid within the two streams of the recuperator. Ideally, it would be desired to have a large variation in the thermodynamic properties of a refrigerant over a wide range of temperatures; however, this is not the case for pure substances. In contrast, a mixed gas zeotropic fluid exhibits large thermodynamic property variations over wide temperature spans, making them superior for use in Joule-Thomson cooling cycles. Therefore, zeotropic refrigerants can widen the enthalpy difference in equation (0.1) resulting in a drastic increase in refrigeration capacity. For example Alfeev (1973) was able to increase the refrigeration capacity by an order of magnitude by using a zeotropic fluid as the refrigerant as compared to pure Nitrogen.

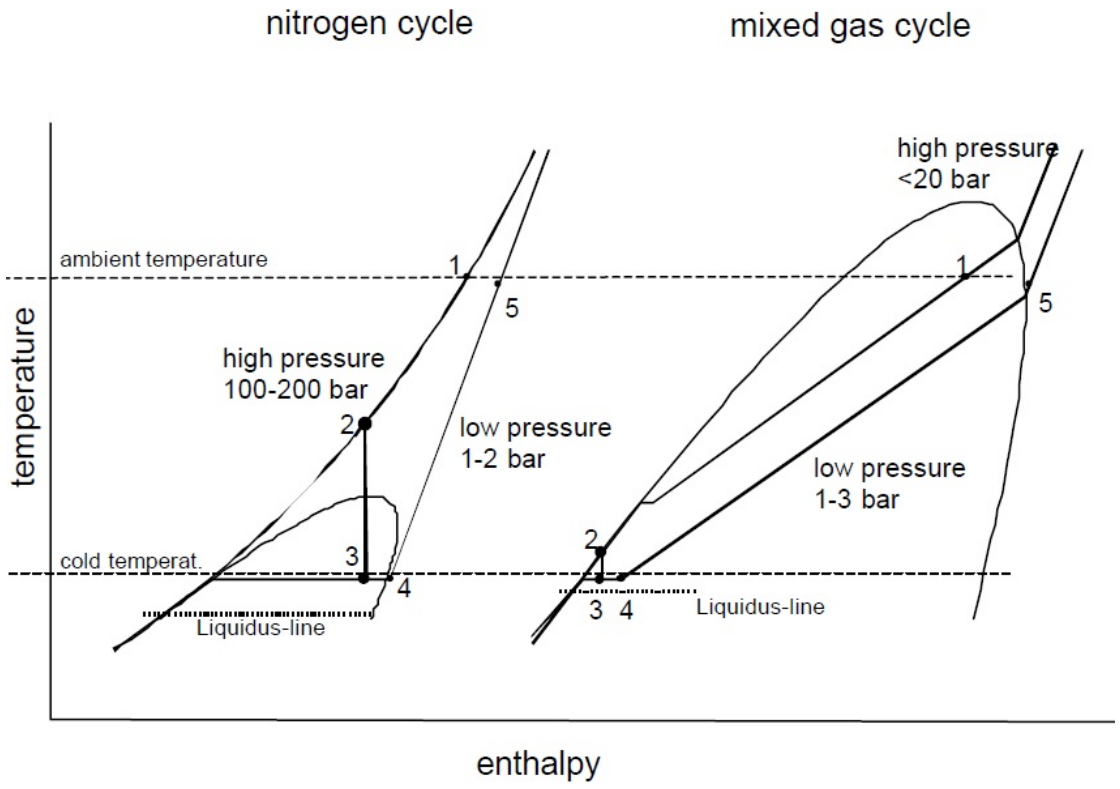

Figure 3. Temperature entropy diagram comparison between a pure refrigerant and a mixed gas zeotropic fluid

1.2.1 Introduction to zeotropic fluid

A refrigerant may be either a pure substance or a mixture of two or more substances. Examples of pure refrigerants are R12, R22 and R134a. Examples of mixtures are R502, R404A and R407C. A mixture can behave either as a pure refrigerant, in which case these are referred to as azeotropic mixtures, or differently as is the behavior of zeotropic mixtures. Despite containing two or more refrigerants, at a certain pressure an azeotropic mixture evaporates and condenses at a constant temperature. Therefore, azeotropic mixtures behave like pure refrigerants in all applications, which provide less benefit to a Joule-Thomson cooling system.

In comparison, zeotropic mixtures have a varying evaporation and condensing temperature, as shown in Figure 4. During a constant pressure phase change, these mixtures experience a change in temperature, known as a temperature glide. Figure 5 shows a phase diagram for an arbitrary

binary mixture. The concentration of the more volatile component, B, is shown in the x-axis and temperature is shown on the y-axis (Hughes 2004).

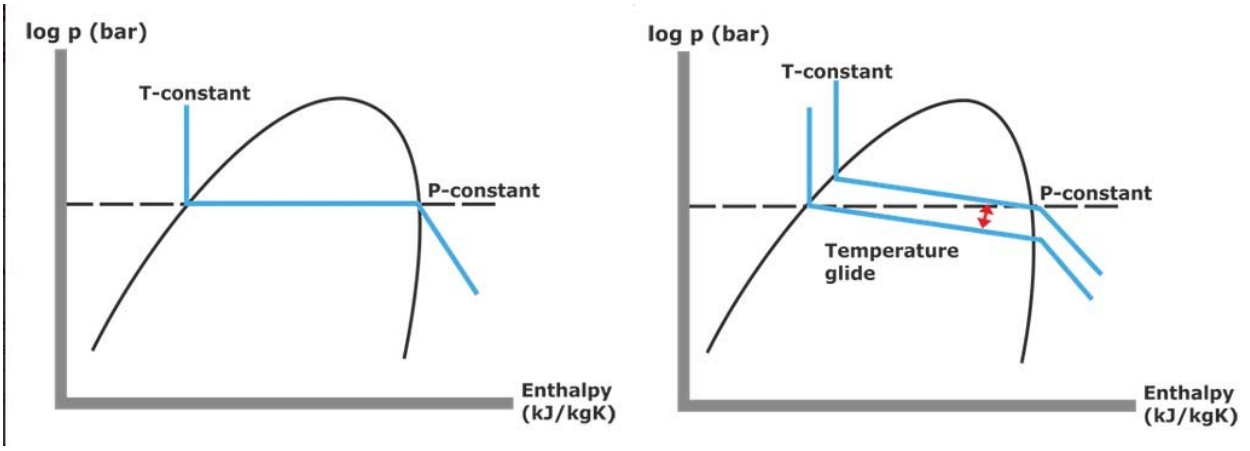

Figure 4. Pressure enthalpy diagram for a pure refrigerant compared to a zeotropic mixture at constant temperatures

The vertical line in Figure 5 shows the behavior of the mixture as it goes through the evaporation process. At point 1 the mixture is all liquid and has a composition C_0. The evaporation process begins at point 2 and the vapor that is produced has concentration of C_{v2}. The vapor has the greatest concentration of the more volatile component at point 2. As the quality increases the liquid phase becomes richer in the less volatile component and the concentration of the more volatile component in the vapor phase decreases. The superheat required to nucleate the vapor phase increases as the liquid phase becomes richer in the less volatile component. The evaporation process does not occur at constant temperature as it would for a pure substance instead, a temperature glide ΔTg results as described by Jung et. al (1989). The concentration gradient between the liquid and vapor suppresses nucleate boiling by creating diffusive mass fluxes. This makes correlations available for pure substances not applicable to mixtures.

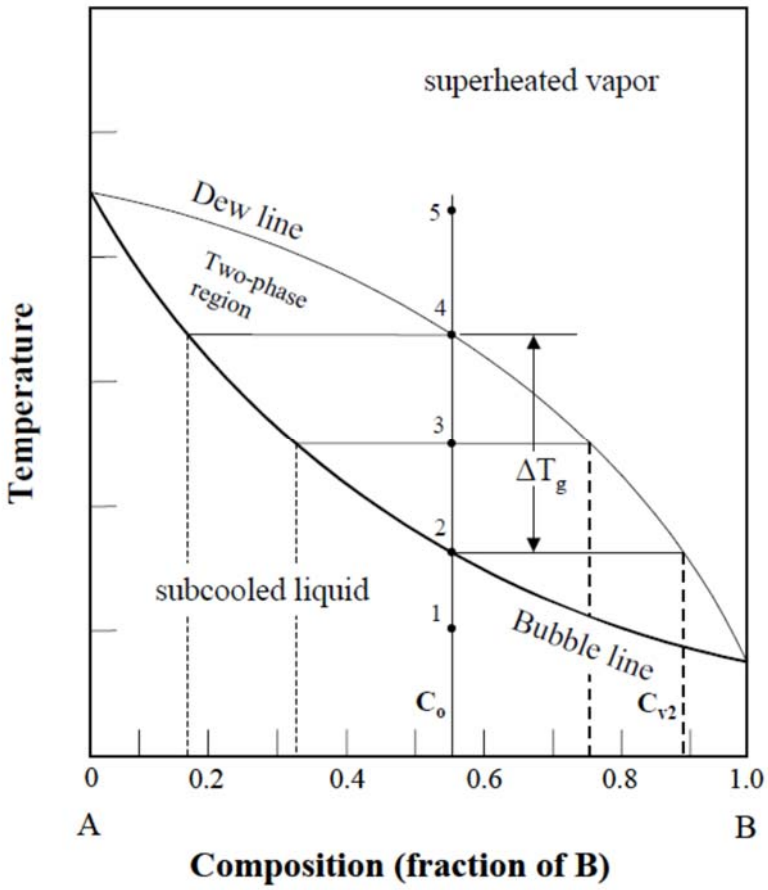

Figure 5. Phase diagram for a binary mixture (Hughes 2004).

1.3 Methods to determine heat transfer coefficients

Various methods can be employed to measure heat transfer coefficients of fluid flow through a duct, such as applying constant heat flux, maintaining a constant wall temperature, or measuring the heat transfer to a secondary fluid in a separate flow stream. It is important that the fluid being researched maintain controlled conditions throughout the experiment. Parameters such as mass flux and pressure should be held constant as the fluid changes phases. In addition, the duct or channel dimensions should be measured and known.

Through the use of a simple resistive wire heater, a constant wall temperature condition can be obtained when wound around a highly conductive material such as copper. Conversely, a constant heat flux condition is created when using a non-conductive material (Jung 1989). This

current and voltage across the heater wire can be measured, which supplies the energy applied to the fluid. Additionally, a heat exchange system can be setup such that a pure fluid is evaporated or condensed across the channel wall. This is typically done in a counterflow arrangement (Kattan 1998), and the applied heat flux is found using an energy balance on the pure fluid as it passes through the heat exchange setup. Typically, a tube-in-tube design is implemented in these applications, and the bulk fluid temperature is measured along with the tube wall temperature. Unfortunately, this method really provides an average heat transfer coefficient, whereas the electrical heater method can provide good approximate local heat transfer coefficient measurements.

Many studies available currently utilize the heat exchange setup described previously; therefore, providing only averaged overall heat transfer coefficients. Such overall heat transfer coefficients of a mixed gas cryogenic refrigerant from the inlet and outlet temperatures of a recuperative heat exchanger in a mixed gas Joule-Thomson cycle system have been measured (Boiarski 1999). Furthermore, using mixed gas refrigerants, Gong (2001) measured the overall heat transfer coefficient over a range of temperatures and compositions using a tube-in-tube heat exchanger. The issue is that these studies do not provide the desired details of the heat transfer characteristics of two-phase zeotropic mixtures. It is necessary to obtain local heat transfer coefficients of these mixtures. The goal of this research is to build on the work of Hughes and Keppler (2004).

1.4 Document outline

An introduction to the project and concepts involved in it were presented in this chapter. Chapter 2 explains the experimental test facility equipment and details the components used in the experimentation. This includes the test Dewar, the data acquisition system, the gas chromatograph.

Chapter 3 goes through the test facility modifications including valve, regulator, oil handling, pressure measurements, new test sections, and equipment protection and safety. The operation procedure is detailed comprehensively in chapter 4 of this work. It simulates the operation of the test facility for the next user. Details of the experimental results are presented in chapter 5. Some additional details of the test facility are given in the Appendix of this work.

2 Experimental Test Facility Equipment

2.1 Overview of Test Facility Design

A test facility design was proposed and constructed by Barraza, to obtain measurements of temperature, pressure, and mass flow rate of mixed-gas refrigerants in a horizontal test section within a controlled environment. The facility consisted of a compression station, coupled to a vacuum evacuated Dewar containing the central element of the test facility, the test section. The compression station was used to control the mass flow rate and supply pressure in the experiment; the piping and instrumentation diagram can be seen in Figure 6. Initial testing was performed using this basic design.

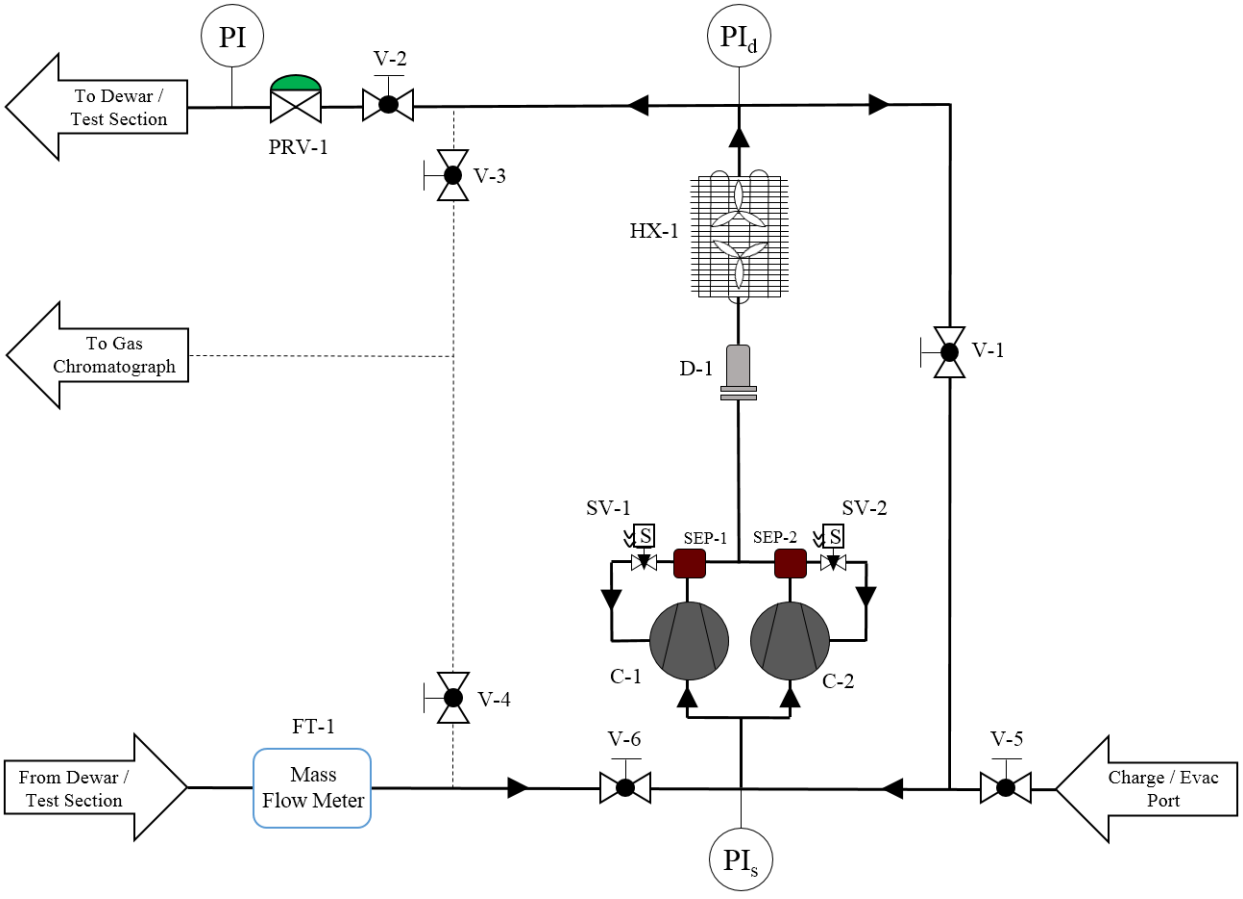

Figure 6. Original compression station process diagram

The Dewar contained the low temperature, thermal control components, along with the test section. It was vacuum evacuated below 10^{-4} Torr to minimize the loss of thermal energy to convection. This was accomplished through the use of a rotary vane pump, as well as a high velocity turbopump. The gas entering the Dewar first passed through a recuperative heat exchanger. Upon exiting the recuperative heat exchanger, it passed through another heat exchanger attached to a cryocooler coldhead, which was used to control the temperature of the gas mixture in conjunction with electric heaters. With the temperature controlled, the gas then entered the horizontally mounted test section. It was here that a known heat flux was applied, and the temperature and pressure changes of the gas were measured. The gas leaving the test section was routed to the recuperative heat exchanger, removing thermal energy from the incoming gas supply as it returned to the compression station. The equipment diagram is shown in Figure 7.

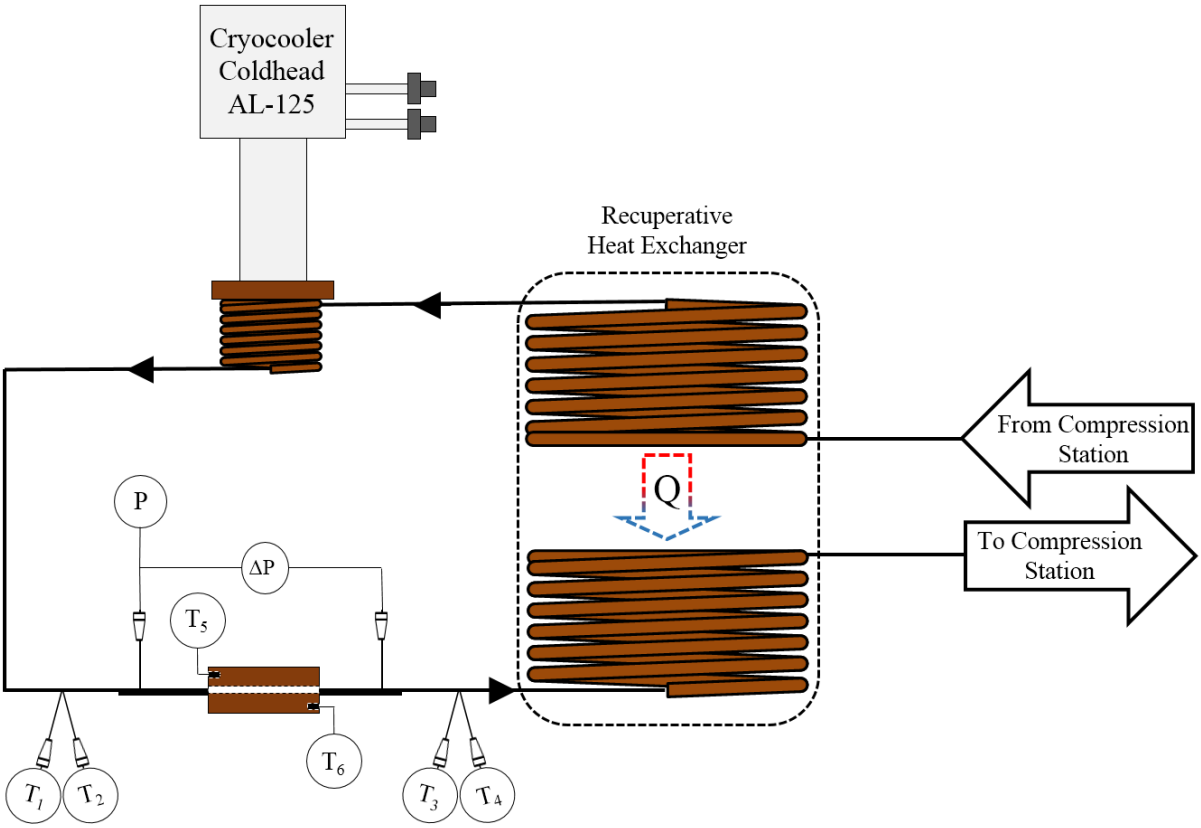

Figure 7. Dewar process diagram

An auxiliary system very important to the experiment is the gas chromatograph (GC). The GC is used to determine the concentration of gas mixtures used in the test facility during collection of experimental data sets. The actual GC used in the experiment is shown in Figure 29.

Samples of the gas mixtures in the system were sent to the GC periodically, to provide a concentration profile for the data collected during each data set. Though the GC is a single instrument, capable of measuring concentration alone, additional components were added to help facilitate sample injections, as well as register the signal output.

2.2 Test Conditions

It was proposed that three test section diameters be fabricated for this research. Two gas mixtures were selected to be tested, one consisting completely of hydrocarbon gases and another of fluorocarbon gases. Each of the mixtures would be diluted twice at 20% and 40% to produce a total of six mixtures. The hydrocarbon mixture would be diluted with pure nitrogen, while the fluorocarbon mixture would be diluted with pure Argon. Furthermore, each mixture would be tested at two different pressures and a single mass flux. The result was a test matrix of 36 test conditions which would provide the necessary information for this research, as can be seen in Table 1. The heat flux shown in the table was determined by estimating the amount of energy required to maintain nearly constant fluid properties across the heating section of the test section.

Table 1. Original test matrix conditions

Mixtures *Concentration Effects*		Test Section Inner Diameter *Geometry Effects*					
		0.5 [mm]		1.5 [mm]		3.0 [mm]	
		Supply Pressure *Pressure Effects*					
		0.1 [MPa]	1.0 [MPa]	0.1 [MPa]	1.0 [MPa]	0.1 [MPa]	1.0 [MPa]
		Mass Flux *Constant*					
		250 [kg/m^2-s]					
		Heater Power *As Calculated*					
45%	Methane Ethane Propane Nitrogen	2.9 [W]	3.6 [W]	27 [W]	32 [W]	107 [W]	129 [W]
36%	Methane Ethane Propane Nitrogen	2.2 [W]	2.5 [W]	20 [W]	22.4 [W]	78 [W]	89.7 [W]
27%	Methane Ethane Propane Nitrogen	1.5 [W]	1.7 [W]	14 [W]	16 [W]	56 [W]	63 [W]
35%	R14 R23 R32 R134a Argon	1.7 [W]	1.8 [W]	13 [W]	14 [W]	51 [W]	55 [W]
28%	R14 R23 R32 R134a Argon	1.3 [W]	1.3 [W]	12 [W]	13 [W]	47 [W]	53 [W]

2.3 Compression Station

The two compressors on the compression station apparatus circulated the gas mixture in the system. Due to the compression process, the temperature of the gas also increased. This required a heat exchanger to reduce the temperature of the gas entering the Dewar, as the gas was ultimately cooled to very low temperatures (<120 K) prior to entering the test section. However, prior to cooling the compressor discharge gas, an oil separation mechanism was required, as the gas was in contact with the compressor lubricant. The best practice for this is to recover the oil immediately downstream of a compressor. Therefore, the high temperature gas was passed through a coalescing-type oil separator after each compressor, which utilized electrically actuated needle valves to periodically empty the separators and return the collected oil to the compressor. In addition, downstream of the oil separators, a filter drier was installed to capture any further oil and moisture that was able to pass through the oil separators. This component arrangement can be seen in Figure 8.

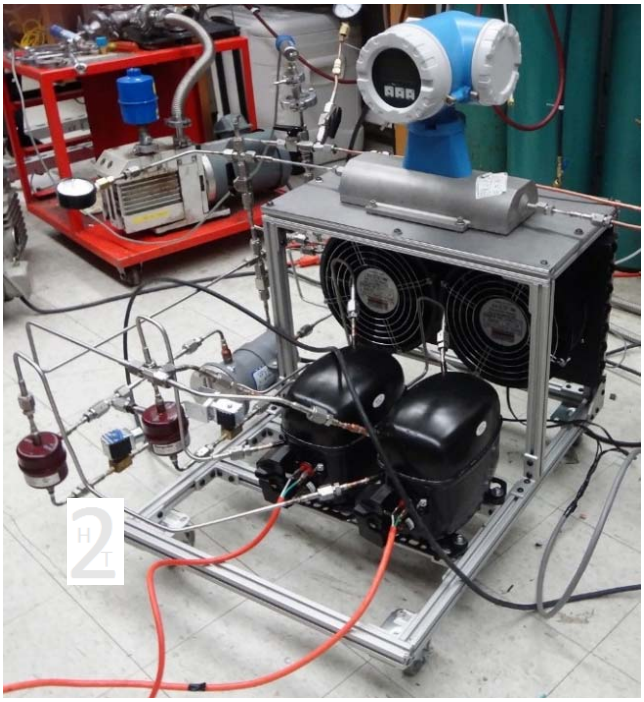

Figure 8. Original compression station design schematic

The clean, dry gas was finally cooled using a copper fin-and-tube type heat exchanger, as described previously. The unit selected to perform the cooling was a Lytron model 6320G3 with two, ten inch fans, as shown in Figure 9. This model uses 0.7mm wall thickness tubing, and is suitable for pressures up to 150 PSIG. It allowed for the gas to be cooled to nearly ambient temperature, which was approximately 25 ± 5 Celsius.

Figure 9. Lytron tube-and-fin heat exchanger setup

Before the gas entered the Dewar, it was necessary to regulate the supply pressure. This was accomplished using a simple spring and diaphragm type pressure regulator. A Swagelok KPR series regulator was selected, using a 0-250 PSIG spring range, as shown in Figure 10. The valve had a low flow coefficient of 0.002, which is indicative of a low flow requirement.

Figure 10. Swagelok pressure regulator, KPR series

As the mass flux through the test section needed to be measured, it was necessary to install a mass flow meter in the test facility. Given that it would have been impractical to install the flow meter inside the Dewar, it was installed and incorporated into the compression station, downstream of the Dewar outlet. The meter selected was a Coriolis sensing type, as shown in Figure 11.

Figure 11. Endress and Hauser mass flow meter

A mass flux of 250 kg/s-m^2 was specified for each of the test sections. This resulted in mass flow rates of approximately 0.05 g/s, 0.44 g/s, and 1.77 g/s for the 0.5 mm, 1.5 mm, and 3.0 mm inner diameter test sections, respectively.

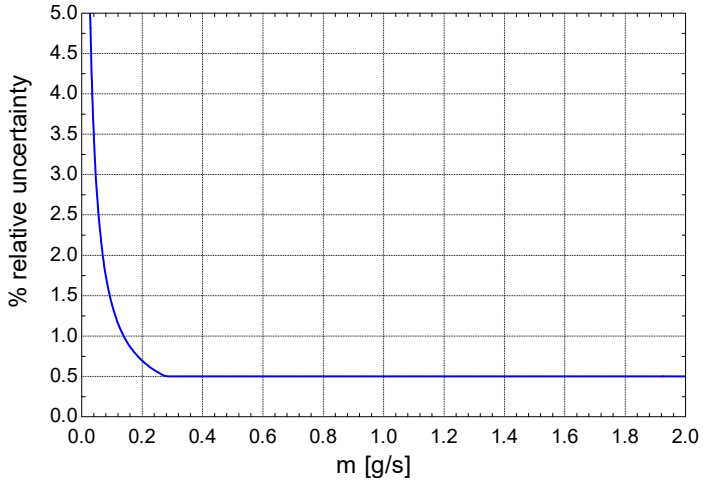

Figure 12. Relative uncertainty curve of coriolis mass flow meter

The relative uncertainty of the mass flow meter will be more significant in the smallest test section, from 2-3%, but only 0.5% in the larger diameter test sections.

2.4 Dewar and Test Section

The Dewar contained the low temperature components, where these items could be isolated in a vacuum environment, thereby effectively eliminating convection losses and reducing cooling requirements. After the gas entered the Dewar, it passed through a tube-on-tube recuperative heat exchanger made of quarter inch copper tubing, roughly 20 meters in length, as shown in Figure 13. A counterflow arrangement was used with the gas leaving the test section. This reduced the cooling load on the cooling system, which proceeded the recuperative heat exchanger.

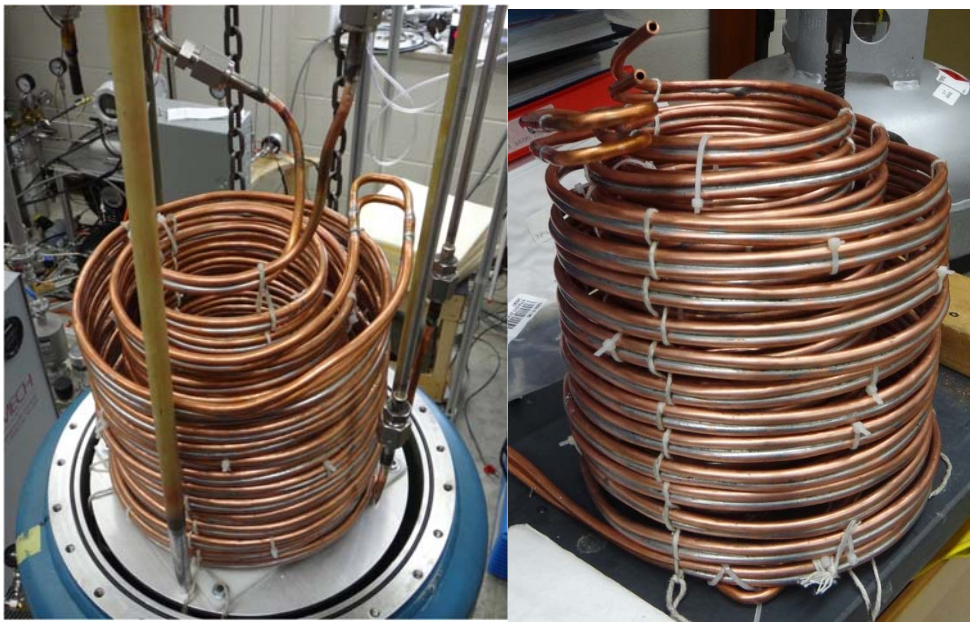

Figure 13. Recuperative heat exchanger, located inside Dewar, installed (left)

The low temperature cooling system utilized for this test facility was a Gifford-McMahon (GM) type cryocooler, model AL-125 coupled to a compressor module, model CP640, each manufactured by Cryomech. A copper heat exchanger was affixed to the cold end of the cryocooler cold head shown in Figure 15 using four mounting bolts to compress a thin layer of 99.99% pure Indium between the two surfaces, thereby increasing thermal contact. The cold head heat exchanger construction was quarter inch copper tubing, coiled around and soldered to a three inch

diameter copper Type L pipe, which had been soldered to a quarter inch thick copper disk, as shown in Figure 14.

Figure 14. Coldhead heat exchanger

Figure 15. Cryomech AL-125 coldhead

Also shown in the figure, protruding from the side of the copper plate at the top of the cold head heat exchanger, is one of two cartridge heaters used to balance the cooling load during operation. These heaters were each capable of providing 100 watts, and were procured from

Lakeshore Cryotronics. Independent DC power supplies provided power to each heater, as shown in Figure 16. The digital displays were very useful when incrementally adjusting the heater power.

Figure 16. BK Precision programmable DC power supplies

The cryocooler cooling capacity as a function of temperature was experimentally determined by Barraza. The testing was performed while the cold head was installed inside the Dewar, operating in a vacuum below 10^{-4} Torr to effectively eliminate the convection losses. Additionally, seven layers of aluminized reflective film were installed over the cryocooler to minimize radiation losses. A T-type thermocouple was installed between the heat exchanger and the cold head, using 99.99% pure Indium to decrease thermal contact resistance. An ultimate low temperature of 28 K was achieved when no heat load was applied. Several measurements were taken from no load, up to 160 watts, changing load upon reaching thermal equilibrium, as shown in the plot in Figure 17.

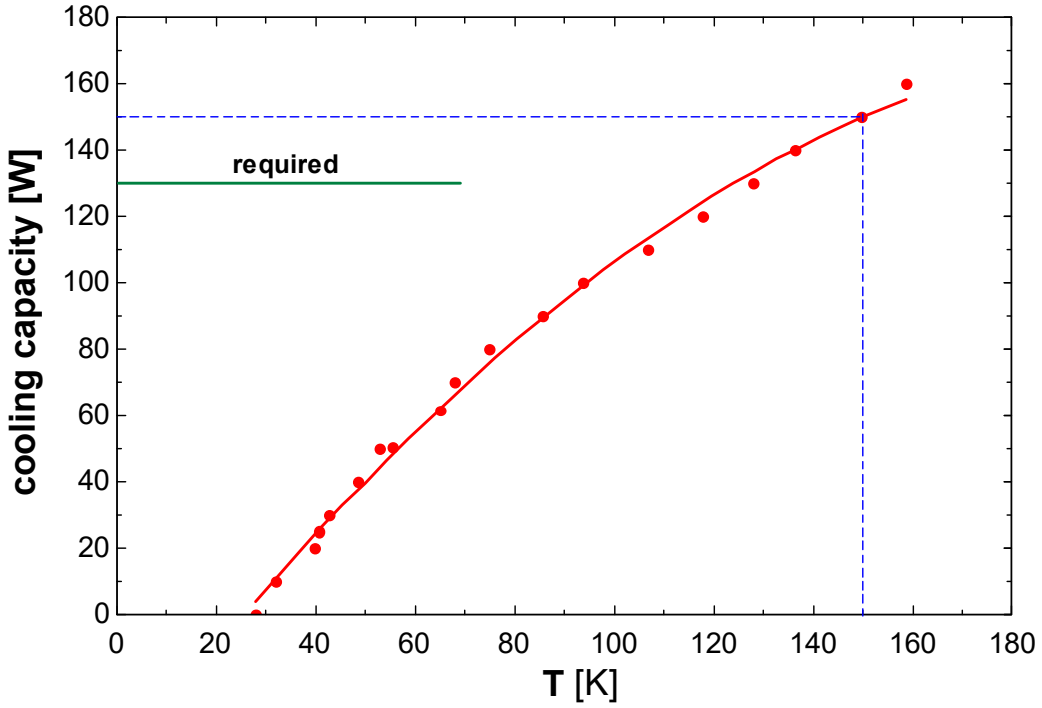

Figure 17. Measured cryocooler cooling capacity as a function of cold head temperature (Barraza)

The central element of this test facility was the test section, which was the combination of temperature and pressure measurement instrumentation, as well as a heating section where a known heat flux was applied. The foundation of the test section was a stainless steel tube, mounted horizontally. Affixed to this tube was a cylindrical copper mass, of relatively larger size in comparison to the tube diameter, with a hole bored in the center to fit the stainless steel tube. This copper mass was brazed to the tubing using a silver brazing alloy, Safety-Silv 45. The purpose of this copper mass was to act as an isothermal heat reservoir, to create an approximately isothermal wall condition inside the test section, and the brazing alloy was used to promote heat transfer to the stainless steel tube.

Nichrome wire, which has a relatively high resistivity of approximately 34 ohms per meter at 305 Kelvin, was uniformly wound around the copper mass, insulated from the copper using thin tissue paper and coated with varnish. Lengths of 0.09, 0.4, and 0.7 meters were selected to produce

the desired heat flux for the 0.5, 1.5, and 3.0 millimeter test sections, respectively. Two copper wire pairs were soldered to each end of this wire to form electrical leads. One wire from each lead was used to supply current from a DC power supply, and the other to create a voltage divider circuit. The wiring diagram is shown in Figure 18. These items formed the heating section.

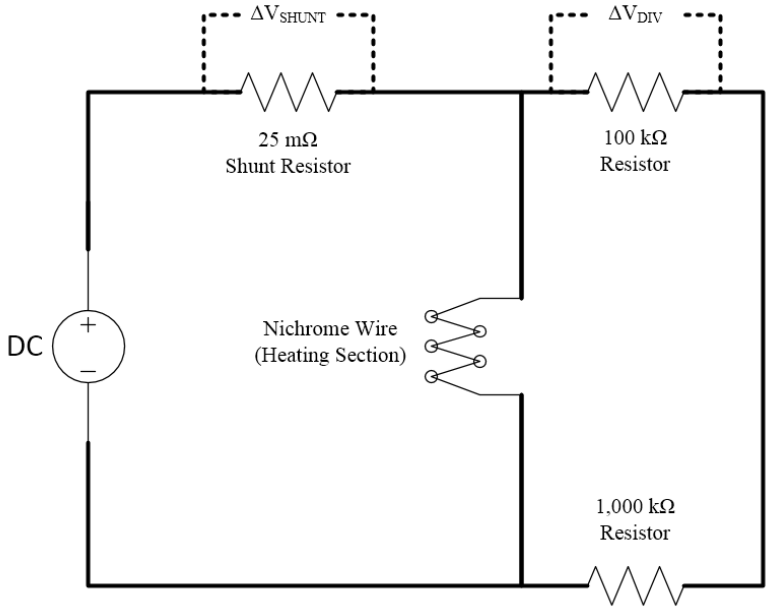

Figure 18. Heating section of test section wiring diagram

The heat applied to the heating section was the product of the current and voltage across the Nichrome wire, each of which needed to be measured. Using the voltage divider circuit and Ohm's Law, the voltage, V, was determined by the following equation:

$$\mathrm{V} = \Delta \mathrm{V}_{DIV} \left(1 + \frac{1{,}000\ \mathrm{k\Omega}}{100\ \mathrm{k\Omega}}\right)$$

Similarly, the current flow through the Nichrome wire can be determined using Ohm's Law and the measured voltage drop across the calibrated shunt resistor. There will be current flow through the voltage divider circuit, but it is negligible in comparison to the Nichrome wire and main circuit. Therefore, the current, I, can be determined by the following equation:

$$\mathrm{I} = \frac{\Delta \mathrm{V}_{\mathrm{SHUNT}}}{25\ m\Omega}$$

The product of the voltage, V, and current, I, represent the heat applied to the heating section copper rod. The circuit components, such as the shunt resistor and voltage divider circuit were calibrated, as installed, using a Hewlett-Packard model 34401A multimeter.

On the inlet and outlet of the test section, pressure taps were installed using custom fabricated copper blocks with holes bored to form a tee fitting, allowing for an inlet pressure measurement, as well as the pressure drop across the heating section. These pressure tap fittings were also brazed in place on the horizontal tube. The inlet pressure was measured using a Setra model 204 sensor, with a pressure range of 0 to 250 PSIA and an uncertainty of 0.28 PSI, or 0.11% of the full-scale range. Similarly, the pressure drop across the heating section was measured using a Setra model 204D sensor, with a range of 0 to 25 PSID and an uncertainty of 0.063 PSI, or 0.25% of the full-scale range.

The inlet and outlet temperature of the gas mixture were measured using Platinum Resistance Thermometers (PRT). The PRT's selected for this experiment were from Lakeshore Cryotronics, model PT-103, and were used in a braided 4-wire configuration. One pair of wires supplied the excitation through a calibrated Lakeshore model 120 current source, while the other pair provided a voltage differential to be measured. Redundant PRT's were been installed to verify the temperatures recorded during operation were correct, while also reducing the uncertainty. The construction was a quarter inch Swagelok VCR gland with the 4-wire leads and a support wire epoxy sealed, as can be seen in Figure 19. A calibration method used is described in appendix B.

Figure 19. PRT assembly used to measure mixture temperatures

Similarly, two additional PRT's installed at each end of the copper rod in milled holes at a known radius, were used to determine the wall temperature inside the test section tubing using a quantifiable thermal resistance network. A vacuum grease, Apiezon N, was applied between the PRT and milled hole in the copper mass to reduce the thermal contact resistance. The redundancy of the PRT's installed in the test section copper mass provided validation that the copper mass was isothermal, or if a difference existed between the inlet and outlet of the heating section.

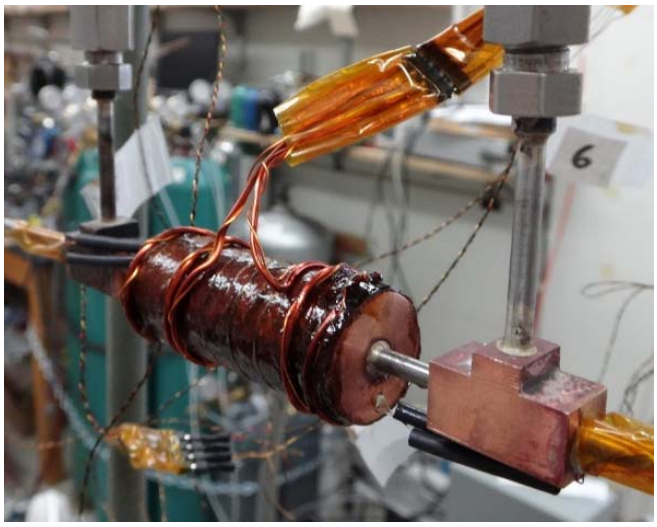

Figure 20. PRT installed into copper mass of heating section in 1.5mm test section

The two locations where pressure was measured was between the locations where the PRT's were installed and the heating section. The inlet location was used to measure the absolute pressure, while the downstream location was utilized in conjunction with the upstream location to

measure the pressure difference across the heating section and the inlet and outlet piping. Again, it should be noted that these pressure sensors are located at known distances from the test section, such that the fittings used to provide access to fluid for the sensors do not disturb the flow entering the test section, ensuring fully developed, undisturbed flow throughout. The uninstalled 0.5, 1.5, and 3.0 millimeter test sections assemblies are shown in Figure 21, Figure 22, and Figure 23, respectively.

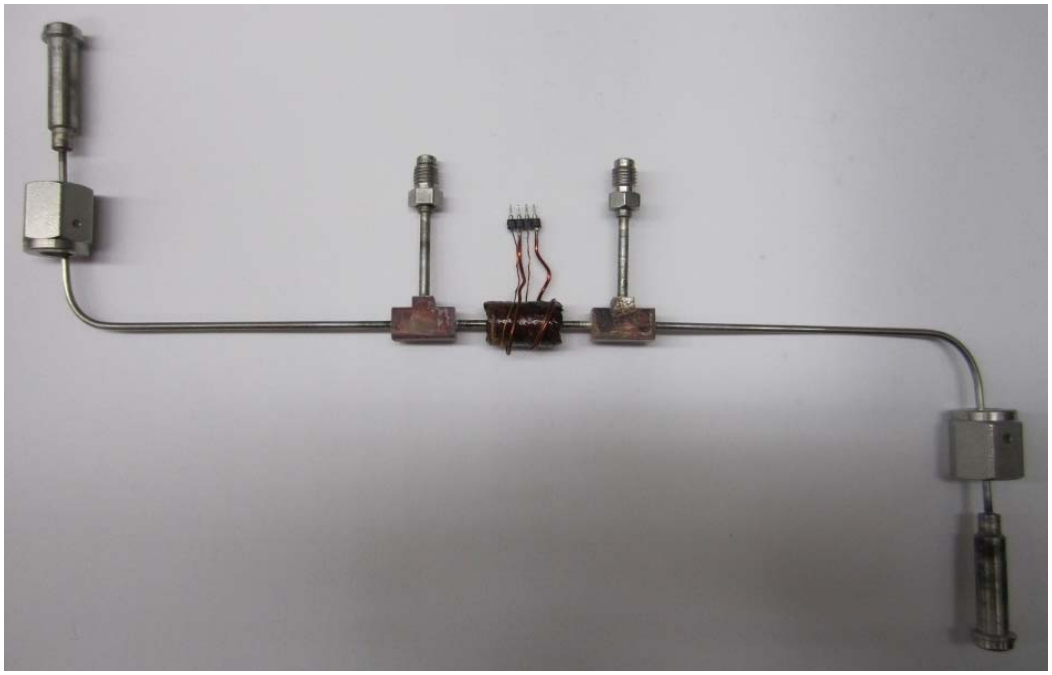

Figure 21. Test section and pressure taps, nominal 0.5mm size

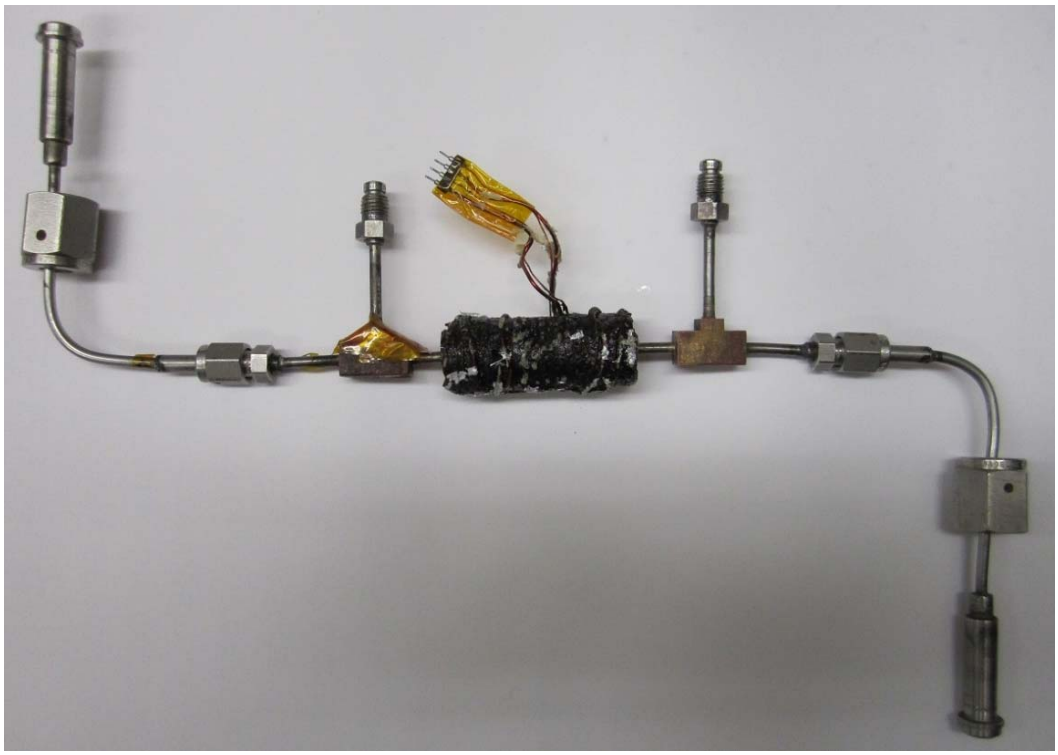

Figure 22. Test section and pressure taps, nominal 1.5mm size

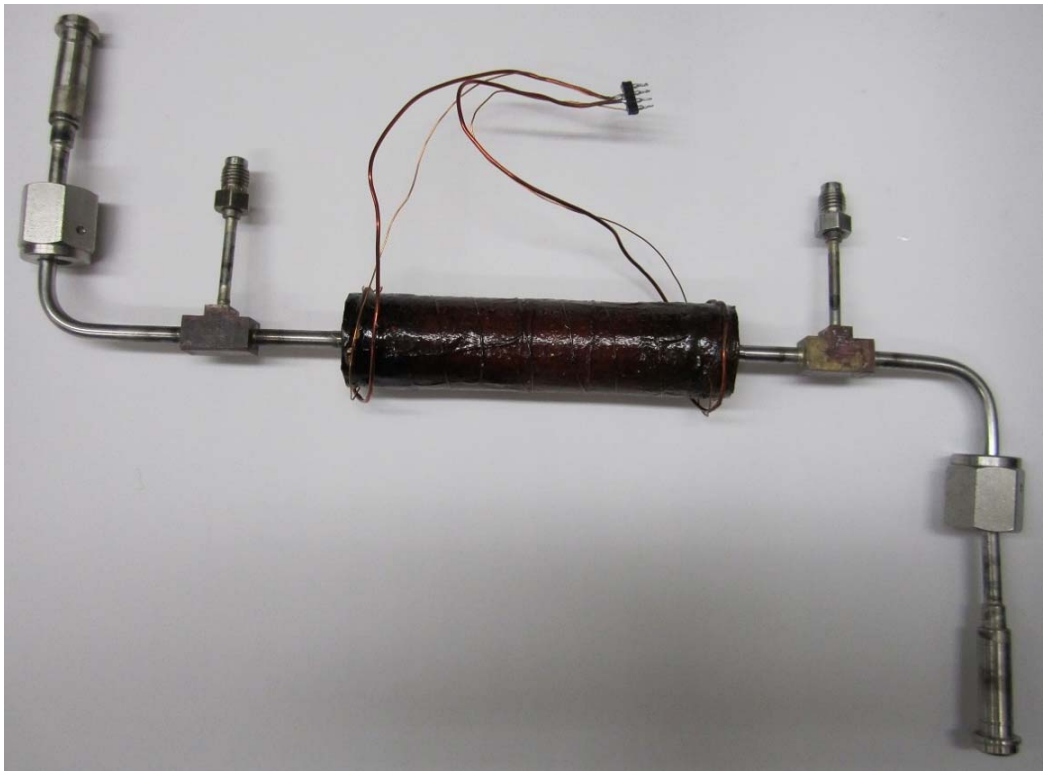

Figure 23. Test section and pressure taps, nominal 3.0mm size

Thermal and fluid analysis was performed by Barraza to determine the locations of the instrumentation, as well as the length and position of the heating section. It was important that the fluid flow through the heating section be fully developed, both thermally and hydrodynamically, as the heat transfer coefficient being measured was effectively derived from an average Nusselt number. This required a minimum length of straight, constant tube diameter flow upstream of the heating section inlet, as well as sufficient length of the copper rod heating section. It has been demonstrated though CFD analysis that at the specified mass flux, the required length of piping to obtain hydrodynamically fully developed flow is approximately ten pipe diameters. Therefore, the temperature and pressure instrumentation was able to be installed this distance from the heating section to measure fluid properties, while still allowing the flow entering to be fully developed hydrodynamically. Similarly, the heating section was determined to require a minimum of 35 pipe diameters of copper. To validate this test facility setup, data using high purity nitrogen was collected and compared to expected results obtained from the Dittus-Boelter equation.

The internal characteristics of the test section tubing were measured, such as diameter and surface roughness, as these would be used in pressure drop calculations. A microscope with imaging software capable of specifying a dimensional scale was used to determine the inner diameter of the tubing. From this, the inner diameter of the 1.5mm test section was found to be 1.515 millimeters. Similarly, using a Zygo optical surface profiler, or profilometer, the surface roughness was measured. A roughness average, or Ra, of 1.949 micron was measured, as shown in Figure 25, which equates to a relative roughness value of 0.0013. These internal characteristics were not measured on the other two test sections.

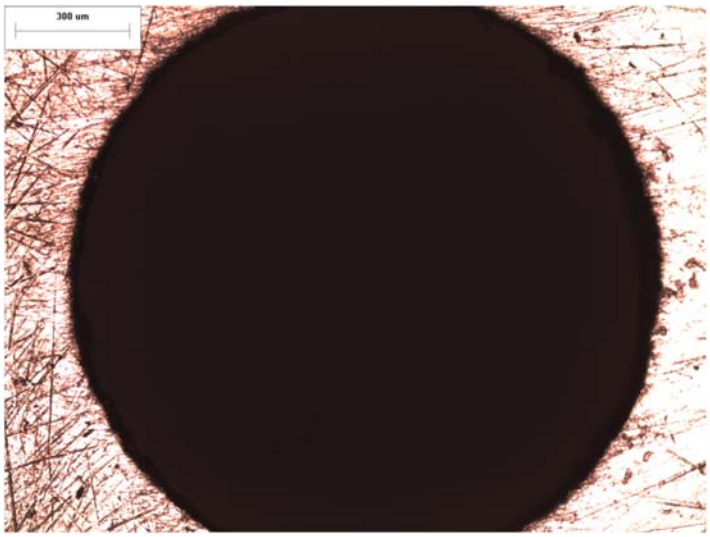

Figure 24. Microscope image used to determine 1.5mm test section diameter with scale

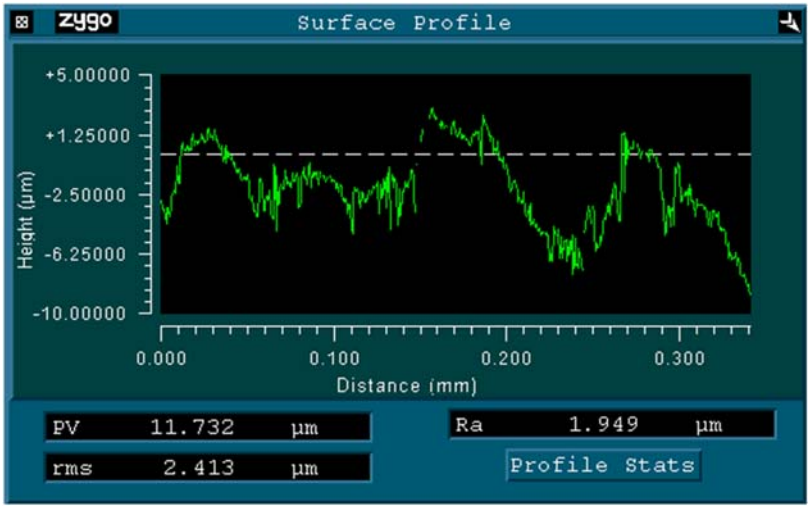

Figure 25. Zygo optical surface profiler output for 1.5mm tube sample

2.5 Radiation Shielding

At the low temperatures expected to be encountered during this research, it is necessary to take steps to mitigate the effects of radiation heat losses. In this experiment, several layers of highly reflective aluminized Mylar sheets were wrapped around the test section, each sheet insulated further with a layer of synthetic woven fabric called Dacron, as shown in Figure 26. A thermal resistance network was proposed and modeled by Barraza, as discussed in Appendix C. From this

model, it was determined that a 95% reduction in radiation loses could be attained by installing five layers of this multilayer insulation (MLI) around the test section and associated cooling components.

Figure 26. Multilayer Insulation (MLI) installed

Furthermore, it was proposed that a greater reduction in radiation losses could be reached by creating an isothermal layer to install around the test section. It was fabricated from 24 gauge copper sheet material, with Mylar secured to the surface using Lakeshore varnish. The sheets were wrapped around the test section and instrumentation, and fastened to the coldhead heat exchanger using machine screws and thermally connected using Indium.

Figure 27. Isothermal radiation shield

Three layers of MLI were installed between the isothermal shield and the test section and associated instrumentation. The installed isothermal shield is shown in Figure 27.

2.6 Data Acquisition System

The data acquisition (DAQ) hardware used for this experimental test facility was a model CR23X-TD datalogger developed by Campbell Scientific. It had the capability of measuring twelve differential or 24 single-ended voltage inputs, and could simultaneously filter 60 Hz noise. The input channels could also be a combination of differential and single-ended voltages, each having a voltage range that could be specified as 5000 mV, 1000 mV, 200 mV, 50 mV, or 10 mV, with a full-scale accuracy of 0.025%. Additionally, there were eight output channels, capable of providing 0 to 5000 mV output signals. The actual datalogger used is shown in Figure 28.

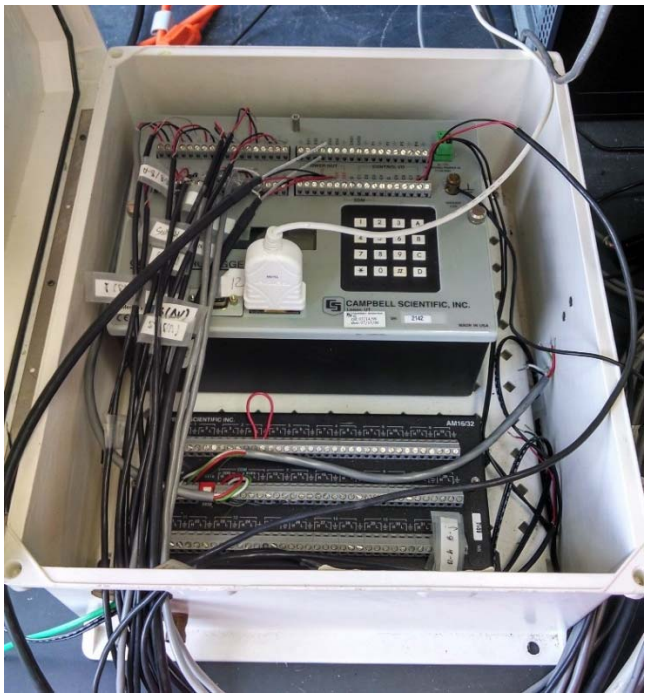

Figure 28. Campbell Scientific CR23X-TD Datalogger, actual unit shown

This hardware was controlled using a software package called LoggerNet version 4.2, also from Campbell Scientific. This software package provided the necessary program modules to create datalogger programs to record, perform calculations, and store signals from the instrumentation used on this test facility to data tables, which could then be automatically stored to a computer hard drive in a useable format, such as CSV or XML. Additionally, there were program modules designed to configure plots and tables to view the data being collected in real-time.

2.7 Gas Chromatograph

An important objective of this research was to determine the concentration of the gas mixture in the test facility during operation at various points of thermodynamic quality in the test section, as it was expected to change as the mixture was condensed in the Dewar components. Shown in Figure 29, a gas chromatograph (GC), Hewlett-Packard model 5890 Series II, was used to measure the concentration of the mixtures. It was adapted from an earlier experiment using it

for the same purpose; therefore, the only requirement to integrate it into the test facility was to install the necessary piping and connect to the sample line.

Figure 29. Hewlett Packard Gas Chromatograph 5890 Series II

The GC was equipped with a Thermal Conductivity Detector (TCD) and a Flame Ionizing Detector (FID). The TCD was used with the mixtures being investigated in this research scope, along with the installed Agilent Technologies packed column. The GC was also previously setup to be used with LabVIEW as a means to communicate with the unit and input or change parameters, such as the injector, detector, and oven temperatures and temperature programs. Also, the signal output was connected to a Hewlett-Packard model 3396A Integrator as shown in Figure 30, which printed the chromatograms to paper.

Figure 30. Hewlett-Packard 3396A Integrator

The GC was setup such that the gas mixture could be sent through a sample line, where pressure and flow rate were measured using analog sensors. The flow rate was measured in a raw form through the use of a differential pressure sensor connected across the injection valve, as well as with rotameter on the sample line discharge. The sample line pressure sensor was connected near the injection valve, approximately in the same location as the differential sensor high pressure port. The pressure and flow rate information was critical in determining the sample size being injected into the GC column, and the pressure sensors were incorporated into the LabVIEW program used to operate the GC, centralizing all of the critical parameters for operation.

The process of injecting the sample into the column from the sample line was essentially automated, as the GC was equipped with a pneumatic injection valve. The valve was programmed to open for 30 seconds, beginning when the start command is sent to the GC from the LabVIEW program, allowing the gas mixture to enter the column. This combination of time, pressure, and flow rate is the method utilized to produce approximately equal and repeatable sample sizes for the GC to measure.

The TCD signal would change from its baseline reading when a component of the gas mixture would elute from the column installed in the oven chamber and pass over the detector.

The time it required for the component to reach the TCD is known as the retention time, which is a function of the oven temperature and the column length and type. The signal profile from the TCD resembles a peak when it is plotted onto paper using an Integrator. The peaks from each component are representative of the mixture concentration, in the form of their respective areas under the signal profile. Peak areas are the product of the peak height from the baseline and the width of the peak at half-height point, which the Integrator calculates automatically.

In order to interpret the results from the Integrator, a correction factor, more commonly referred to as a response factor, needed to be applied to these area results. As it pertained to this experiment, two methods were utilized to determine these correction factors. The first method was to test several samples from a certified mixture containing the gases used in the mixtures being investigated as part of this research, such as the hydrocarbon mixture. A certified mixture could be obtained with a mixture uncertainty within 1% of the actual concentration. Again, by keeping the GC injection pressure and flow rate as consistent as possible, the areas obtained from the samples for each mixture component could be averaged. The product of this averaged area and the desired response factor, RF_{gas}, was expected to produce the specified component molar concentration, as shown below.

$$A_{peak} \times RF_{gas} = M_{gas}$$

The second method to be utilized involved using high purity gas samples of each component in the mixtures being investigated. Again, several samples of each gas would be taken and averaged, using the same GC injection pressure and flow rate to effectively maintain nearly the same sample sizes. These values were then treated as values expected with a pure solution sample of the gas, and as the area values are linearly correlated with concentration, the area of each component from a mixture could be divided by this value to determine the effective

concentration. An additional calculation was implemented to normalize the concentrations, such that the sum of the concentrations would be 100%, reducing the effects of inconsistencies in sampling. The equation for an 'n' component gas mixture would be calculated as shown below, where A_n represents the measured area value from the Integrator, and $A_{n,pure}$ represents the averaged pure sample areas.

$$\frac{\frac{A_1}{A_{1,pure}}}{\frac{A_1}{A_{1,pure}} + \frac{A_2}{A_{2,pure}} + \frac{A_3}{A_{3,pure}} + \cdots + \frac{A_n}{A_{n,pure}}}$$

The uncertainty of the GC was not known; however, using these methods it is reasonable to determine the uncertainty by performing several samples. Also, the major source of uncertainty lies in the sampling technique using the pressure and differential pressure sensors. It is unlikely that the same pressure and differential pressure is achieved for every sample. For use in this experiment, a minimum of five samples from each of the reference gases will be taken to calibrate the methods discussed.

3 Experimental Test Facility Modifications

3.1 Overview of Testing Issues

Control of the mass flow rate proved to be difficult with the original test facility design. The most significant issue was that the compressor oil separation and collection system disturbed the mass flow rate to the test section when the emptying valves were opened. Also, the ball valves were nearly impossible to use to control and adjust backpressure in the system piping, as slight adjustments with the valve handles translated to large changes in flow rate. Additionally, the pressure regulator selected for the test facility did not allow for fine adjustments in the outlet pressure, likely due to the spring range being too large.

Given the need for gas mixtures for use in testing, there was an obvious requirement to either source the mixtures from a gas supplier or create the mixtures in the lab. Costs of the mixtures were obtained from various suppliers. The hydrocarbon mixture was relatively inexpensive, whereas the fluorocarbon mixture was substantially more expensive to purchase. Therefore, it was determined that the hydrocarbon mixture would be purchased from a supplier, and the fluorocarbon mixture would be created in the lab using the gas chromatograph. This required the addition of a mixing tank. After reviewing the design, it was determined that such a tank could be added and piped into the bypass line of the compression station. This would also alleviate another testing issue, which was the large reduction in system charge pressure due to the condensing gas, as the volume of the tank could be added as needed.

In regards to the test section, the determination of the inlet and outlet pressures and temperatures could not be made with a high degree of confidence due to pressure drop between the sensors and the test section, resulting in a decrease in the temperature of the gas mixture, a phenomenon known as the Joule-Thomson effect. A reconfiguration of the measurement setup

surrounding the test section was required. In conjunction with the measurement modifications, the pressure sensor taps were also modified to reduce the perturbations in flow entering and exiting the test section by using a smaller pressure tap diameter. Lastly, the cross sectional area of the test section tubing allowed significant heat leak due to conduction.

The original test parameters specified in the research proposal for this project were thought to require more time to collect than was available. Therefore, a new set of test parameters was created to reduce the number of data sets required, while still maintaining the same level of investigative usefulness. Further evaluation of the test parameters and time available to collect the data produced a test matrix that would investigate the effects of different heat and mass fluxes, in addition to diameter, pressure, and concentration effects. A binary data set was also added.

Finally, as the data sets for this experiment commonly would take longer than 12 to 15 hours, an attempt at leaving the system operating unattended was made. Consequently, the gas mixture in the system changed from two-phase to solely vapor during this time, which resulted in a reduction in the heat transfer in the test section and coldhead heat exchanger. The experiment was severely damaged, as the coldhead heat exchanger became unsoldered from the base attached to the coldhead, removing the only cooling capacity in the system, resulting in gas temperatures in excess of 450 Kelvin. The thermometer assemblies were destroyed, and the radiation shielding and thermometer wires were burned. The recuperative heat exchanger was the only undamaged piece in the Dewar, as even the cryocooler coldhead displacer needed to be replaced. Various changes were made to protect the equipment from this failure occurring again.

To address these design issues, modifications to the original design were made by the author of this work as will be described in detail in this section. The additional pressure sensors were added in the Dewar piping, as shown in the updated diagram in Figure 31. Similarly, Figure

32 shows the process diagram of the compression station, which was the most significantly modified. There were no changes required for the gas chromatograph and its associated equipment.

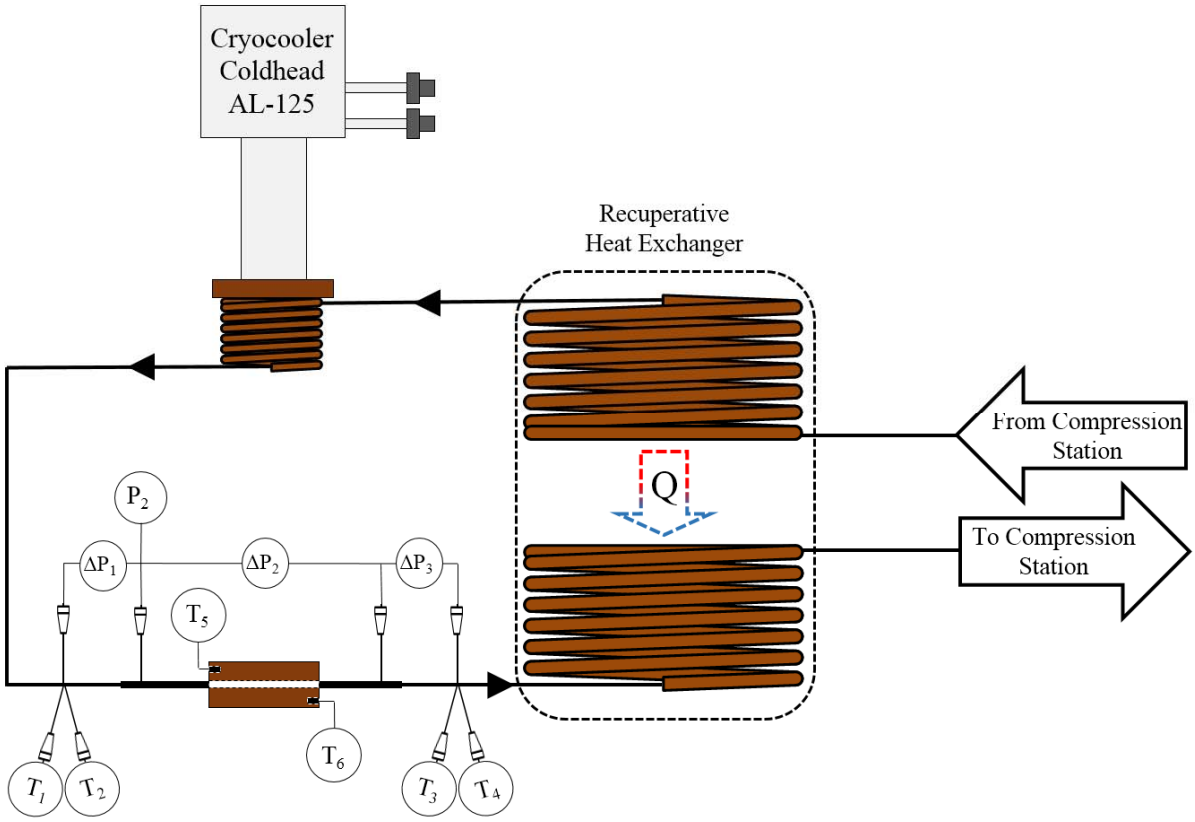

Figure 31. Dewar process diagram with modifications

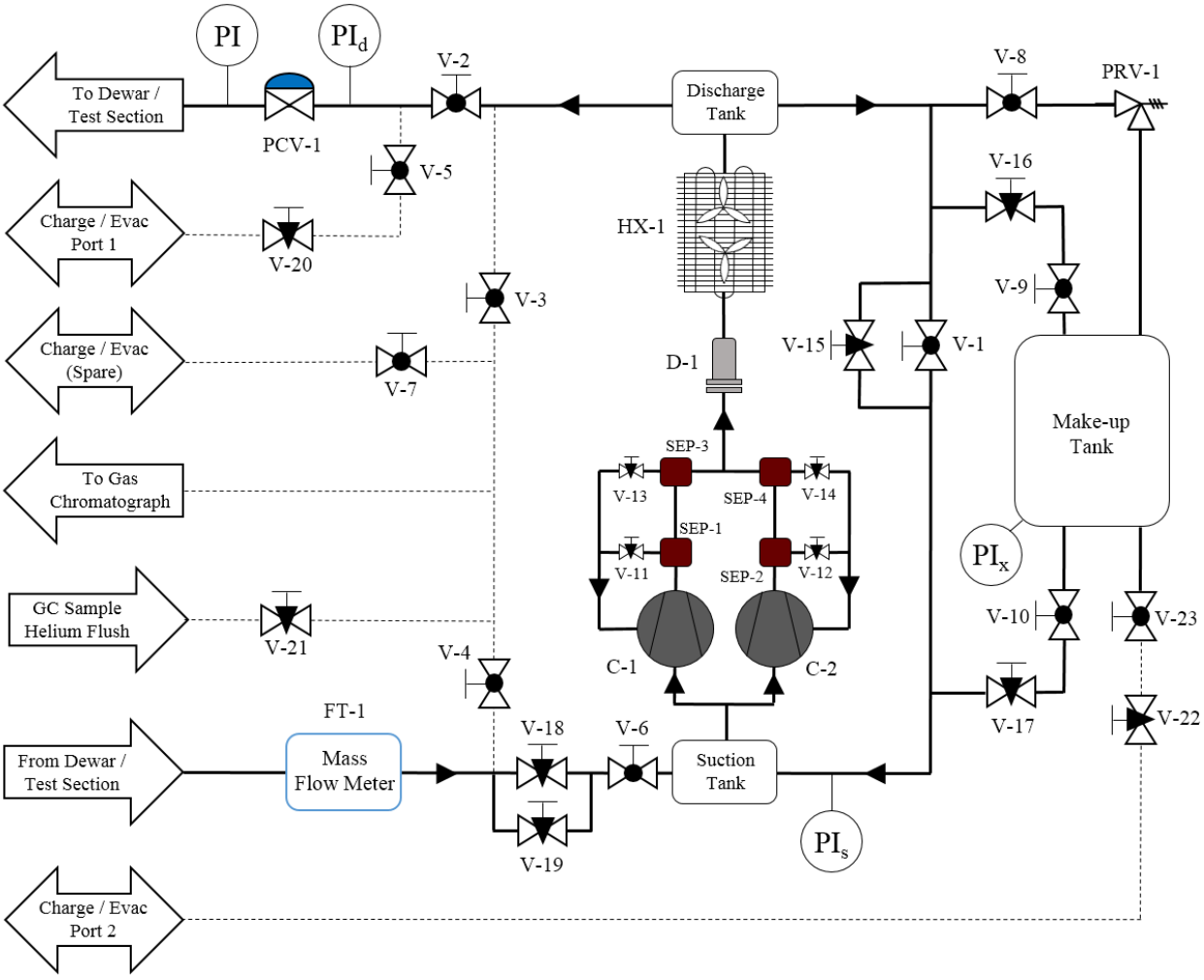

Figure 32. Compression station process diagram with modifications

3.2 Oil Separator Modification

As stated in the previous chapter, the compressors used to move the gas mixture through the system required lubricating oil, which was in contact with the mixture. As a result, some of this oil left the compressor with the mixture, but was captured by the oil separators. From the initial testing of the facility, it was observed that the drier element had become saturated with compressor oil. It was proposed that an additional oil separator on each compressor would increase the amount of oil captured, and subsequent testing showed a marked improvement. Alternatively, a properly sized oil separator could have been used, but there was no sizing information available to determine a suitable model for this application.

Furthermore, the oil separator drain valve emptying sequence proved to be problematic, as it disturbed the steady-state flow of gas to the test section and displayed a hysteretic effect. The flow rate would not return to the rate at which it was prior to the separator emptying sequence. To correct this issue, the electrically actuated valves were replaced with manually operated, regulating-type needle valves to allow for continuous drainage of the separators during operation. Testing has shown the setup in Figure 33 to be the ideal solution for this test facility.

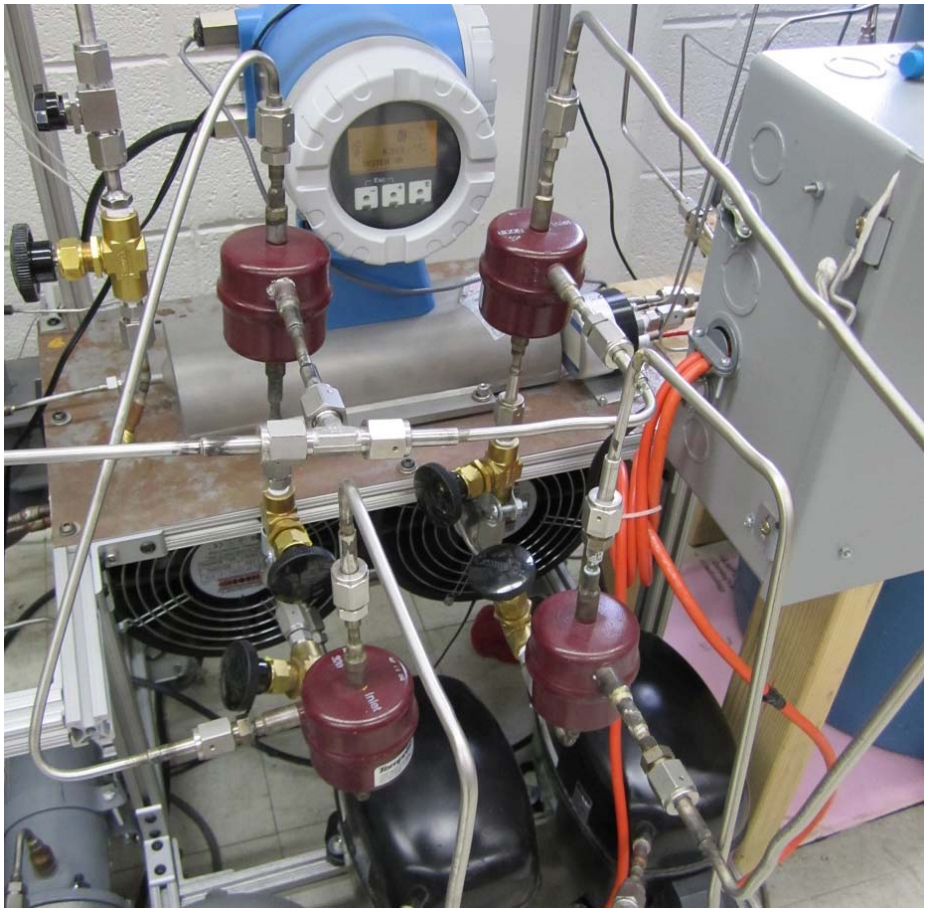

Figure 33. Oil separator modifications

3.3 Buffer Volume Modification

Another noticeable issue with the mass flow was the pulsating flow pattern that resulted from the compressors, as the compressors were of the reciprocating type. The method selected to dampen the fluctuations was to install two vessels, with a volume of roughly one US gallon, at the

compressor inlet and outlet. In addition to providing a volume in which the pulsating flow could be dampened, another proposed benefit of having a vessel installed upstream of the compressor was to provide a volume from which the compressors would draw, regardless of the fluid conditions elsewhere in the system. Such concerning conditions would include condensing the mixture to saturated liquid in the test section. Again, after testing, it was determined that the vessels provide significant dampening from pulsations in the flow. The installed vessels can be seen in Figure 34.

Figure 34. Buffer volume tanks installed

3.4 Valve Modifications

The previously discussed flow control modifications were implemented to alleviate fluctuations in the flow, but would do little in regards to controlling a set flow rate during operation. The original test facility design utilized manual ball valves for both shutoff and regulation of flow. Initial testing of the facility proved that the ball valves were not a sufficient means to control the flow rate; therefore, it was proposed that needle valves could be used as a more precise means to control the flow rate through the piping. Brass needle valves were installed in two locations, with one valve placed downstream of the mass flow meter and the other in the

bypass loop, as shown in Figure 35. These locations proved to be more useful in adjusting flow rate and pressure, and post-installation testing has shown these valves provided a significant improvement in flow control.

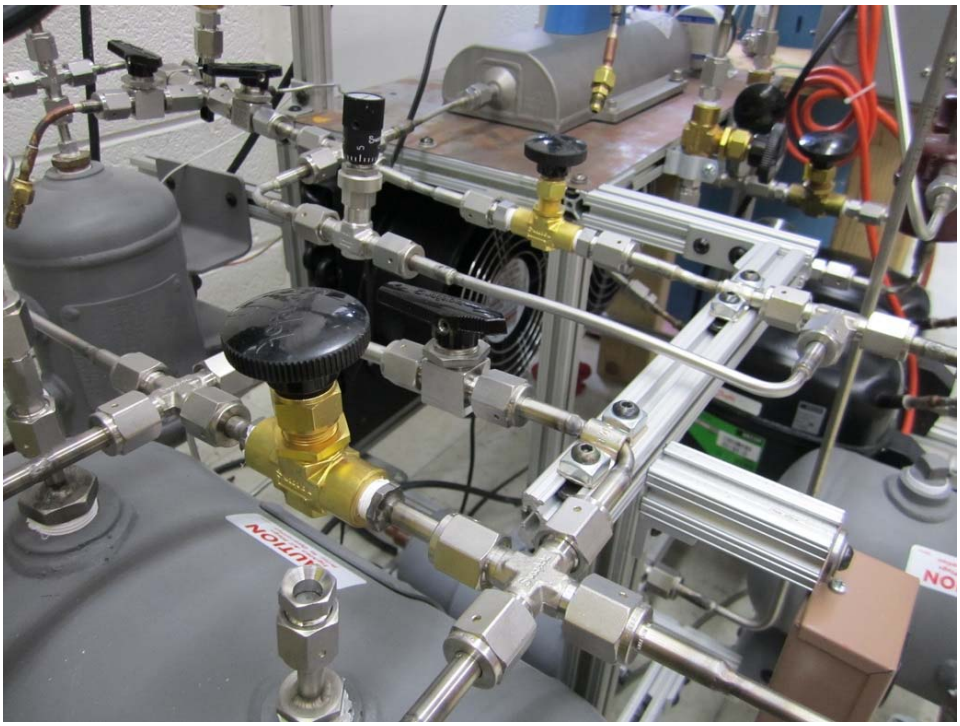

Figure 35. Needle valves installed on bypass and compressor return line

3.5 Pressure Regulator Modification

In addition to the needle valve modifications discussed above, it was determined from initial testing that the flow coefficient for the pressure regulator was likely too small for the flow rate required to achieve the specified mass flux through the two, larger test section diameters. The valve would not achieve the required flow rate without significant pressure drop across the valve. The issue with that scenario is that the heat exchanger used to cool the compressor discharge gas, which was upstream of the regulator, was not rated to such high pressures to allow for that. The other issue with the regulator was the spring range in combination with the number of turns allowed by the valve. The range was nearly double what was required, and the number of turns allowed

were not enough to make fine adjustments in the range needed. A new Swagelok regulator with a larger flow coefficient, more reasonable spring range, and relatively low droop was procured. This new regulator, shown in Figure 36, worked well for all flow conditions specified for this experiment.

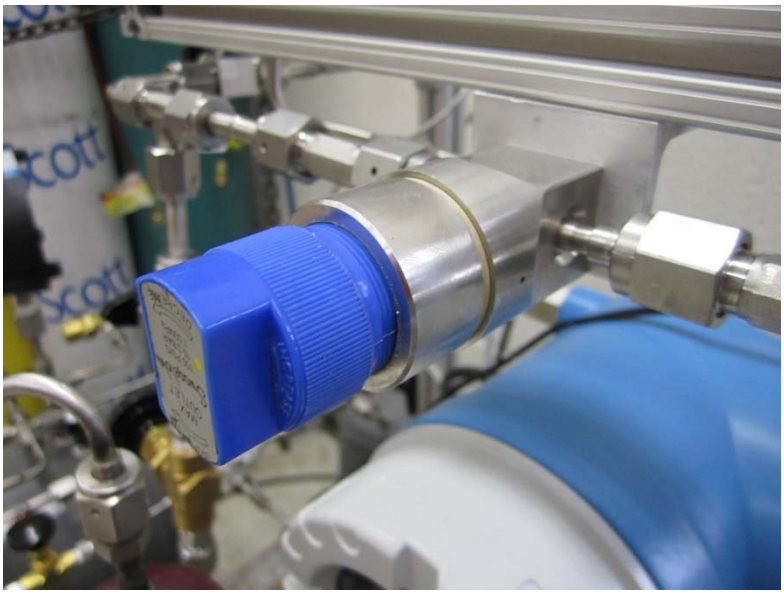

Figure 36. Swagelok pressure regulator with higher flow range

3.6 Make-up Tank

The primary purpose of the make-up tank was to provide a vessel in which new mixtures could be created and after achieving the correct concentrations, added to the vacuum evacuated test facility. After reviewing the necessary components required for this, it was determined that the vessel could be connected into the bypass line using a few more valves and used to regulate the amount of gas mixture in the system. This was originally the purpose of adding a surge tank to the compressor suction described above, but it seemed that the volume of the two vessel was not sufficient make-up volume when the mixture was being condensed to saturated liquid. Testing showed that this larger tank, 4.5 US gallons, was more beneficial in this respect than as a mixing tank, and as a result, it was never utilized for creating the gas mixtures independent of the

remaining system volume. Through a pressure relief valve, it also provided a safe location to release gas from the system when the pressure in the compressor discharge heat exchanger became unintentionally high. The installed tank is shown in Figure 37.

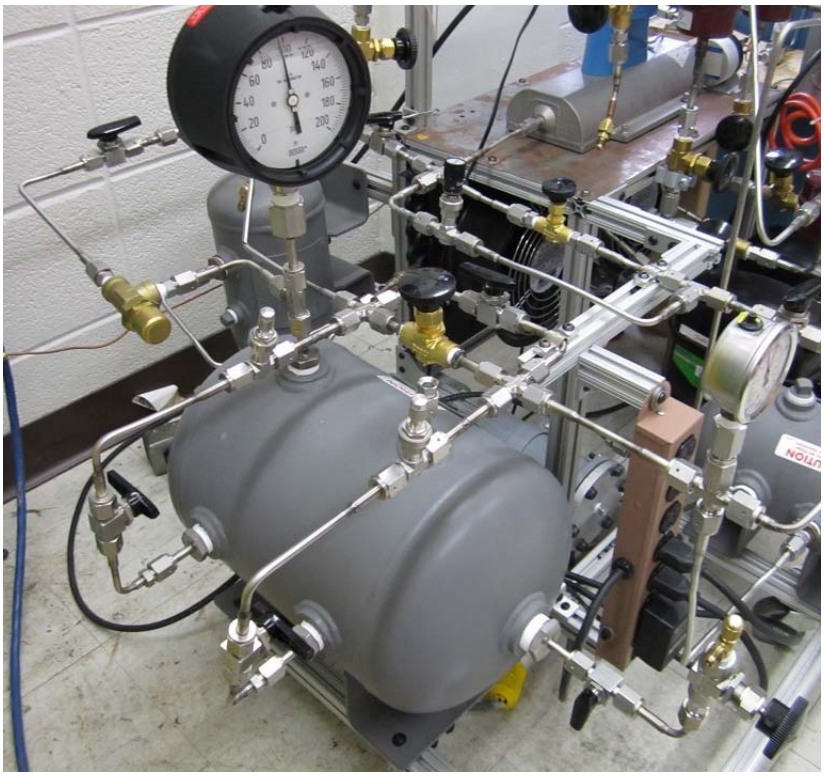

Figure 37. Make-up tank installed

3.7 Pressure Measurement Modifications

The primary issue with the original design of the test section and surrounding instrumentation was that the configuration measured temperature and pressure in different locations, succumbing to the inherent effect of a zeotropic mixture. It was noted during initial testing that in the absence of an applied heat flux to the copper rod, the outlet temperature of the gas mixture was lower than the inlet temperature. Again, this cooling phenomenon is the result of the Joule-Thomson effect. Due to the nature of zeotropic mixtures, having a single measurement of either temperature or pressure at a given location is not useful in the determination of fluid properties. Therefore, new locations to measure pressure were added in approximately the same

locations where inlet and outlet temperatures were measured, as shown in Figure 38. The diameter of the hole that penetrated into the inner diameter of the flow channel was created using a 72 gauge drill bit, which has a diameter of 0.635 mm.

Figure 38. Pressure tap additions to temperature measurement locations

Two custom configured, differential pressure transducers made by Omega were added at these new locations in such a way that gauge pressure sensor at the inlet of the test section could be translated to the locations where temperature was measured. This allowed for an improvement in the degree of certainty in specifying the inlet and outlet temperatures of the fluid flowing through the test section. With these new pressure sensors, a relationship between temperature and pressure was established and validated for the mixture in the test facility. This is graphically shown in Figure 39.

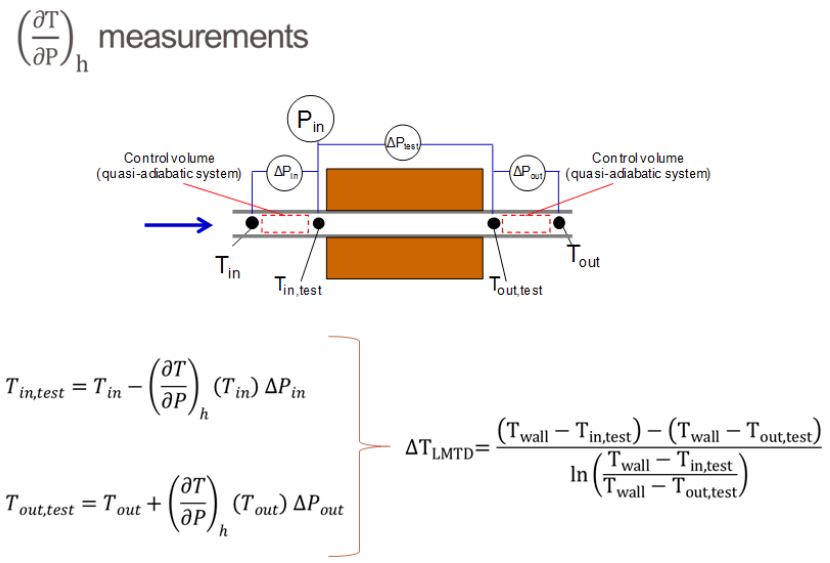

Figure 39. Graphical representation of Joule-Thomson effect as it related to the test section instrumentation

3.8 Test Section Modifications

An equally concerning issue pertaining to the test section was that the stainless steel tubing used in each of the three test sections had a relatively thick wall, which resulted in higher than desirable conduction losses from the copper mass. To reduce this undesirable heat loss, stainless steel tubing with thinner wall thicknesses were procured.

The pressure tap design was also reconfigured and utilized a custom fabricated group of Swagelok VCR type fittings on the inlet and outlet of the test section. It consisted of a quarter inch blind VCR gland with a centered hole bored approximately 0.01 inches over the outer diameter of the test section tubing. Welded to this piece was an eighth inch VCR gland, where the pressure tap hole would be drilled. Again, the diameter of the hole that penetrated into the inner diameter of the tubing created using a 72 gauge drill bit. Due to the torque required to tighten the VCR fittings and the thin wall tubing of the test section to which these were brazed, flats were machined onto these custom fabricated fittings to allow a wrench to grasp while tightening into the test facility piping. An example of the fittings fabricated for this purpose is shown in Figure 40. The final test

sections for the nominal 1.5 millimeter and 3 millimeter size are shown in Figure 41 and Figure 42, respectively.

Figure 40. Test section pressure tap custom fabricated fitting

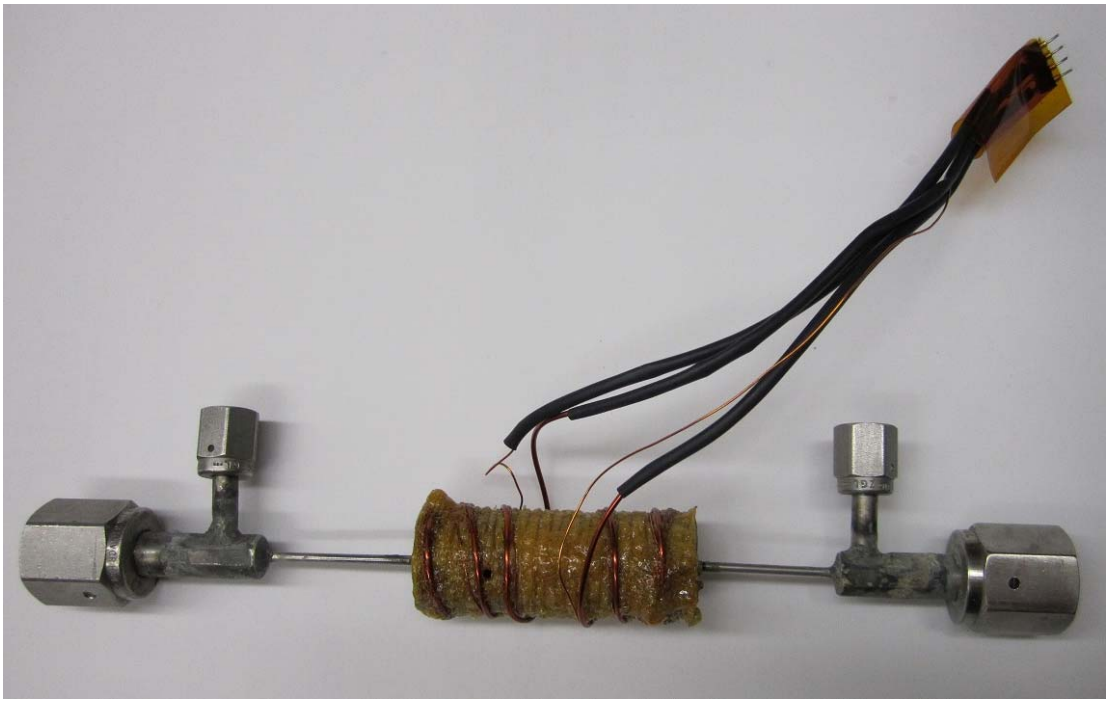

Figure 41. Modified 1.5mm test section

Figure 42. Modified 3mm test section

Figure 43. Test section stainless tube brazed to copper mass

3.9 Test Matrix Revision

The initially proposed test matrix, shown in Table 1, specified 36 different test conditions resulting from six mixtures at two pressures and three different test section diameters. These variations maintained the same heat and mass flux throughout all three test section diameters. After some thoughtful discussion, a new test matrix was proposed to reduce the number of test conditions without sacrificing the experimental intent of studying heat transfer capabilities of these mixtures. This new test matrix is shown in Table 3 and specifies the heat flux (q), pressure (P), and mass flux (G) for the corresponding mixture composition and test section diameter. The subscripts on

the parameter symbols provide identification for shared values. The test shown in red indicate deviations from the control condition specified in the 1.5 millimeter test section size.

The primary benefit of the new test matrix was a reduction in the number of test conditions from 36 to only 24, reducing the time required to obtain the data. The reduction resulted from the proposition that the effect of pressure could be observed in a single test section diameter. In addition, the heat and mass flux will now be varied in one of the test section diameters for each of the undiluted mixture concentrations. Following this new test matrix, it is believed that the scope of the desired analysis from the original test matrix was still maintained, while investigating additional variables and the resulting effects on the measured heat transfer data.

Though not shown in the new text matrix, but noteworthy, is the need to obtain a set of data for temperature and pressure drop for instances where the mass flux, pressure, and concentration change. This was done to confirm the fluid property data obtained from a National Institute of Standards and Technology (NIST) program called REFPROP version 9.1, which was used to perform calculations of the mixture thermodynamic quality and account for the Joule-Thomson effect. Furthermore, a binary mixture was added to the scope of this research, as it was proposed that a binary mixture was less complex than the other mixtures being investigated. The proposed test matrix can be seen in Table 2.

Table 2. Binary hydrocarbon mixture test matrix

Mixture		**Test Section Inner Diameter** *Geometry Effects*		
		0.5 [mm]	**1.5 [mm]**	**3.0 [mm]**
40% 60%	Methane Ethane	P_1 q_1 G_1	P_1, q_1, G_1 *Control Condition*	P_1 q_1 G_1
			P_2, q_1, G_1 *PuressureEffects*	
			P_1, q_2, G_1 *Heat Flux Effects*	
			P_1, q_1, G_2 *Mass Flux Effects*	

Table 3. Modified test matrix conditions

Mixtures *Concentration Effects*		**Test Section Inner Diameter** *Geometry Effects*		
		0.5 [mm]	1.5 [mm]	3.0 [mm]
45% 35% 20% 0%	Methane Ethane Propane Nitrogen	P_1 q_1 G_1	P_1, q_1, G_1 *Control Condition* P_2, q_1, G_1 *PuressureEffects* P_1, q_2, G_1 *Heat Flux Effects* P_1, q_1, G_2 *Mass Flux Effects*	P_1 q_1 G_1
36% 28% 16% 20%	Methane Ethane Propane Nitrogen	P_1 q_1 G_1	P_1 q_1 G_1	P_1 q_1 G_1
27% 21% 12% 40%	Methane Ethane Propane Nitrogen	P_1 q_1 G_1	P_1 q_1 G_1	P_1 q_1 G_1
35% 15% 15% 35% 0%	R14 R23 R32 R134a Argon	P_1 q_3 G_1	P_1, q_3, G_1 *Control Condition* P_2, q_3, G_1 *PuressureEffects* P_1, q_4, G_1 *Heat Flux Effects* P_1, q_3, G_2 *Mass Flux Effects*	P_1 q_3 G_1
28% 12% 12% 28% 20%	R14 R23 R32 R134a Argon	P_1 q_3 G_1	P_1 q_1 G_1	P_1 q_3 G_1
21% 9% 9% 21% 40%	R14 R23 R32 R134a Argon	P_1 q_3 G_1	P_1 q_1 G_1	P_1 q_3 G_1

3.10 Equipment Protection and Safety

Nearly all of the data sets required more than 12 hours to collect, and several required more than 20 hours to completely collect. Therefore, it was desired to leave the test facility operating at a steady-state condition between days, allowing for the data collection to resume from this point. In order to safely leave the test facility operating while unattended, several safety precautions were required. The failures that occurred from the excessive heating were the primary focus. Some were programmed into the data acquisition, while others were simple electronics.

The first implementation was to integrate solid-state relays into the cryocooler power circuit to deactivate it, as shown in Figure 44. These relays received a five volt DC signal from the datalogger using its data collection program created using the Campbell Scientific program called Edlog. The two programmed interlocks instructed the datalogger to stop the signal when the inlet temperature of the fluid reached 300 Kelvin and when the mass flow meter was not detecting flow. When either condition occurred, the respective relay would disconnect the power to the cryocooler, which in turn deactivated all power supplies controlling the heaters through another relay using the cryocooler power.

Figure 44. Relays used to disable cryocooler

Further precautions were taken in regards to the test section heater after the Nichrome wire was destroyed by sending a current that the wire could sustain at startup. The DC power supply control knob had been adjusted to a high current setting while the unit was powered off, which destroyed the wire when powered on. To eliminate the possibility of this failure occurring again, a one amp fuse was integrated into the heater circuit, ahead of the Nichrome wire on the test section. Similarly, to avoid any issue with the coldhead heat exchanger heaters, a two amp fuse was installed into each circuit between the DC power supply and the heater element. The three fuses were installed into a fuse block, as shown in Figure 45.

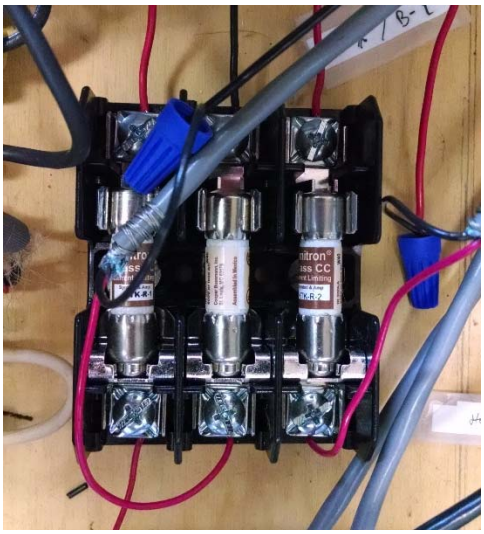

Figure 45. Heater DC power supply fuses

As a result of the thermal damage that occurred while the test facility was operating unattended, much of the equipment inside the Dewar needed to be repaired, such as the coldhead heat exchanger, the thermometers, and the radiation shielding. A new coldhead heat exchanger was fabricated in a similar manner as the original, except the base was brazed rather than soldered, and was then compressed between an additional copper plate and the coldhead using bolts. The four damaged thermometers used to measure the gas mixture temperature were discarded and remade using the same design. Finally, the radiation shielding, specifically the copper isothermal

envelope was modified to be much simpler, consisting of only two sheets that would encase the test section and surrounding instrumentation. It was affixed to the lower plate on the coldhead heat exchanger using a rectangular bolt flange and indium to reduce contact resistance, as shown in Figure 46.

Figure 46. Isothermal envelope modification in radiation shielding

Shortly after the thermally damaged components were repaired and data collection resumed, the turbopump used on the Dewar seized and needed to be replaced. The cause of the failure was unclear, but it is likely the result of one of two operating conditions: vibration and off-gassing inside the Dewar. The turbopump was mounted directly to the Dewar with no vibration isolation installed, where the coldhead displacer produced noticeable vibration. These

turbopump rotors operate at very high rotational velocities, and vibrations are not acceptable. Additionally, the varnish used to seal the Nichrome wire around the copper mass of the test section showed signs of off-gassing after being heated during the tests, in the form of small bubbles on the surface. The varnish is an adhesive substance, which could have accumulated in the tight tolerance spaces of the turbopump. The turbopump was mounted to the adjacent wall using flexible hose as shown in Figure 47, and the varnish was baked at a temperature above the expected highest temperature of 380 Kelvin. Upon implementing these corrections, no further issues arose from the turbopump.

Figure 47. Remote mounted turbopump modification

4 Operation

4.1 Gas Chromatograph and Sampling

There are many components comprising this test facility; however, most instrumentation works independently and requires manual operation. When preparing for a data set collection, it is advisable to begin by preparing the gas chromatograph. To do this, begin by initiating carrier gas flow to the GC by opening the valve on the carrier gas supply cylinder and adjusting the regulator. In this particular experiment, helium was utilized for the carrier gas; however, other gases, such as nitrogen, argon, or hydrogen may be used on this gas chromatograph. The flow and pressure can be verified by checking that the integral column pressure gauge displays pressure and responds to adjustments at the carrier gas cylinder regulator. The actual GC column pressure gauge is shown in Figure 48. A range of 55-65 PSIG was used for this experiment.

Figure 48. Gas chromatograph integral column pressure gauge

With the carrier gas flowing, it is acceptable to power the GC on and input the desired temperature program using the LabVIEW data acquisition program from Cornell University (http://ceeserver.cee.cornell.edu/mw24/Software) installed on the connected computer. It should be noted that the Cornell program has been modified to suit the needs of this experiment, with the addition of two pressure sensor measurements installed in the gas sample supply line. The program main window can be seen in Figure 49.

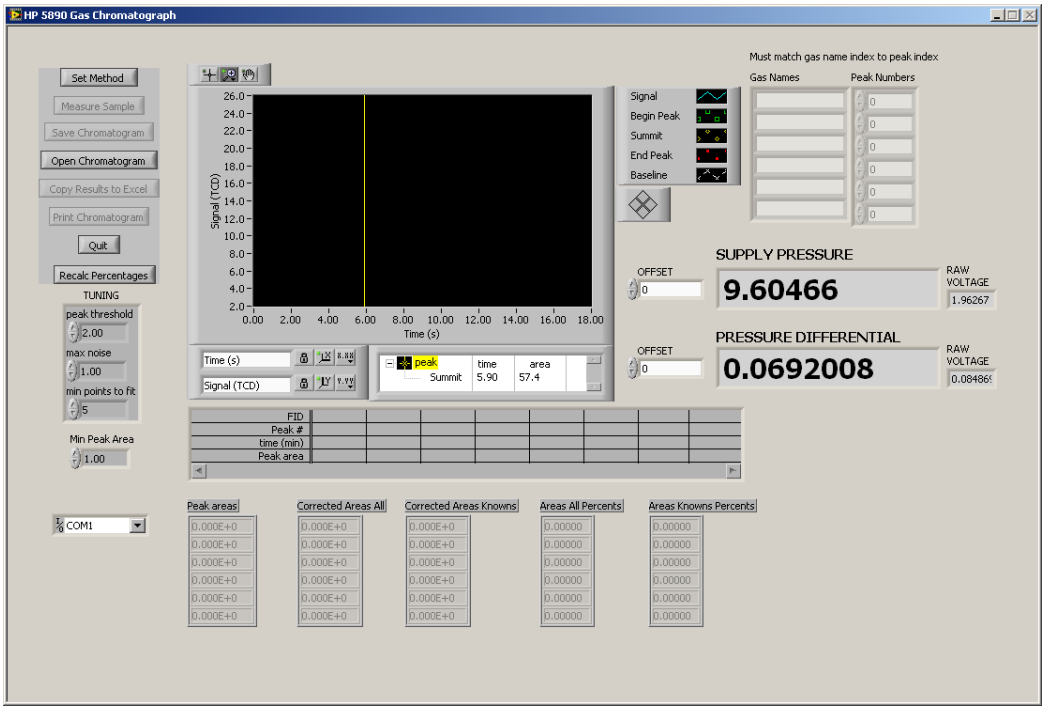

Figure 49. Cornell University gas chromatograph LabVIEW program initial start screen

To set the temperature program, select the 'Set Method' button located in the upper left corner of the screen. This will bring up a second window, shown in Figure 50, where the desired temperature program can be input and sent to the GC. The various settings related to sampling temperature can be set in this interface, such as injector, detector, and oven temperatures. The oven temperature program can be a constant temperature, or have up to three ramp functions occurring at specified temperature rates [C/min] and times [minutes].

Figure 50 shows an example of a temperature program utilizing a single ramp function. Ramp functions were necessary for the diluted mixtures, as constant temperature programs did not allow for adequate column separation of the diluting gas and the mixture component that was first to elute from the column. The lower initial oven temperature allowed for an increased separation. Upon inputting the desired settings, the 'OK' button should be pressed to send the parameters to the GC.

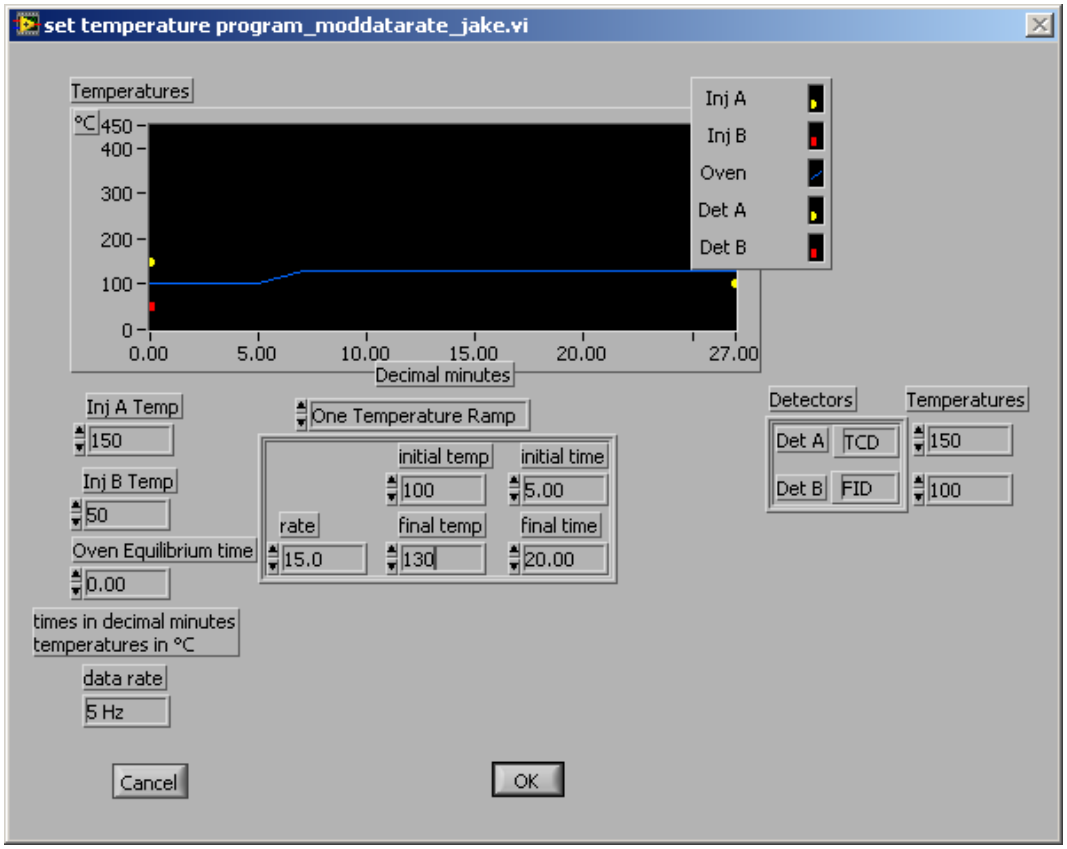

Figure 50. GC temperature program input screen; ramp function shown

Immediately following this action, a window will appear, indicating the actual temperatures of the instrumentation, as well as the active status of the detectors. This screen allows the sensing instrumentation to be activated, such as the Thermal Conductivity Detector (TCD), which was utilized in this experiment. From initial startup, it is necessary to change the activation of the TCD switches on the screen. This is accomplished by clicking the red 'OFF'

button located below the TCD label, as well as the red toggle switch above it, as shown in Figure 51. A window will appear, asking for confirmation that the carrier gases are flowing to the GC, as the TCD can be damaged if activated and heated with no carrier gas flowing through it.

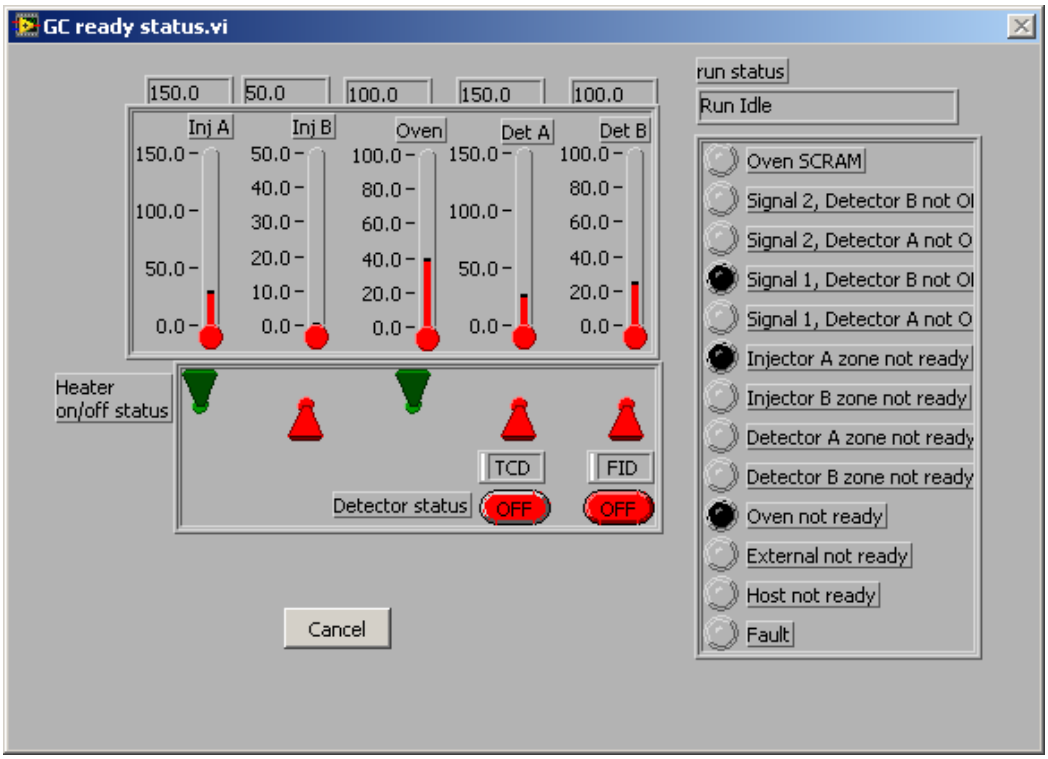

Figure 51. GC ready status screen, shown with TCD sensor not active and temperatures not ready

At the time the instrumentation is ready, an ‘OK’ button will appear at the bottom of the window, as can be seen in Figure 52. This indicates that the parameters specified have been met and the GC is ready for a sample. Selecting the ‘OK’ button will return the main program window screen, where the controls to begin a sample test are located.

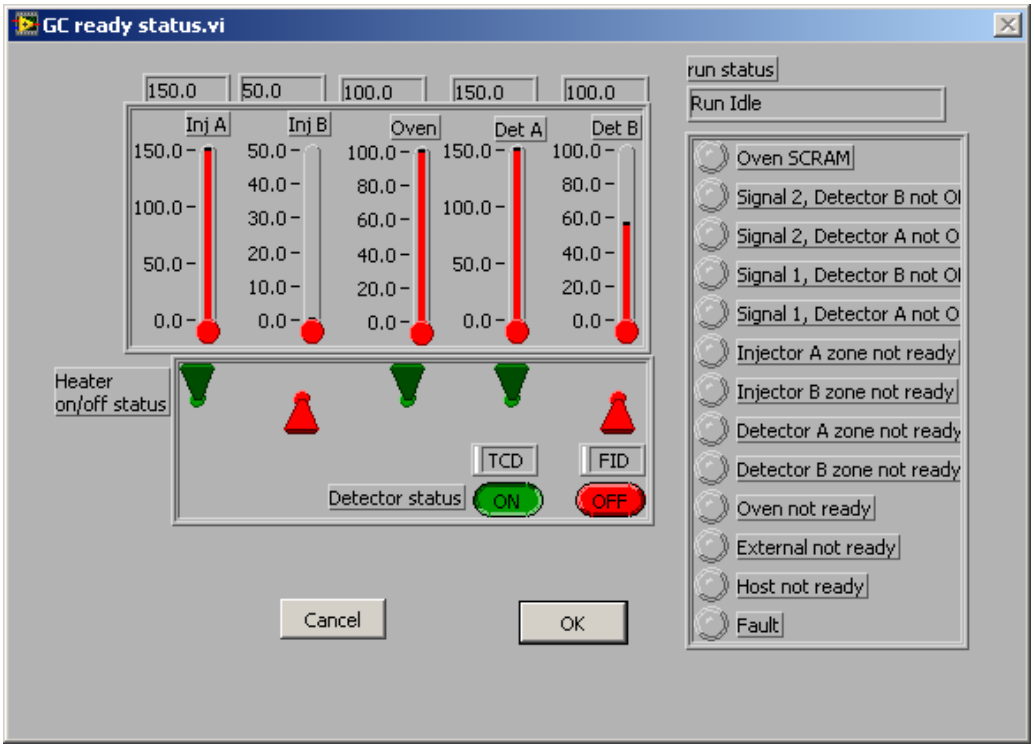

Figure 52. GC ready status screen, shown as ready to proceed

Though the LabVIEW program from Cornell University is capable of providing chromatograms with peak areas and retention times, the external Integrator was preferred. It was often observed that the chromatogram in the LabVIEW program would stop recording during a sample test. In addition, it was less difficult to save and record the paper copies from the Integrator.

While preparing the gas chromatograph as described above, the Integrator can be started and setup. The Integrator is powered on using a switch located on the backside of the device. It will need to go through a warm-up sequence, but two green lights will appear when ready. The first settings to input should be the date and time. On the Integrator keyboard, simply type the letters TIME, followed by the actual time in HH:MM:SS format. Pressing the ENTER button will complete the action. Similarly, for the date, type DATE, followed by the desired date in MM/DD/YYYY format. Again, pressing the ENTER key will complete this step.

There are two settings related to the output control that should be changed from their default settings, prior to recording a sample. The peak attenuation should be set to 5, by pressing the ATT2↑ button twice, followed by the 5 key and ENTER key. The threshold level setting should be also set to 5 in the same manner, except using the THRSH key. These settings should scale the peak heights to fit on the Integrator paper.

The equipment is now ready to accept a sample; however, it is best to perform a helium gas flush of the sample line to remove any contaminants. The piping installed from the helium supply cylinder to the experimental test facility at the sampling location and isolated by a single needle valve, should be used for this purpose. The brass needle valve, shown in Figure 53, can be opened to initiate the flushing procedure.

Figure 53. Gas sample valves on compression station for GC sampling

It is recommended that the helium flush take place for a minimum of five minutes, at a rate of 10-20 cc/min as indicated on the rotameter at the GC sample line outlet, as this proved successful in clearing the sample line. This flow rate can be controlled using the integral valve on the rotameter. After this time has elapsed, the needle valve isolating the sample line from the helium

cylinder should be closed. The residual helium in the sample line should be purged to atmosphere by opening the integral valve on the rotameter for another five minute period, or until the supply pressure and differential pressure sensor values on the main program screen do not change with time.

The baseline measurement of the TCD should also be checked for stability. This can be done by pressing either the SIG 1 or SIG 2 button on the GC user interface keyboard. One of those two buttons will be associated with the TCD sensor. A baseline of 3.5 to 5 was common for this experiment, and was related to the carrier gas pressure supplied to the GC. It is important to have a measurement baseline that does not change with time, as this is the reference from which the sample components are measured.

The integral valve on the rotameter should be nearly closed prior to sending the gas sample to the GC. The supply pressure and differential pressure sensor readouts should be set to zero, or approximately zero, as the values will fluctuate. This is done to provide consistent sample sizes to the GC from the test facility.

A sample from the test facility can be sent by opening one of the two isolation ball valves located near the helium flush valve used earlier. The purpose of having two valves is to allow for a sample to be sent from either the supply or return of the Dewar, or rather the test section. When the supply pressure value on the main program screen reads above 30 [PSIG], the isolation valve can be closed, as this is sufficient pressure in the sample line to inject a sample. The valve on the rotameter can be slowly opened to allow the gas sample to flow through the sample loop.

The valve should be used to control the flow rate of the gas sample. Target values of approximately 18 [PSIG] and 0.11 [PSI] were specified for the supply pressure and differential pressure, respectively, for sample consistency in this experiment. The ‘Measure Sample’ button,

located in the upper left corner of the main program screen, can be selected to introduce the sample to the GC. This will actuate the GC sampling valve, which remains open for a specified time of 30 seconds. All of the menu button icons will disappear and a single button will appear, which is used to end the sample run after all the gas components have eluted from the column. Figure 55 shows the main program screen after a sample run has completed. Similarly, the Integrator should be stopped by pressing the 'STOP' key on the keyboard.

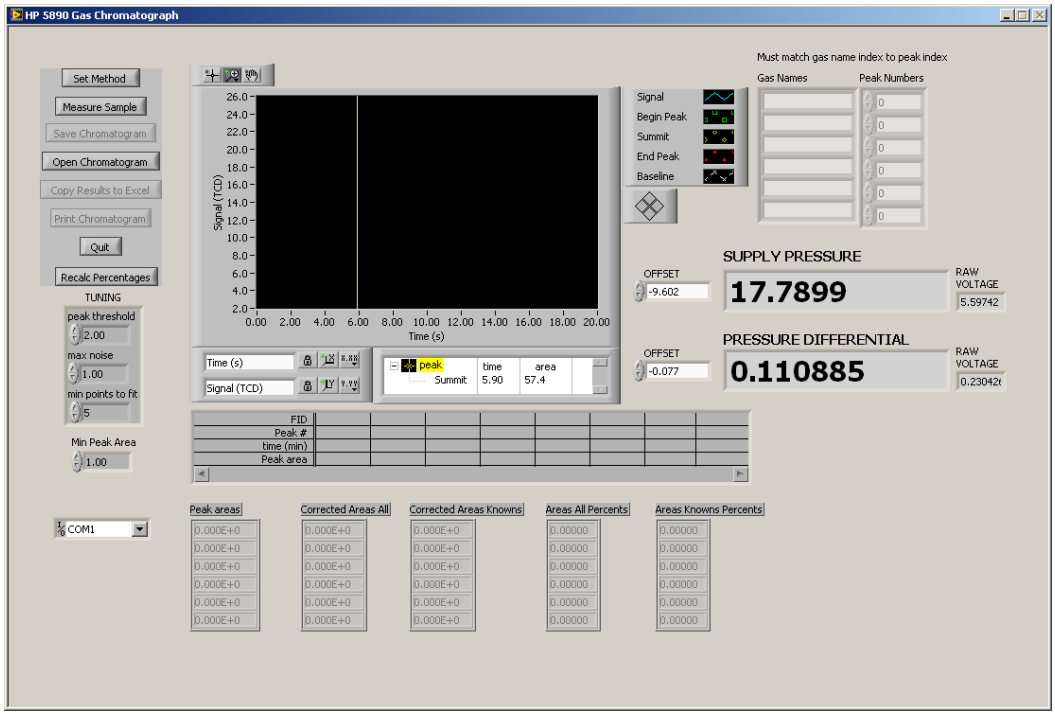

Figure 54. Gas chromatograph main screen, ready for sample

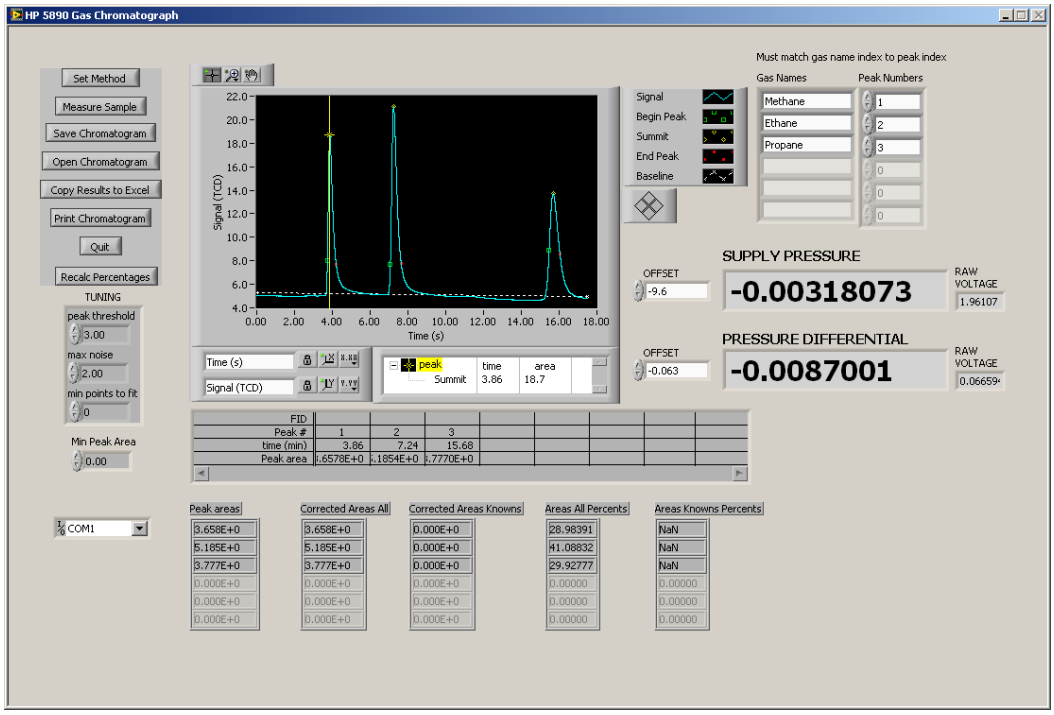

Figure 55. Gas chromatograph main screen, end of sample

4.2 Data Acquisition

On the computer connected to the Campbell Scientific datalogger, open the LoggerNet program interface. A menu screen should appear, as shown in Figure 56.

Figure 56. Campbell Scientific LoggerNet menu screen, 'Main' menu selected

Select the 'Main' menu, as highlighted in the figure, and click on the 'Connect' option. This will open the data output interface, as shown in Figure 57. This screen can be used to verify whether the data appear to be acceptable, or if changes are required.

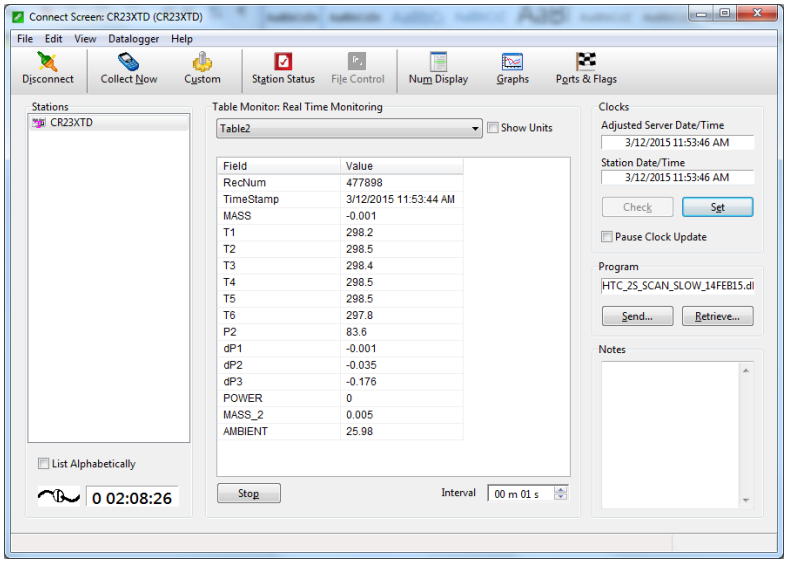

Figure 57. Connect screen, used as the data output interface

Typically, the differential pressure sensors will need to be set to zero prior to activating the compression station. To do this, return to the main program interface and select the 'Program' menu and click the 'Edlog' option, as shown in Figure 58.

Figure 58. Loggernet interface, 'Program' menu selected

This will open the programming environment shown in Figure 59 for creating and modifying the code, or set of instructions, used by the datalogger to interpret input and output signals. The code can then be modified to adjust the offset of the differential pressure sensors. Once adjusted, the program file can be saved to record the changes.

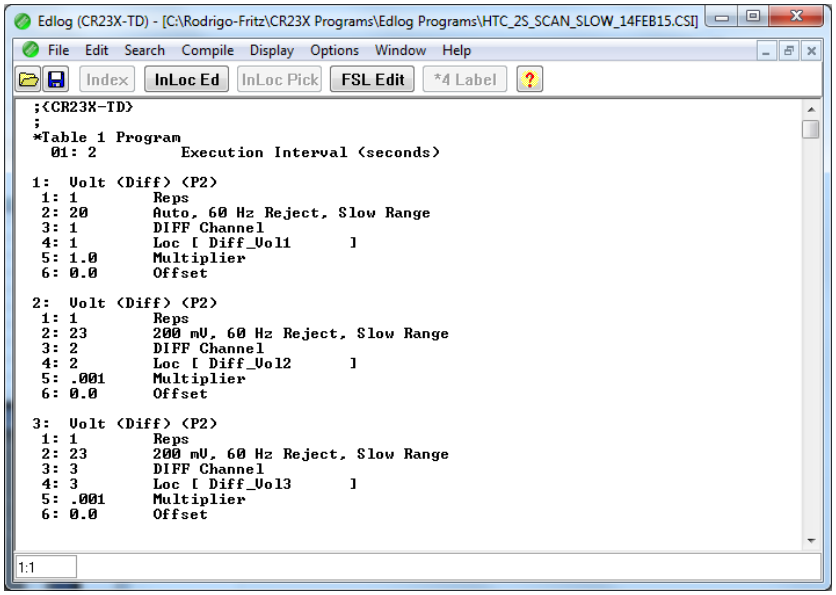

Figure 59. Edlog programming environment

The next step is to upload the program to the datalogger. This is done by returning to the Connect screen, shown in Figure 57, and clicking on the ‘Send…’ button located on the right side of the window, under the ‘Program’ section. This will open a file explorer window, from which the newly modified Edlog program can be selected. Additional prompts will appear to verify the action, as once the program is uploaded, it will clear the memory on the datalogger. This is desired for beginning a new data set.

Alternatively, the program upload process can be done through this ‘Setup’ window. The ‘Setup’ window is opened through the LoggerNet interface menu by selecting it in the ‘Main’ menu option, as can be seen in Figure 56. Finally, navigate to the ‘Program’ tab and click the ‘Send…’ button, as shown in Figure 60. This will similarly clear the datalogger memory when the new program is uploaded. If the tabs do not appear, it is likely due to the datalogger not being selected in the left window pane, under ‘Entire Network’ section.

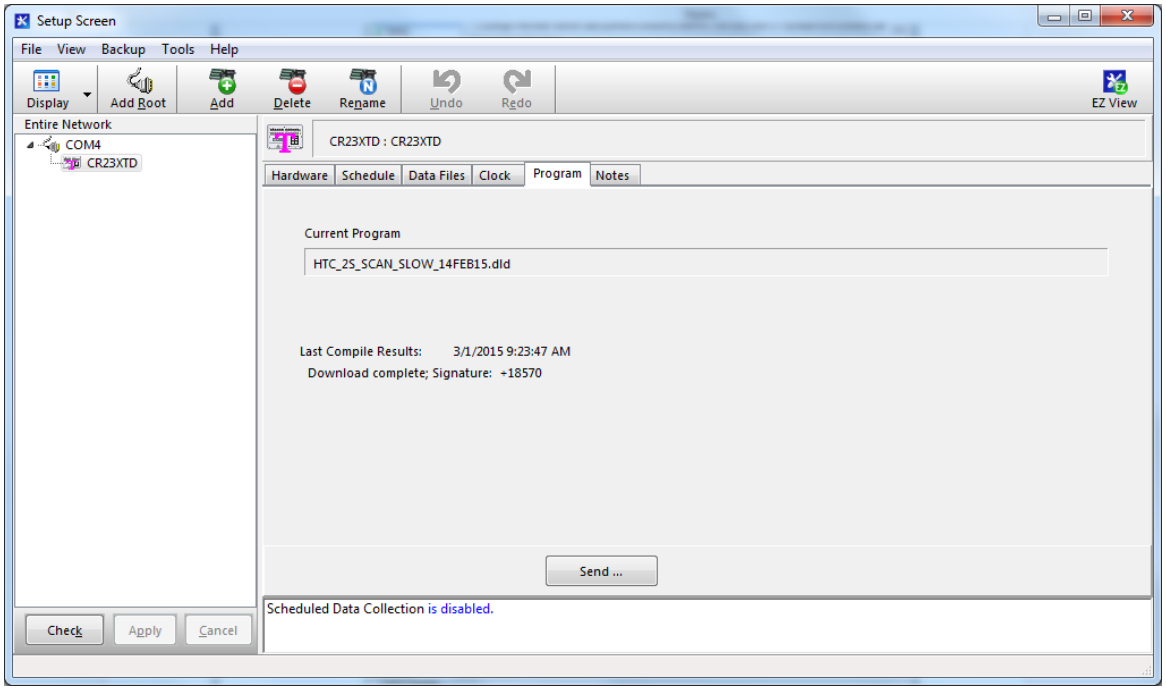

Figure 60. Setup screen, showing the Program tab for sending a new program to the datalogger

Data saved to the datalogger need to be recorded to a computer for permanent storage, as the datalogger will only save the most recent data. In this experiment, a cable from the RS-232 port on the datalogger is connected to a USB port on a computer used for data storage, as well as programming. The program sent to the datalogger will only specify how to store the data in the datalogger.

In order to store the data to the computer, a location needs to be specified in the 'Setup' window. Again, this is done by returning to the LoggerNet menu interface, selecting the 'Main' menu and clicking the 'Setup' option. From this window, navigate to the 'Data Files' tab and specify the file storage location of any tables being created as instructed by the Edlog program in the datalogger. For example, in Figure 61 below shows seven tables being created, five of which are being recorded, as the box labeled 'Included For Scheduled Collection' has been checked. This is graphically displayed by the green checkmarks and red X-marks in the table list.

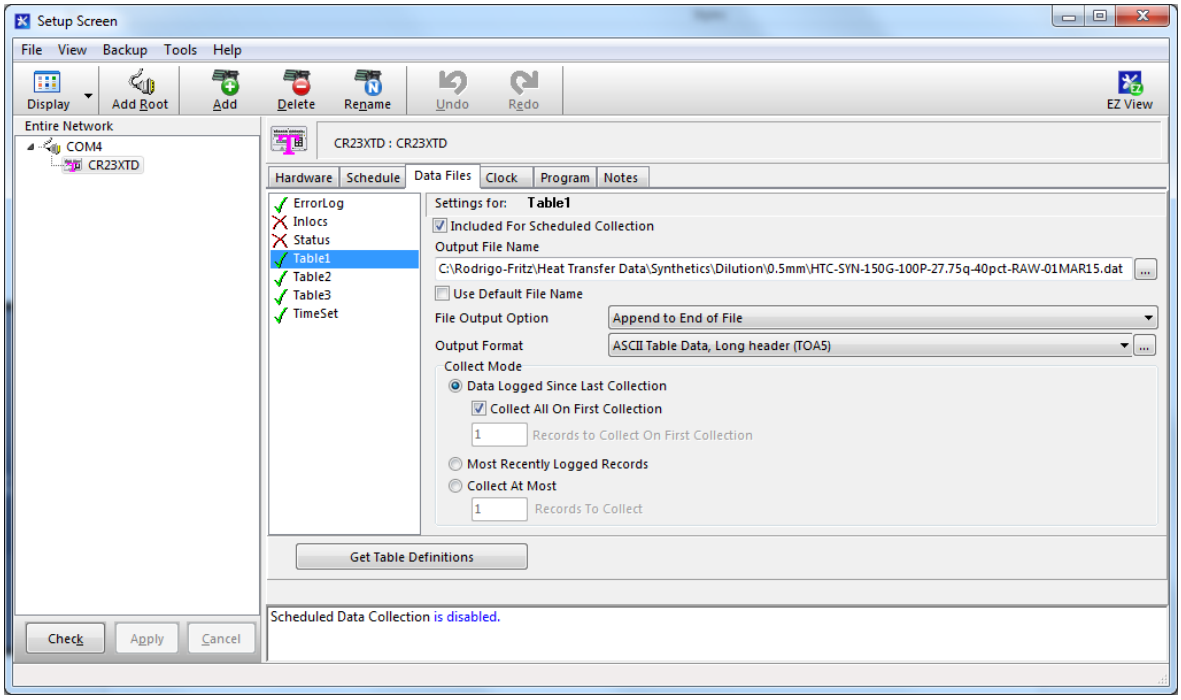

Figure 61. Setup screen, showing Data Files tab where data storage is specified

With the file storage locations specified as desired on the connected computer, an additional feature of the LoggerNet software can be used. The data stored on the datalogger must be retrieved, either automatically or manually. The automatic collection feature, referred to as Scheduled Collection, can be enabled in the 'Setup' screen by navigating to the 'Schedule' tab, as can be seen in Figure 62. This is the ideal practice for collecting large data sets taking place over an extended period of time, such as an entire day as is the case for this experiment.

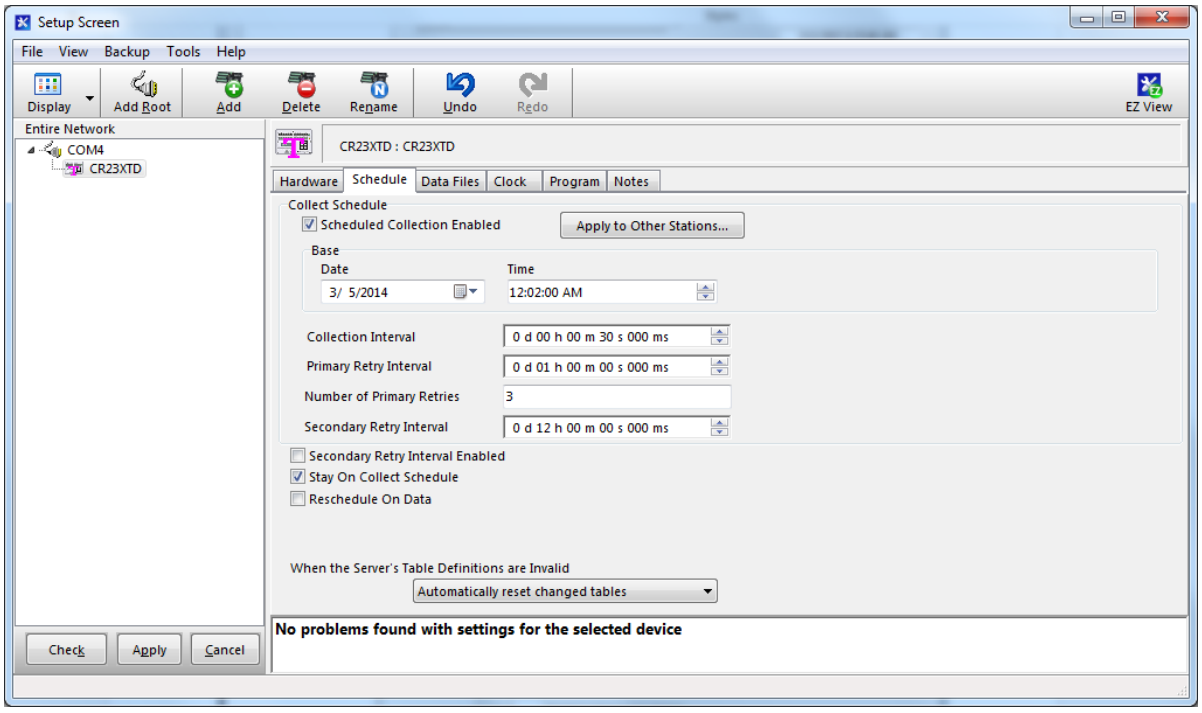

Figure 62. Setup screen, showing the Schedule tab

The important parameters to set are the base date and time, as well as the collection interval. The date and time simply need to be any date or time in the past, from which the program can use as a reference. Conversely, the collection interval requires additional thought. This is the amount of time that will pass between each transfer of new data to the computer for storage, which may be different from the datalogger collection interval. In this experiment, it was beneficial to select a time of less than one minute for use in plotting the data. After the desired settings have been made, clicking the apply button in the lower left corner of the screen will save the changes and initiate the collection process.

Alternatively, a manual collection can be done from the Connect screen, by clicking the Custom menu icon button located near the top of the screen, as can be seen in Figure 57. This will open the window shown in Figure 63 allowing for customized collection of data, such as the number of records, file name, and file location. This is mostly useful for single collections of

particular records from the datalogger, for use in creating a file, or many files, to store in another location.

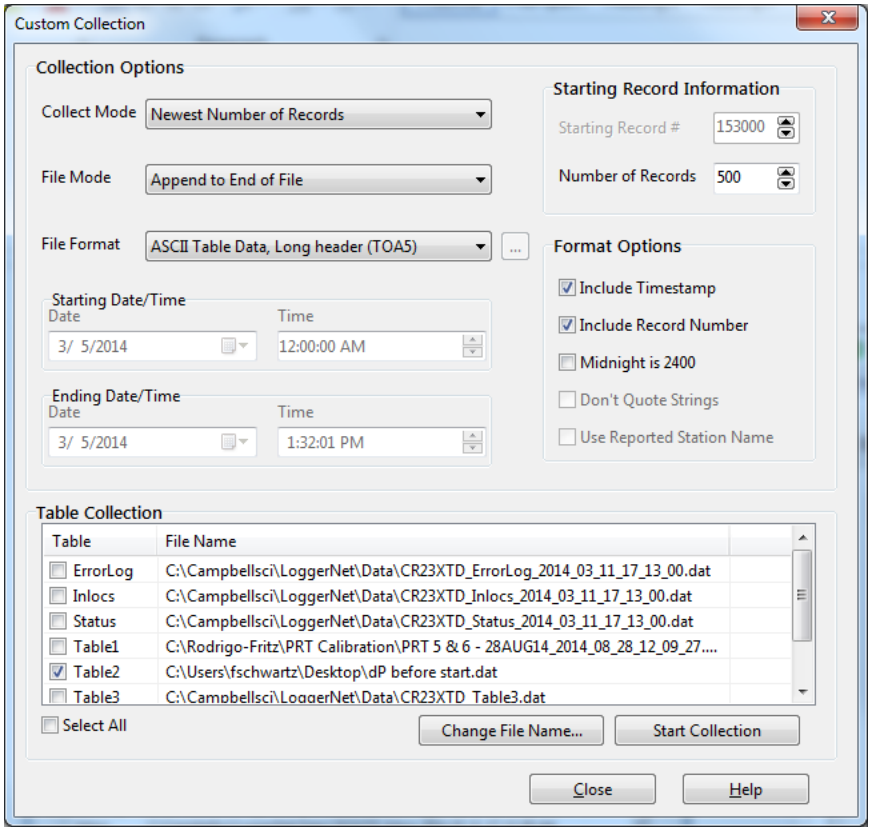

Figure 63. Custom Collection screen used for manual data collection from datalogger

At this point, the data are being collected, stored to the computer, and can be viewed using the LoggerNet software. There are multiple ways to view the data graphically, as well as in the default tabular format as stored on the datalogger. The most practical way to view the data during a data set collection is to use the Run-Time Development software, which can produce graphs of the data at specified update intervals from the files being stored to the computer. To open the development package, return to the LoggerNet menu interface, select the 'Data' option to open the menu and click the 'RTMC Development' option, as can be seen in Figure 64. A screen similar to the one shown in Figure 65 will appear.

Figure 64. LoggerNet interface, Data menu selected

This program can be used to create real-time plots of the data being collected. As was done in this experiment, plots showing all of the temperature measurements and mass flow rate were created to monitor the test section response to changes made to the compression station and electric heaters on the coldhead and test section copper mass. As can be seen in Figure 65, many tabs can be created to show data graphically. This feature can only be used when the Scheduled Collection feature is enabled, and the plots will update at the rate specified by the automatic collection interval.

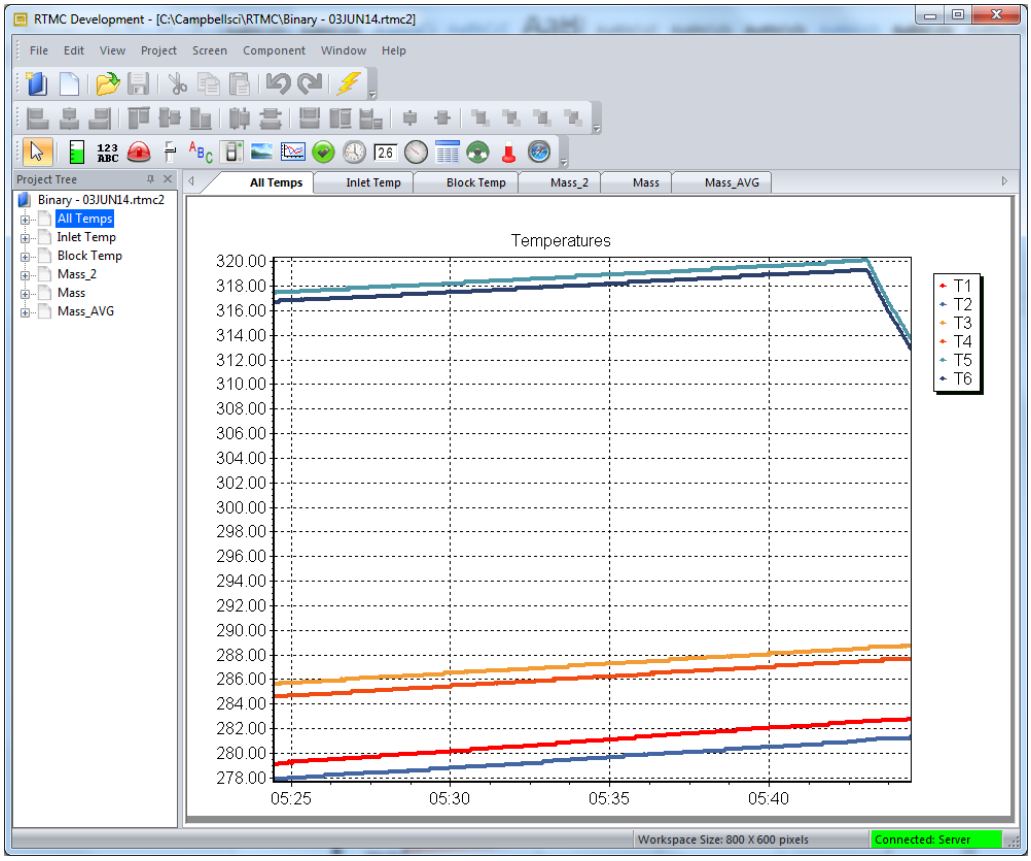

Figure 65. Run-Time Development interface, shown with various screens of plots configured

Once any modifications are made and determined to be acceptable, the project can be saved and run by pressing the 'Save and Run' icon, shown in the above figure as a yellow bolt of lightning. This will produce the actual window where the data will be displayed and updated according to the scheduled collection parameters specified earlier.

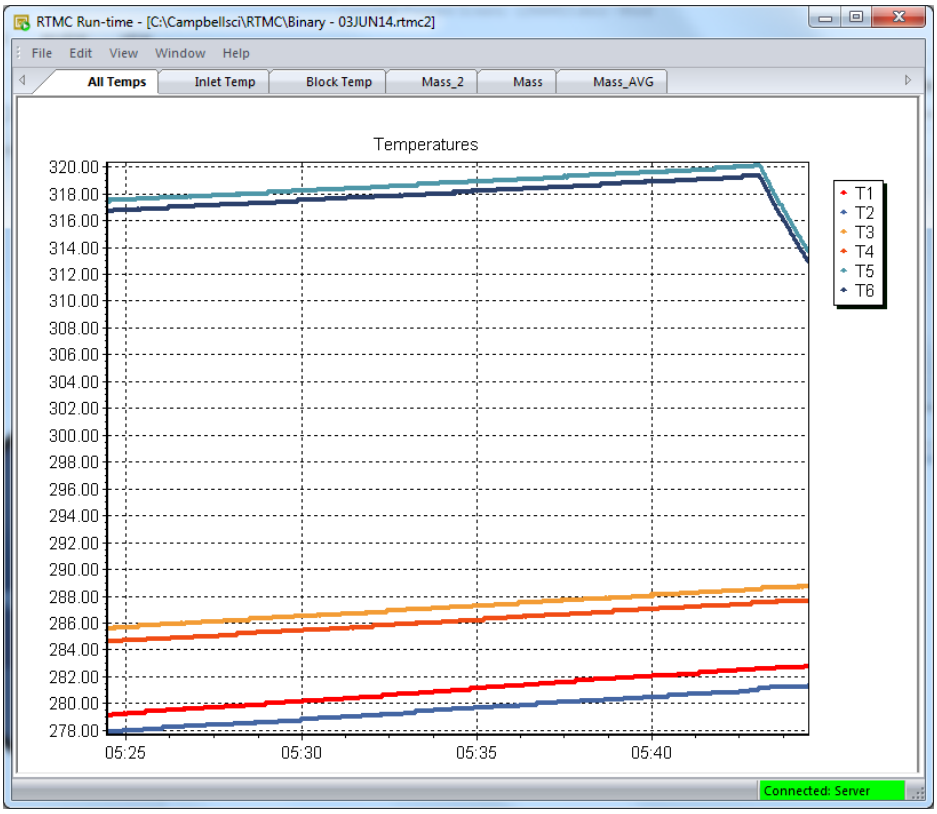

Figure 66. A Run-Time project during data collection

As a way to verify that the data are being collected as desired, another LoggerNet program can be used to view the actual stored files. The program is called View Pro and can be opened through the LoggerNet menu interface, in the Data option, as shown in Figure 64. A window will open, and the table files stored to the computer can be viewed by using the open command. An example of a data file opened in View Pro is shown in Figure 67; the colored columns indicate that each has been selected.

The selected columns can be plotted by selecting the plot icon at the top of the screen, as highlighted in the figure. This is the most practical way to view the data files collected from the datalogger. A plot, similar to the one shown in Figure 68, will appear. There are many options to change the plot viewing area, such as the number of records. As the plot was created using the entire data file, it is possible to scroll through the entire set graphically.

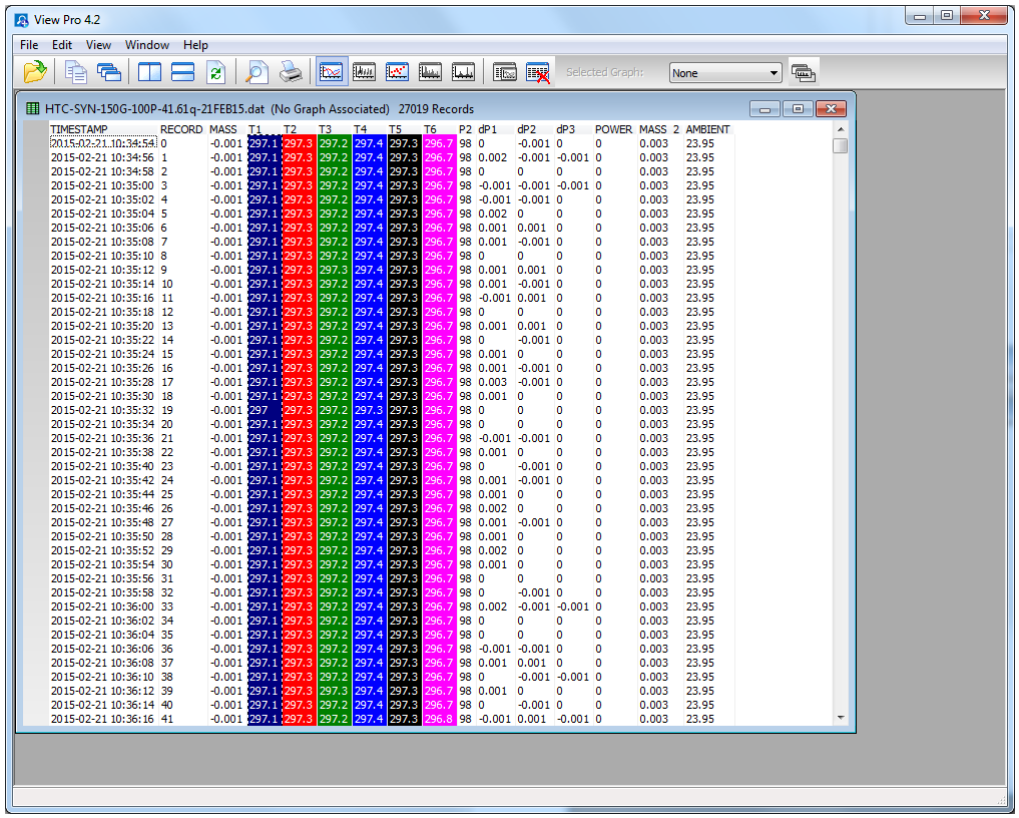

Figure 67. Data file open in View Pro window

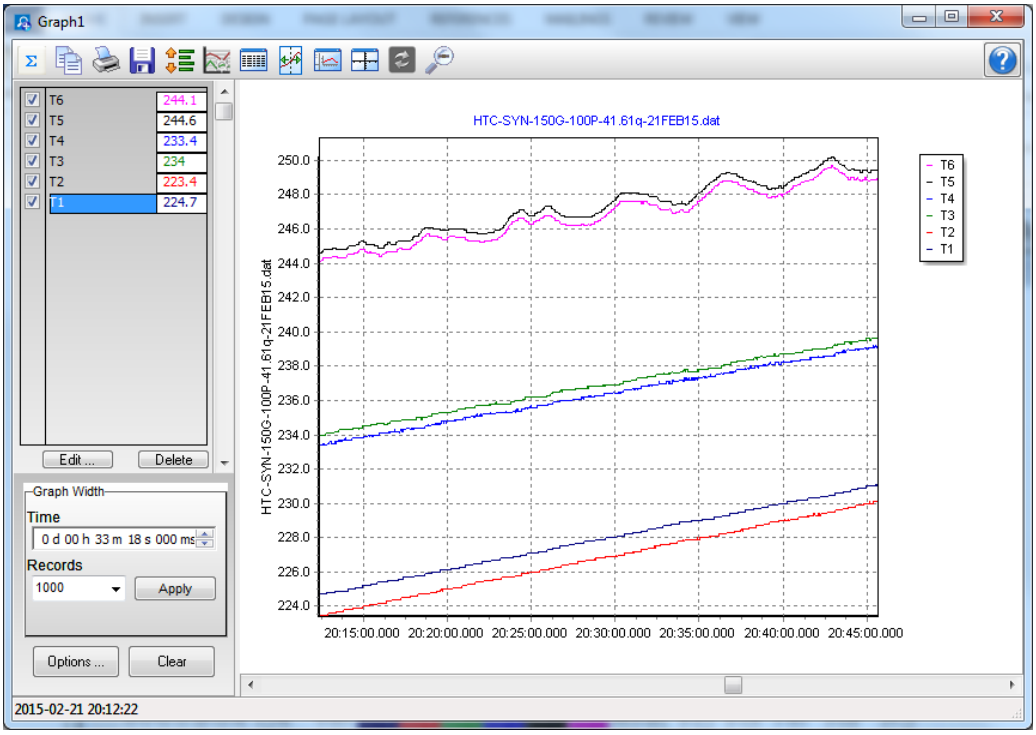

Figure 68. Plot of data created using View Pro.

4.3 Compression Station Flow Balancing

It is acceptable to initiate flow in the compression station after the gas chromatograph and data collection systems are ready. First, however, it is necessary to verify that the appropriate valves are in the correct positions. The ball valve on the bypass line should be fully opened, as this will ensure the discharge pressure does not unintentionally go above the 150 PSIG pressure rating of the compressor discharge heat exchanger. Additionally, the ball valve isolating the pressure relief valve should be opened, as this protects the heat exchanger from high pressure. The four needle valves connected to the oil separator drain ports should be opened partially; a quarter to an eighth of a turn is sufficient. Finally, the needle valves downstream of the mass flow meter should be opened to reduce the upstream pressure, as it will be adjusted in conjunction with the pressure regulator after the compressors are started.

With the flow paths fully open, the compressors can be powered on with the toggle switch installed on the topside of the gray electrical panel mounted on the compression station. As there are two compressors installed in parallel, an option to utilize only one at a time was made available with the installation of a power toggle switch for each compressor, inside this electrical panel. It is necessary to verify that the desired compressor switches are in the correct position. Also, an auxiliary fan should be used to cool the compressors during operation.

The pressure in the system should increase at the discharge of the compressors. To achieve the desired flow rate and supply pressure to the test section, it is necessary to balance the bypass loop needle valve, the pressure regulator, and the needle valves downstream of the mass flow meter. To begin, decrease the amount of mass flow being diverted to the bypass loop by closing the ball valve and opening the needle valve. It is preferable to use the needle valve for this, as it will allow for finer adjustments throughout the data set collection. Depending upon the pressure

upstream of the pressure regulator and the mass flow rate through the test section, it may or may not be necessary to adjust the needle valves downstream of the mass flow meter.

The bypass loop valves will control the amount of mass flow that is diverted from the test section. Closing the valves at this location will increase the discharge pressure of the compressor, as well as increase the mass flow rate to the test section. The opposite will result from opening these valves. Similarly, closing the needle valves downstream of the mass flow meter will decrease the mass flow rate through the test section, but will increase the pressure of gas entering the test section. Again, the opposite effects result from opening these valves. Lastly, the pressure regulator works very similarly to these valves, as adjustments will increase or decrease the gas flow rate and pressure.

The most reliable and steady data set collections resulted from a pressure in the range of 120 to 140 PSIG at the pressure regulator inlet, therefore, this should be the target range when starting the compression station. During the data set collection, it will be necessary to make adjustments to the same valves discussed above, as the viscosity of the mixture will change with its changing temperature, or more appropriately, its thermodynamic quality.

Typically, only slight adjustments to the pressure regulator and needle valves downstream of the mass flow meter were required. Although, as the mixture was condensed to saturated liquid, the compressor discharge pressure decreased due to the decrease in gas volume in the test facility. To counter this, the bypass valve can be closed further, but this decreased the suction pressure at the inlet of the compressors, which had an adverse effect on the mass flow rate. The lower pressure gas has a lower density, and therefore each stroke of the compressor was moving less mass. When this occurs, it is necessary to introduce additional gas mixture to the system from the make-up tank.

The make-up tank ties into the bypass loop in two locations, one upstream and one downstream of the bypass valves. Each location has a ball valve to provide positive shutoff, and also a needle valve to regulate the flow rate through the line. In the situation where more gas is needed, the valves downstream of the bypass loop valve should be used to introduce gas to the compressor suction. Conversely, if gas needs to be removed, as is the case when the gas mixture is changing from saturated liquid to two-phase in the test section, the other valves can be used to accomplish this.

Alternatively, the make-up tank can be used as a bypass loop, by appropriately balancing the two needle valves on the lines that are piped into the original bypass loop. Instead of being required to add or remove gas in large quantities while not bypassing through the make-up tank, the needle valves on the tank lines can be used to adjust the pressure drop across the tank where sufficient volume is available. The benefit of using this approach is it becomes easier to regulate the pressure at the suction and discharge of the compressors.

4.4 Cryocooler and Heaters

Prior to starting the cryocooler compressor, cooling water needs to be supplied to its cooling system. This is done by using the water supply assembly shown in Figure 69. With the solenoid valve controlling the water flow connected to a power source, the manual shutoff valve can be opened by pressing the green push-button to actuate the solenoid valve. This will allow the water to flow through the piping and tubing to the compressor cooling system heat exchanger. A simple flow switch with normally open contacts, was mounted at the cooling loop discharge and integrated into the solenoid valve circuit. The intention is to reduce the possibility that a gross leak of cooling water would occur in the lab.

Figure 69. Cryocooler compressor cooling water supply assembly

With cooling supply water flowing and the compression station activated, the cryocooler compressor may be powered on to initiate cooling at the cold head. If the compression station is actively flowing the gas mixture, the interlocks programmed in Edlog will be made and complete the circuit to the compressor power switch relays. It is recommended that the compressor bypass valve be open during startup, as the cooling power can be increased in a controlled manner by slowly closing the valve. It should also be noted that the desired static charge pressure in the cryocooler compressor system was between 175 and 200 PSIG, which could be verified by the compressor supply and return pressure gauges located on the front of the enclosure. These two gauges, the bypass valve, and the power button can be seen in Figure 70.

Figure 70. Cryocooler compressor, front of enclosure

The electric heaters installed in the coldhead heat exchanger can be used to balance the cooling load provided by the cryocooler, thereby controlling the temperature of the gas entering the test section. The typical operational method involves achieving a steady-state condition with the coldhead heaters by adjusting the power supplied manually with the control knobs on one or both of the DC power supplies. It was preferred that the beginning steady-state condition be in either saturated liquid or vapor for data set collections.

The gas mixture being used and its respective flow rate have a significant effect on the amount of heat needed from the coldhead heaters, as the capacitance rate of the mixture will vary. For example, it was determined that the cryocooler was only necessary to condense the mixtures to saturated liquid for the low flow data sets, and the heat applied to the test section was enough to gradually increase the inlet temperature alone. The most challenging control issue was maintaining the pseudo steady-state temperature during the phase changes, as the heat transfer increased significantly in the two-phase regime of the mixtures.

The test section heater was only operated when the steady-state condition was roughly 5 to 10 Kelvin above the dew point of the gas mixture, as the heat transfer in the vapor region was relatively poor, resulting in high temperatures in the copper mass. Upon reaching a steady-state

condition, the power to the coldhead heaters can be adjusted to produce the pseudo steady-state condition desired to measure the entire range of temperatures in the two-phase regime of the mixture. The pseudo steady-state condition as defined for this experiment was determined by setting the change in internal energy of the test section copper mass to two percent of the heat applied to the test section. Dividing this value by the mass and heat capacity of the copper mass provided a rate of change in temperature that could be targeted using the coldhead heaters. A noteworthy observation regarding the test section heater was that very minor adjustments were required, as the resistivity of the nichrome wire changed with temperature.

4.5 Charging and Evacuating Test Facility Mixtures

The importance of reducing impurities in the gas mixtures was of the utmost importance in this study. Each gas mixture component used had a minimum purity of 99.5% to avoid introducing significant impurities. Therefore, it was critical to be certain that the mixture was being charged into a completely evacuated, empty test facility. Two methods were utilized to produce this environment: repeated flushing and vacuuming with a purge gas or a simple extended vacuum period. It was determined that both methods worked sufficiently well for this experiment based on results from the gas chromatograph, but the extended purge method was most commonly used, though both will be described below.

The flushing method required connecting a rotary vane vacuum pump to an evacuation port on the test facility piping. The post-modification test facility included multiple locations to do this, as shown earlier in Figure 32. A refrigeration manifold manufactured by Yellow Jacket, was used to connect the test facility to the vacuum pump, as well as the flushing gas cylinder. Typically, the flushing gas used was nitrogen, but argon and helium could also be used to accomplish the same

results. The advantage of using this manifold was that it was equipped with pressure gauges, and it allowed the line connecting the gas cylinder to be evacuated with the test facility.

It was considered good practice to control the rate at which the test facility was evacuated. A target rate of 10 PSI per minute was specified, as this reduced the concern of evacuating at a rate that could move the compressor oil in undesired locations in the test facility piping. Therefore, prior to activating the vacuum pump, the needle valve on the evacuation port was always closed completely, which could then be slowly opened and the evacuation rate could be monitored using the test section inlet pressure gauge. As the pressure in the test facility decreased, it was possible to open the needle valve more until it was fully opened.

When the pressure in the test facility had reach a low vacuum, such as 200 millitorr as read by the Series 275 Kurt J. Lesker Convectron vacuum gauge at the vacuum pump suction, the vacuum pump was isolated from the charge manifold by closing the valve on the respective port. Immediately following this action, the flushing gas was slowly added by opening the cylinder valve and adjusting the cylinder regulator. It was considered good practice to close the evacuation port needle valve on the test facility and utilize it to control the rate of gas addition to the test facility piping. The flushing gas was added until a pressure of 10 PSIG was displayed by the test section inlet pressure gauge, as shown on the LoggerNet connect screen interface, and then removed in the same controlled manner described above. This process was repeated two additional times, resulting in a triple flush.

The extended evacuation method followed the same steps, but no flushing gas was used. Instead, the vacuum pump was left to pull a vacuum on the test facility piping for a minimum of 12 hours. The cylinder connected to the charging manifold was to be whichever gas or gas mixture required to be added to the test facility. The evacuation was considered successful when the

convectron gauge on the vacuum pump displayed a value below 100 millitorr, with typical values around 50 millitorr being attained.

Following successful evacuation, the desired gas mixture or mixture component could be added to the test facility. Again, the rate of addition was the same rate described above to avoid moving the compressor oil. The process for adding a pre-mixed gas is very simple and only requires that the gas be added to the desired charge pressure, which ranged from 80 to 110 PSIG in this experiment. This range allowed for adequate mass in the make-up tank to account for the vapor that would condense in the Dewar during the cooling sequence of the data collection process. Conversely, for a mixture that is not a pre-mixed gas, the individual mixture components were to be added separately.

The most practical way to arrive at the desired mixture concentration is to add the components to the test facility such that the partial pressure of each is approximately equal to the desired concentration. This will produce actual concentrations within five percent of the desired concentration, and smaller amounts of each component can be added until the desired concentration is achieved. It is a time consuming process that involves sampling the mixture in the test facility using the gas chromatograph as described above.

Considerations such as allowing the added gas to attain thermal equilibrium with the other gas components in the test facility and also the miscibility of the gas with the compressor oil were important. Though not an issue with the hydrocarbon mixtures, the fluorocarbon mixture concentration would be affected by the R14 and R134a being absorbed into the oil. As this mixture was created using individual high purity gases which were slightly miscible with the compressor oil, this mixture was measured using the gas chromatograph after running the compression station for approximately ten minutes. It was determined that the amount of gas absorbed into the

compressor oil was dependent on the pressure; therefore, the desired flow and pressure target values were used throughout the mixing process. Furthermore, if additional gas was required to be added to attain the desired concentration, the compression station was deactivated and the pressure allowed to equilibrate before adding the gases.

5 Discussion of Results

The actual test matrix describing the data collected for this research is shown in Table 5, and the additional binary hydrocarbon mixture collected is shown in Table 4. The conditions specified in the modified test matrix discussed in a previous chapter were investigated, but with slight adjustments. In the 0.5 and 3.0 millimeter size test sections, an additional run was added to investigate the effects of heat flux in all test section diameters, rather than only one test section. This presented an issue which would require another test matrix modification, as the power supply controlling the electrical current to the test section was not capable of attaining the higher heat flux value of 87 kW/m^2. It was determined that the desired effects could be investigated by using a value below the low heat flux value of 56 kW/m^2, by roughly the same factor as it should have been above. Furthermore, the undiluted hydrocarbon mixture being tested in the 1.5 millimeter test section used the lower pressure of 270 kPa as the other parameters were changed, as it was desired to test the lower pressure originally. After testing the effects of pressure, it was determined that it was less difficult to control the test section conditions at the higher pressure, and was therefore designated as the pressure for the control condition. Again, the text shown in red indicate the deviations from the control condition used in the 1.5 millimeter test section.

Table 4. Binary Mixture Test Matrix - Final Results

Mixtures *Concentration Effects*		**Test Section Inner Diameter** *Geometry Effects*		
		0.5 [mm]	1.5 [mm]	3.0 [mm]
40% 60%	Methane Ethane	P_1: 790 [kPa] q_1: 56 [kW/m^2] G_1: 144 [kg/m^2-s]	P_1, q_1, G_1 *Control Condition*	P_1 q_1 G_1
			P_2: 270 [kPa], q_1, G_1 *PuressureEffects*	
		P_1 q_2 G_1	P_1, q_2: 87 [kW/m^2], G_1 *Heat Flux Effects*	P_1 q_3: 39 [kW/m^2] G_1
			P_1, q_1, G_2: 240 [kg/m^2-s] *Mass Flux Effects*	

Table 5. Test Matrix - Final Results

Mixtures *Concentration Effects*		Test Section Inner Diameter *Geometry Effects*		
		0.5 [mm]	1.5 [mm]	3.0 [mm]
45% 35% 20% 0%	Methane Ethane Propane Nitrogen	P_1: 790 [kPa] q_1: 56 [kW/m^2] G_1: 144 [kg/m^2-s]	P_1, q_1, G_1 *Control Condition* P_2: 270 [kPa], q_1, G_1 *PuressureEffects*	P_1 q_1 G_1
		P_1 q_2 G_1	P_2, q_2: 87 [kW/m^2], G_1 *Heat Flux Effects* P_2, q_1, G_2: 240 [kg/m^2-s] *Mass Flux Effects*	P_1 q_3: 39 [kW/m^2] G_1
36% 28% 16% 20%	Methane Ethane Propane Nitrogen	P_1 q_1 G_1	P_1 q_1 G_1	P_1 q_1 G_1
27% 21% 12% 40%	Methane Ethane Propane Nitrogen	P_1 q_1 G_1	P_1 q_1 G_1	P_1 q_1 G_1
35% 15% 15% 35% 0%	R14 R23 R32 R134a Argon	P_1 q_4: 27 [kW/m^2] G_1	P_1, q_4, G_1 *Control Condition* P_2, q_4, G_1 *PuressureEffects*	P_1 q_4 G_1
		P_1 q_5 G_1	P_1, q_5: 39 [kW/m^2], G_1 *Heat Flux Effects* P_1, q_4, G_2 *Mass Flux Effects*	P_1 q_6: 18 [kW/m^2] G_1
28% 12% 12% 28% 20%	R14 R23 R32 R134a Argon	P_1 q_4 G_1	P_1 q_4 G_1	P_1 q_4 G_1
21% 9% 9% 21% 40%	R14 R23 R32 R134a Argon	P_1 q_4 G_1	P_1 q_4 G_1	P_1 q_4 G_1

Further issue resulted from selecting a lower mass flux, specifically in testing the 0.5 millimeter test section. The mass flow rate required was 0.029 gram per second, which was found to be below the measurement sensitivity of the coriolis mass meter. A calorimetric type, model FMA1820 manufactured by Omega was obtained and installed into the test facility upstream of

the coriolis meter. The meter needed to be calibrated for each mixture. It was known that the signal output voltage from the meter was linearly correlated with mass flow rate. Therefore, several measurements were taken at steady-state conditions using both the coriolis and new calorimetric meters.

The coriolis flow measurements were plotted against the calorimetric signal voltage measurements and a linear correlation was fit to the data points, which would provide the equation to calculate the flow rate from the calorimetric meter. As mentioned previously, the required flow rate for the data sets was lower than could be measured by the coriolis, but the linear relationship of the the calorimetric output signal voltage allowed for the meter to be calibrated against the coriolis at higher flow rates.

A data set showing the temperature sensor measurements is shown in Figure 71. The data was obtained using the hydrocarbon mixture with no dilution. The mixture was cooled to the liquid state, at which point it was heated to reach the desired pseudo steady-state condition until it reached the vapor phase. The three distinctly visible pairs of lines represent the inlet, outlet, and block temperatures of the test section. As expected, the inlet temperture is lowest, followed by the outlet and copper mass temperatures.

Though this plot does not show the heat transfer coefficient directly, the phase changes and magnitude of improvement in heat transfer can be demonstrated. The temperature region where the fluid changes phase from either vapor or liquid to two-phase was always clearly identifiable by a rapid change in the temperature of the copper mass on the test section. These increased temperature rate changes can be seen at either end of the plot. The phase change temperature was confirmed using the program REFPROP.

As the design of the test section utilized a highly conductive material heated by a constant heat flux, the difference in temperature between the fluid measured at the inlet and the copper mass can provide details on the heat transfer rate. The two-hase region clearly provides the best heat transfer, as can be deduced from the relatively small difference in temperatures. The y-axis interval is 5 Kelvin, showing a difference of approximately 48 Kelvin in the vapor region and 12 Kelvin at the point where the fluid is in the two-phase regime at the inlet and outlet of the test section. Using this information, it is expected that the heat transfer coefficient would be approximately four times greater upon entering the two-phase region.

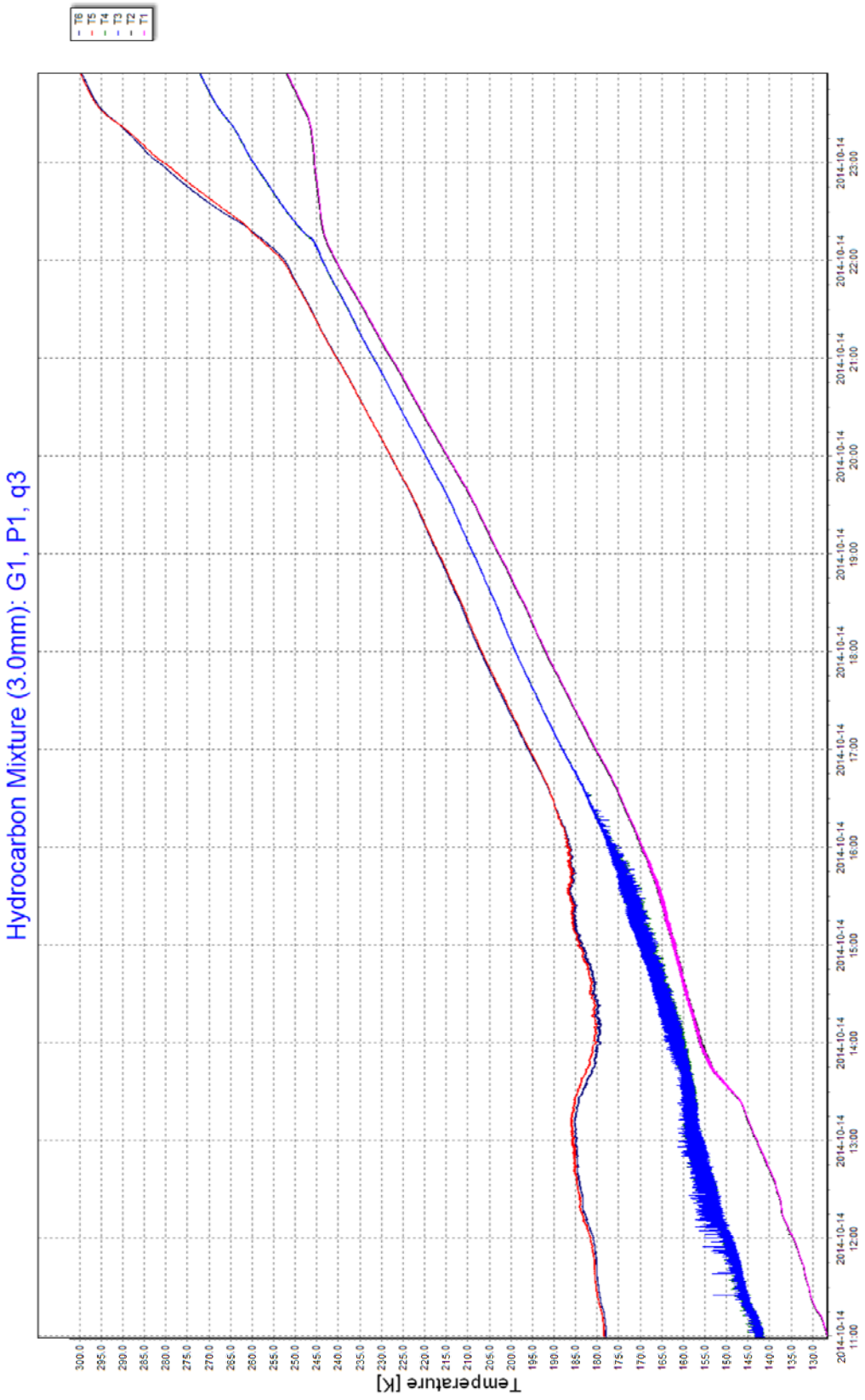

Figure 71. Temperature profile of hydrocarbon mixture from saturated liquid to vapor

The mixture concentration was measured for each data set specified in Table 4and Table 5, and plotted against the average of the inlet and outlet temperatures of the fluid flowing through the test section. Similar data sets were plotted together, such as the mixtures diluted to the same concentration with either Argon or Nitrogen for all test section diameters, or the same mixture with varying heat flux in a single test section diameter. The test parameters were labeled to match those shown in the test matrix in Table 4 and Table 5.

From the plots, it can be shown that the concentration of a particular mixture component in nearly all the data sets does not change more than 5%, with none changing more than 10% from the original concentration. It was expected that the concentration would change, due to the condensing or evaporating of the mixture components during the collection of a data set, in order of their respective dew points or boiling points. As a mixture component condenses to liquid, it reduces the volume of the gas phase in the test facility being measured by the gas chromatograph. The plots below demonstrate the significances of this phenomenon.

The parameters used in the gas chromatograph are summarized for each mixture in Table 6 for reference. These are the settings used to calibrate the gas chromatograph using the pure gases or certified mixtures. These are the settings chosen to provide the best separation of the gases in the column.

Table 6. Gas chromatograph measurement settings for each mixture

Mixture		Oven Temperature	Injector Temperature	Detector (TCD) Temperature	Column Head Pressure
		°C	*°C*	*°C*	*PSIG*
40% 60%	Methane Ethane	150	150	150	55-60
45% 35% 20%	Methane Ethane Propane	150	150	150	55-60
36% 28% 16% 20%	Methane Ethane Propane Nitrogen	35 for 7.5 min 50°C/min to 200 for 20 min	150	150	55-60
27% 21% 12% 40%	Methane Ethane Propane Nitrogen	35 for 7.5 min 50°C/min to 200 for 20 min	150	150	55-60
35% 15% 15% 35%	R14 R23 R32 R134a	130	150	150	55-60
28% 12% 12% 28% 20%	R14 R23 R32 R134a Argon	100 for 5 min 15°C/min to 130 for 20 min	150	150	55-60
21% 9% 9% 21% 40%	R14 R23 R32 R134a Argon	100 for 5 min 15°C/min to 130 for 20 min	150	150	55-60

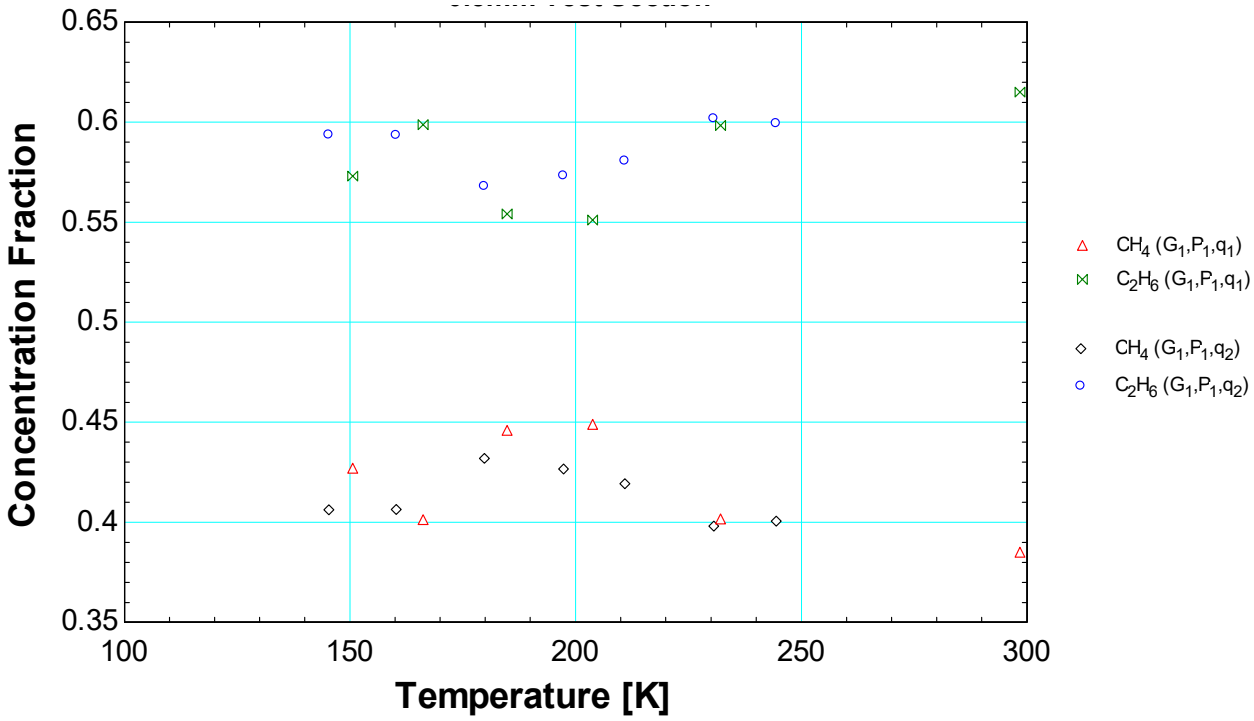

Figure 72. Molar concentration as a function of the average temperature of the fluid flowing through the 0.5mm test section for the binary mixture

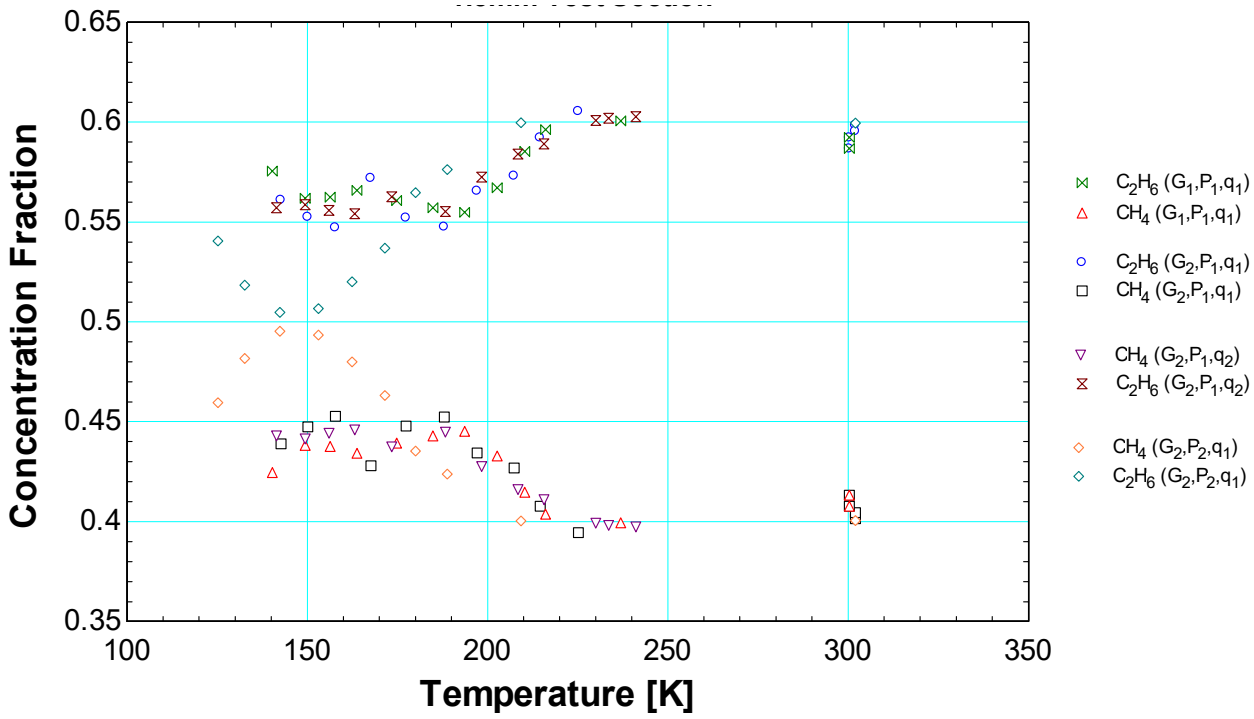

Figure 73. Molar concentration as a function of the average temperature of the fluid flowing through the 1.5mm test section for the binary mixture

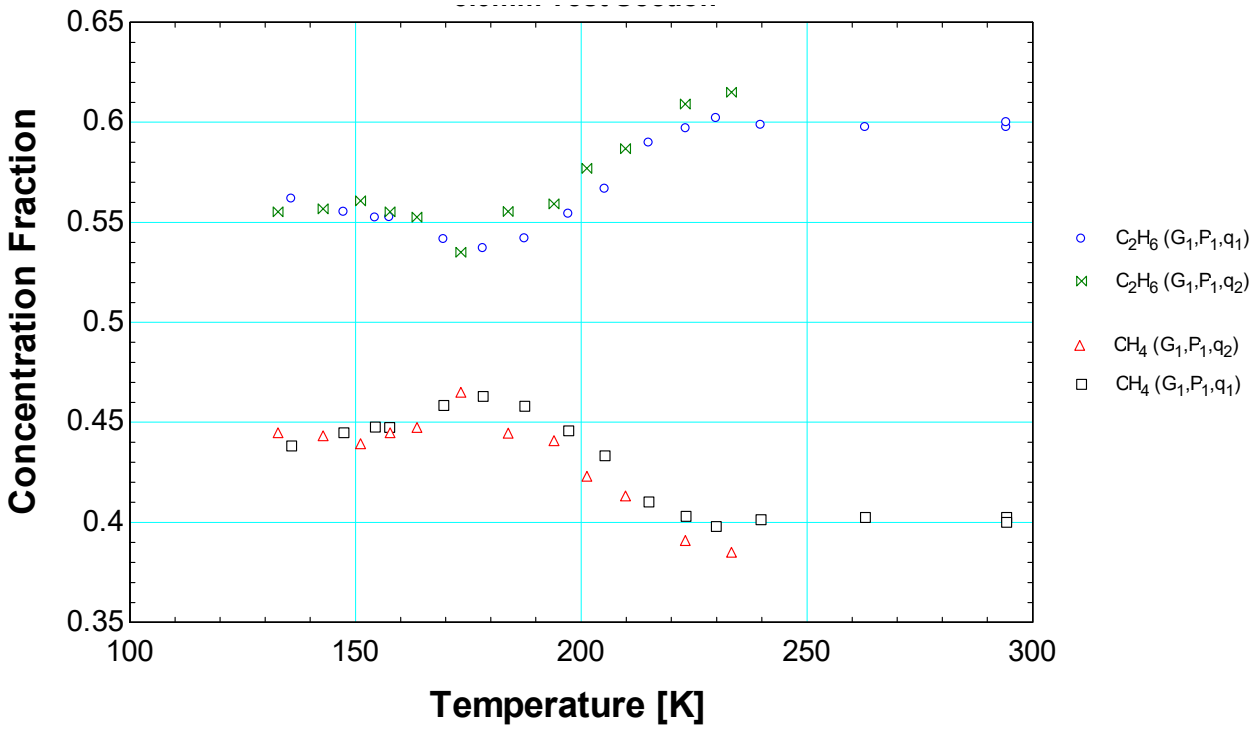

Figure 74. Molar concentration as a function of the average temperature of the fluid flowing through the 3.0mm test section for the binary mixture

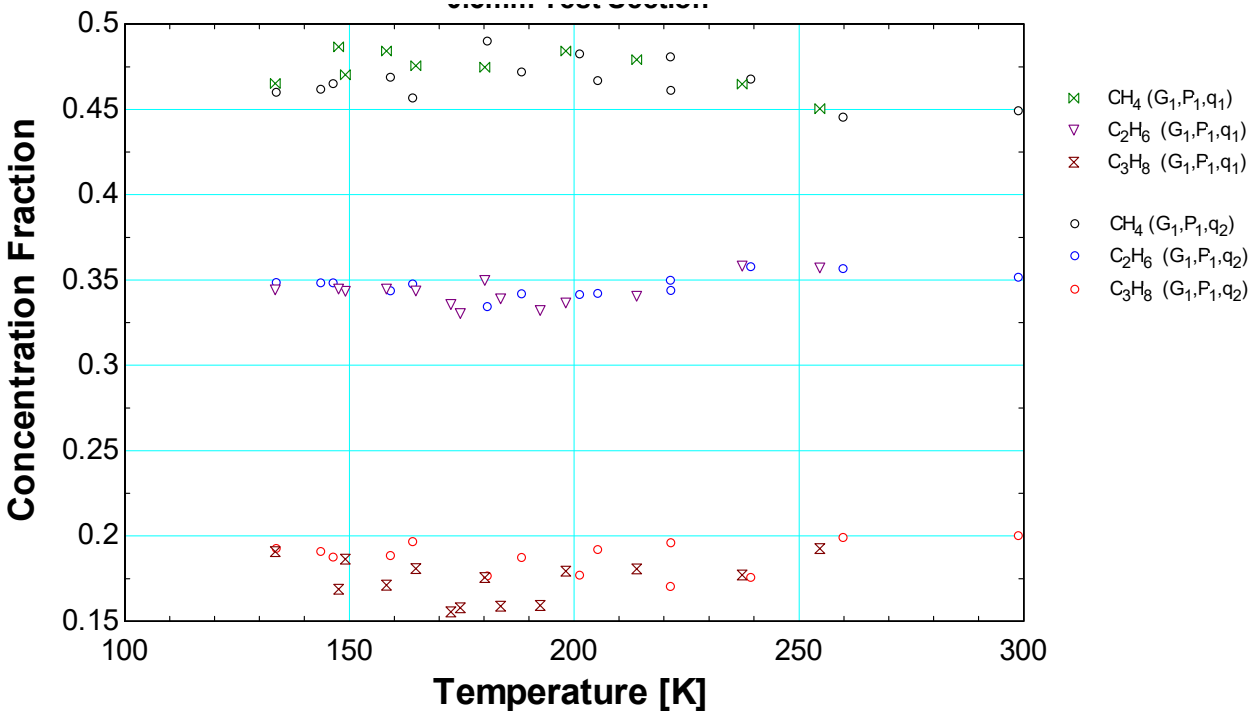

Figure 75. Molar concentration as a function of the average temperature of the fluid flowing through the 0.5mm test section for the hydrocarbon mixture

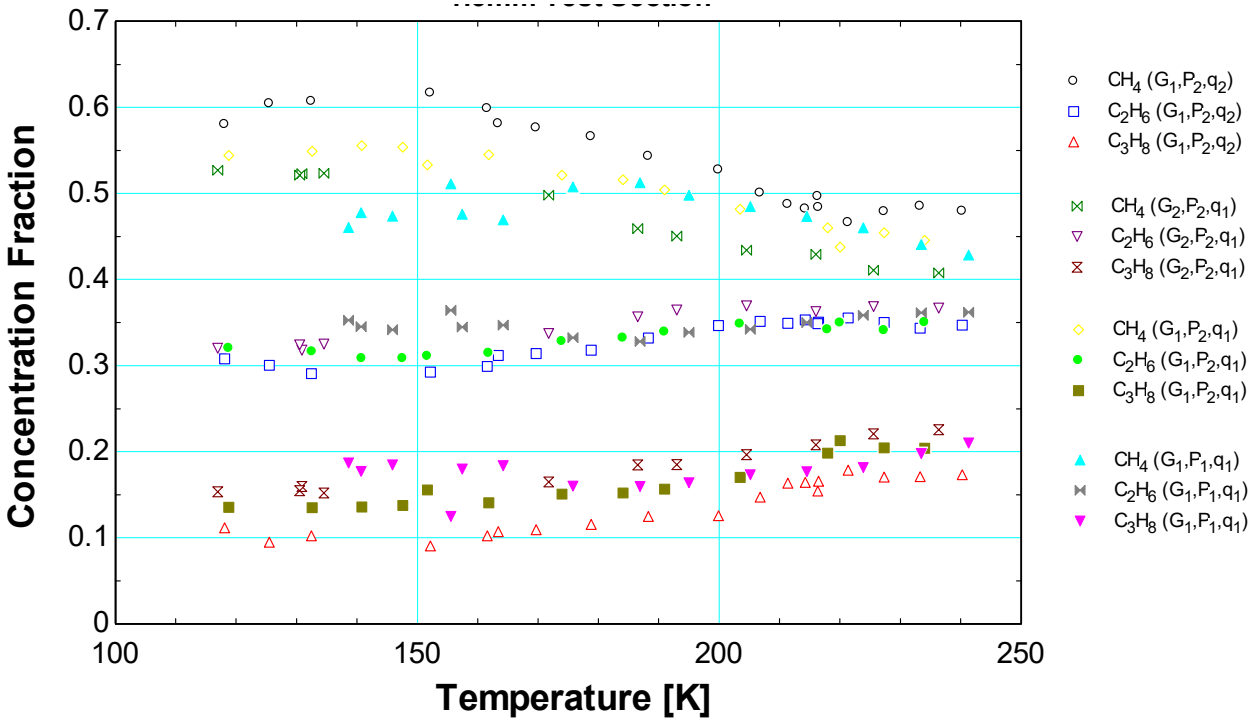

Figure 76. Molar concentration as a function of the average temperature of the fluid flowing through the 1.5mm test section for the hydrocarbon mixture

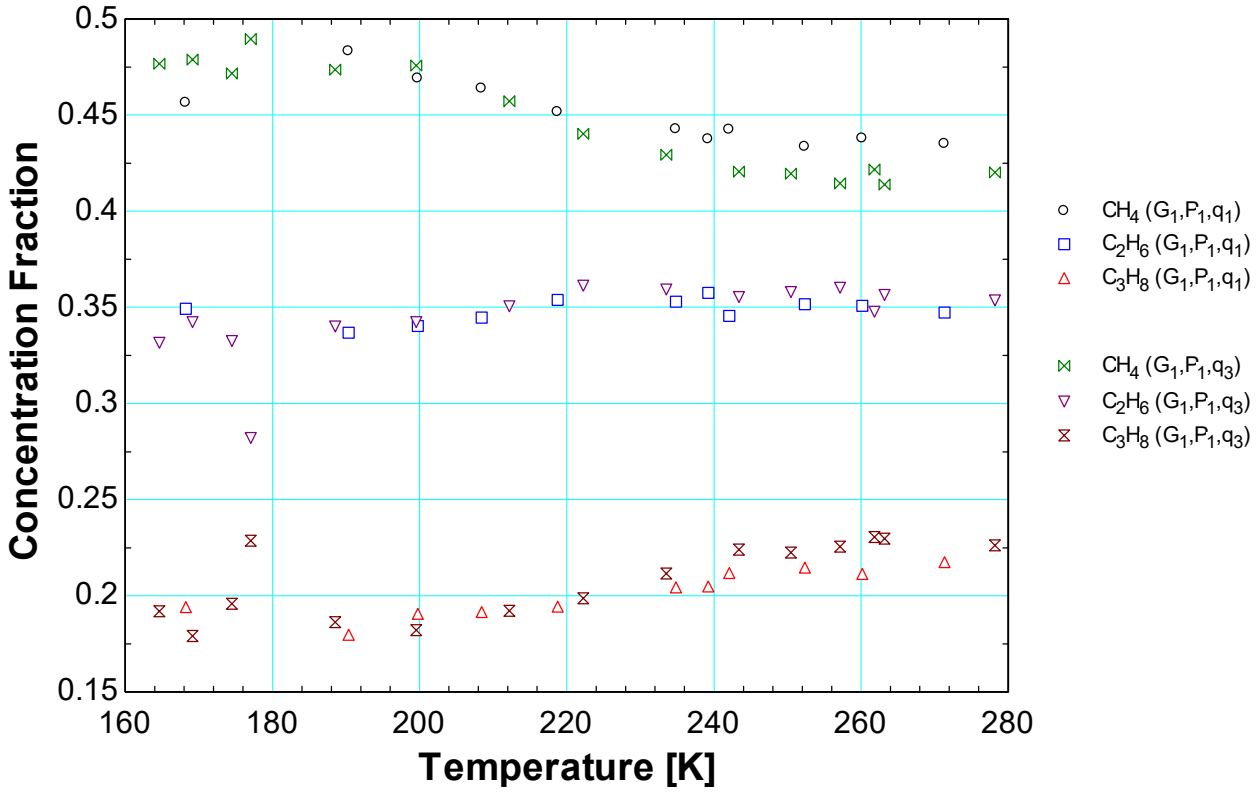

Figure 77. Molar concentration as a function of the average temperature of the fluid flowing through the 3.0mm test section for the hydrocarbon mixture

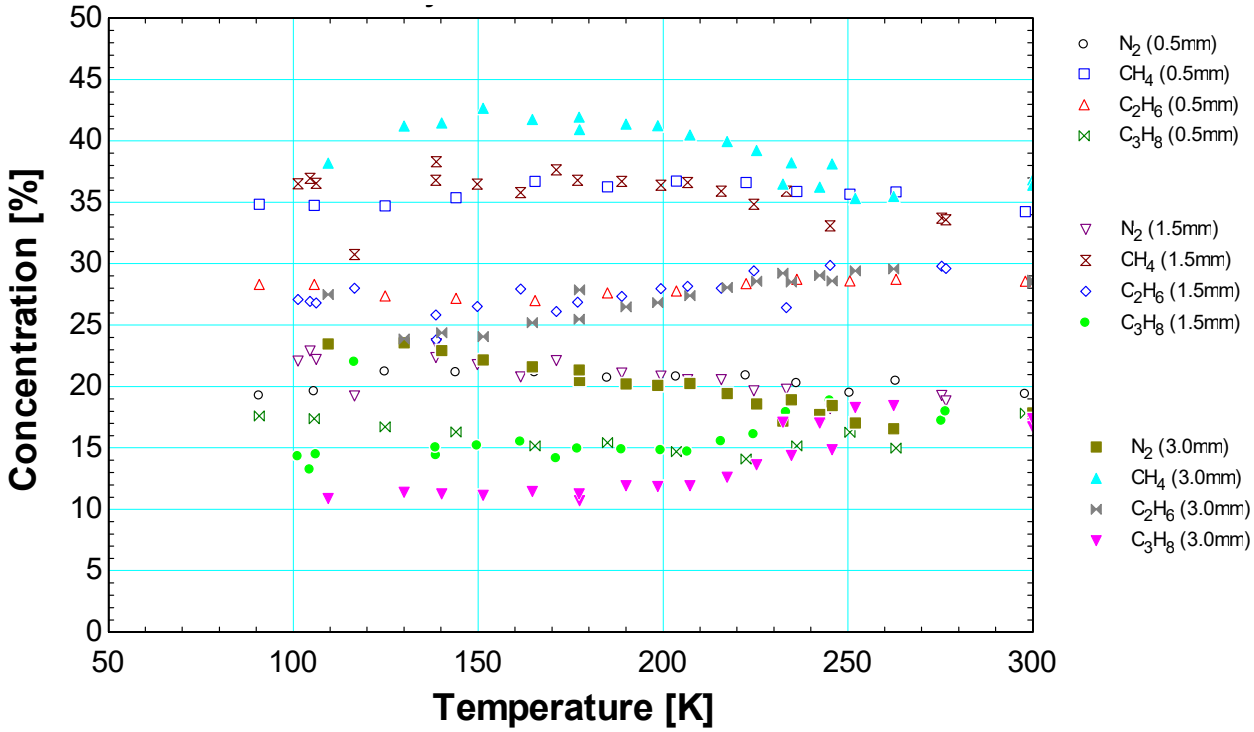

Figure 78. Molar concentration as a function of the average temperature of the fluid flowing through all test section diameters for the hydrocarbon mixture diluted with 20% Nitrogen

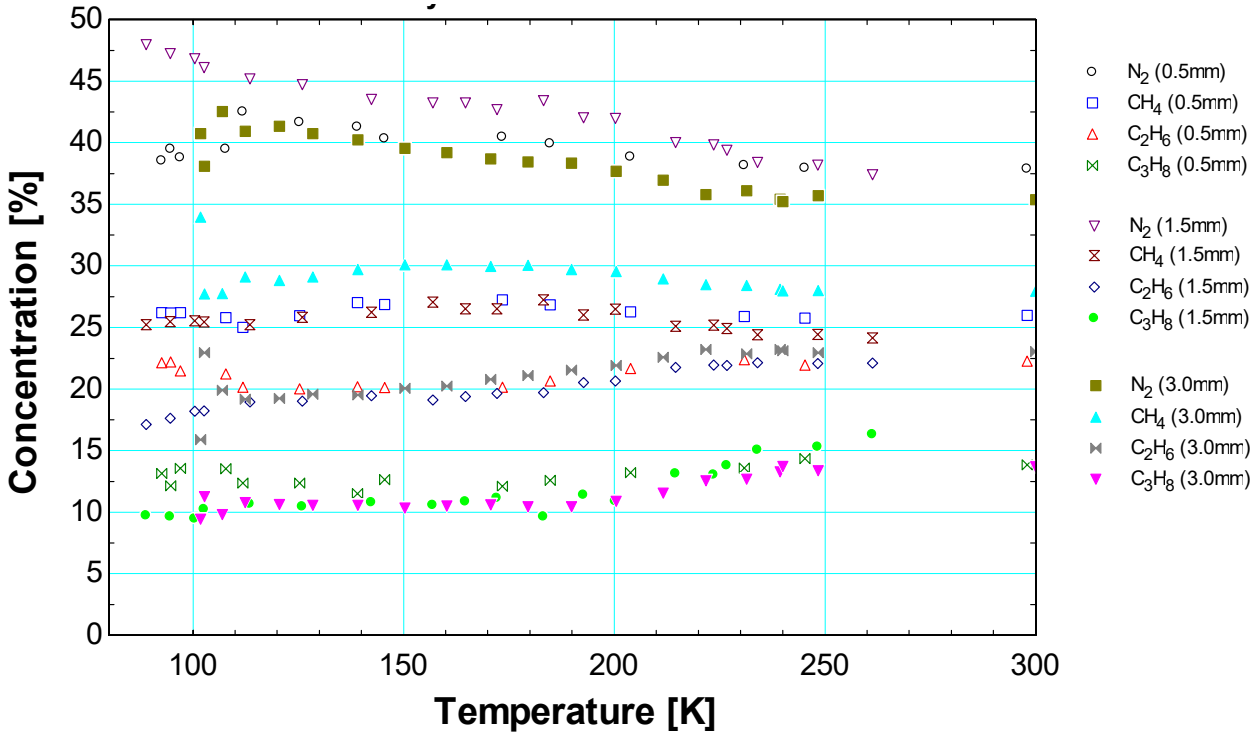

Figure 79. Molar concentration as a function of the average temperature of the fluid flowing through all test section diameters for the hydrocarbon mixture diluted with 40% Nitrogen

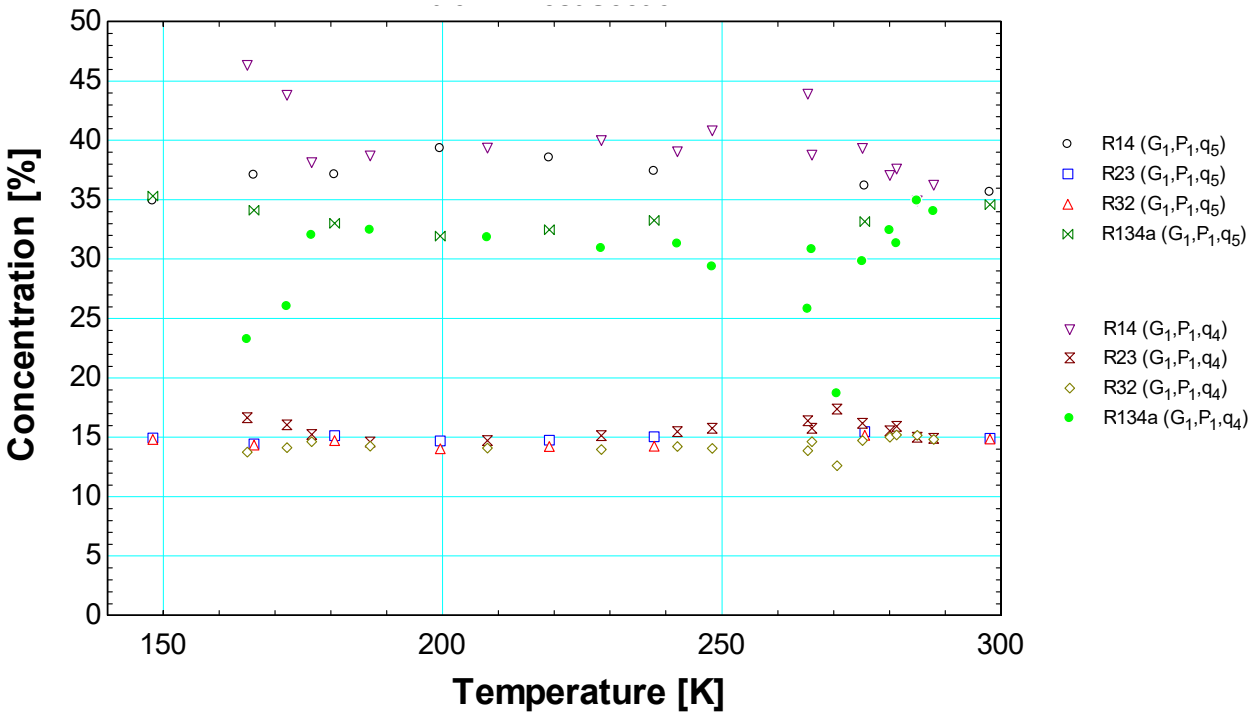

Figure 80. Molar concentration as a function of the average temperature of the fluid flowing through the 0.5mm test section for the fluorocarbon mixture

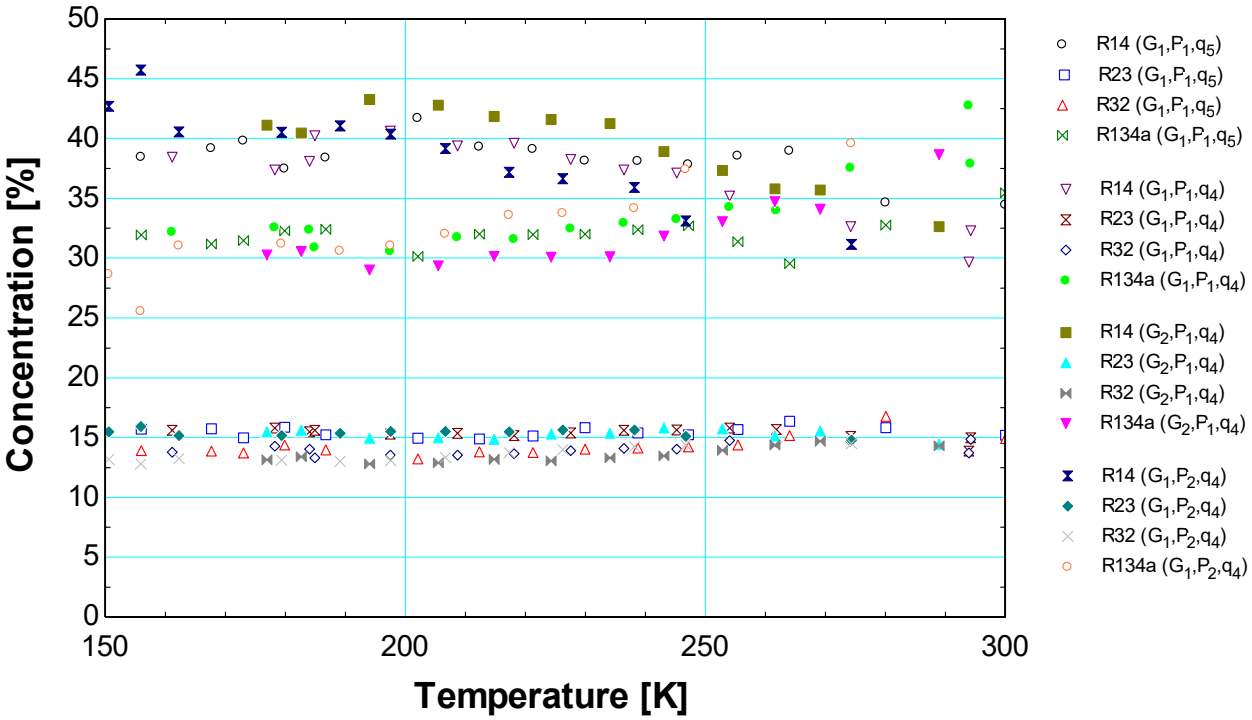

Figure 81. Molar concentration as a function of the average temperature of the fluid flowing through the 1.5mm test section for the fluorocarbon mixture

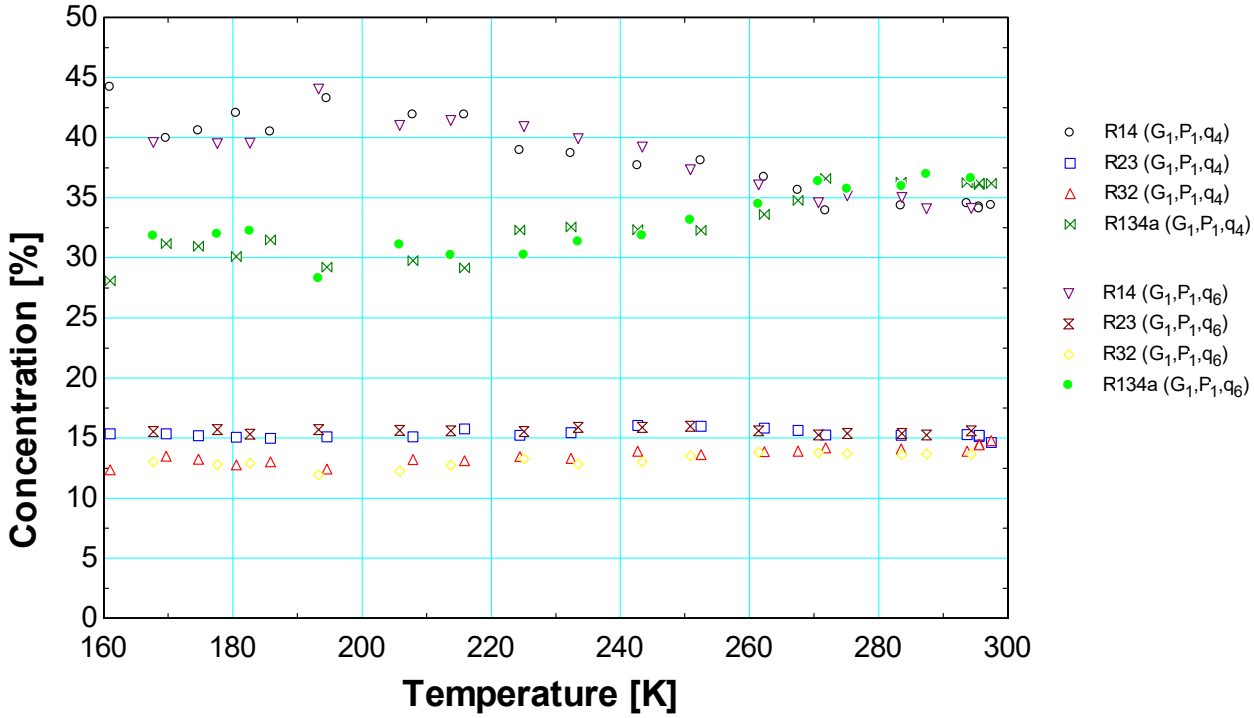

Figure 82. Molar concentration as a function of the average temperature of the fluid flowing through the 3.0mm test section for the fluorocarbon mixture

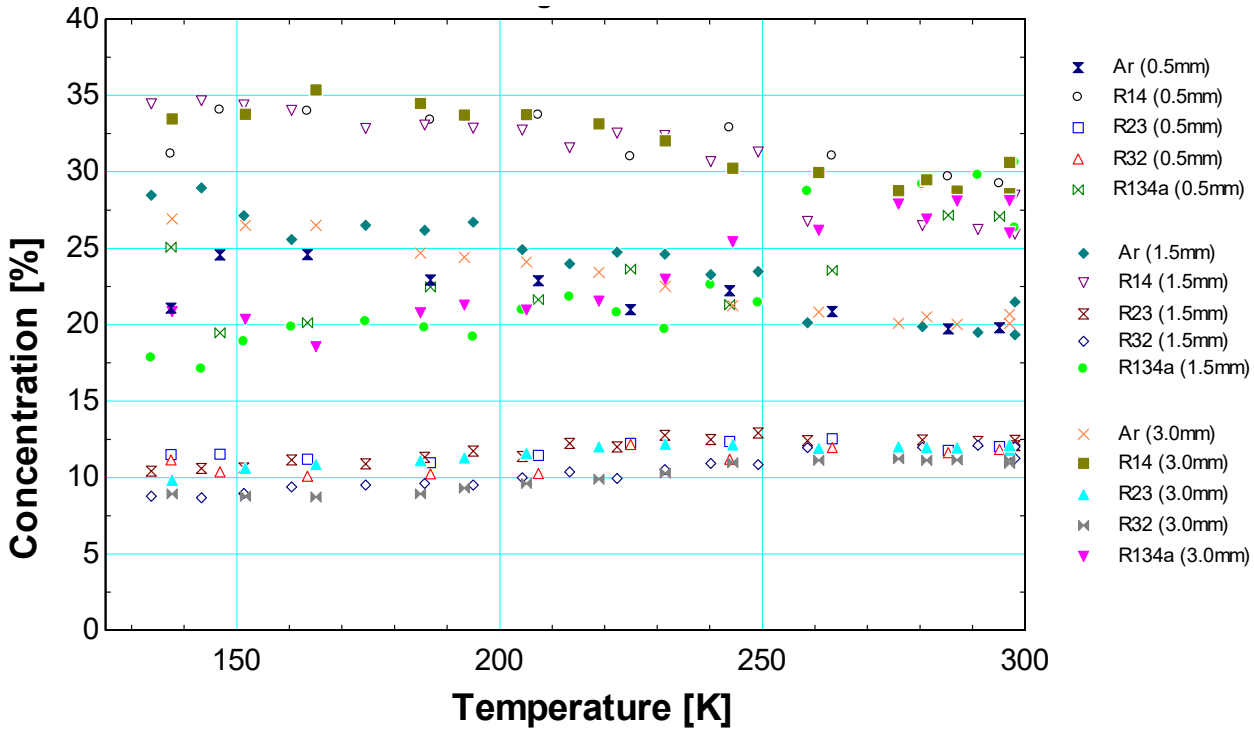

Figure 83. Molar concentration as a function of the average temperature of the fluid flowing through all test section diameters for the fluorocarbon mixture diluted with 20% Argon

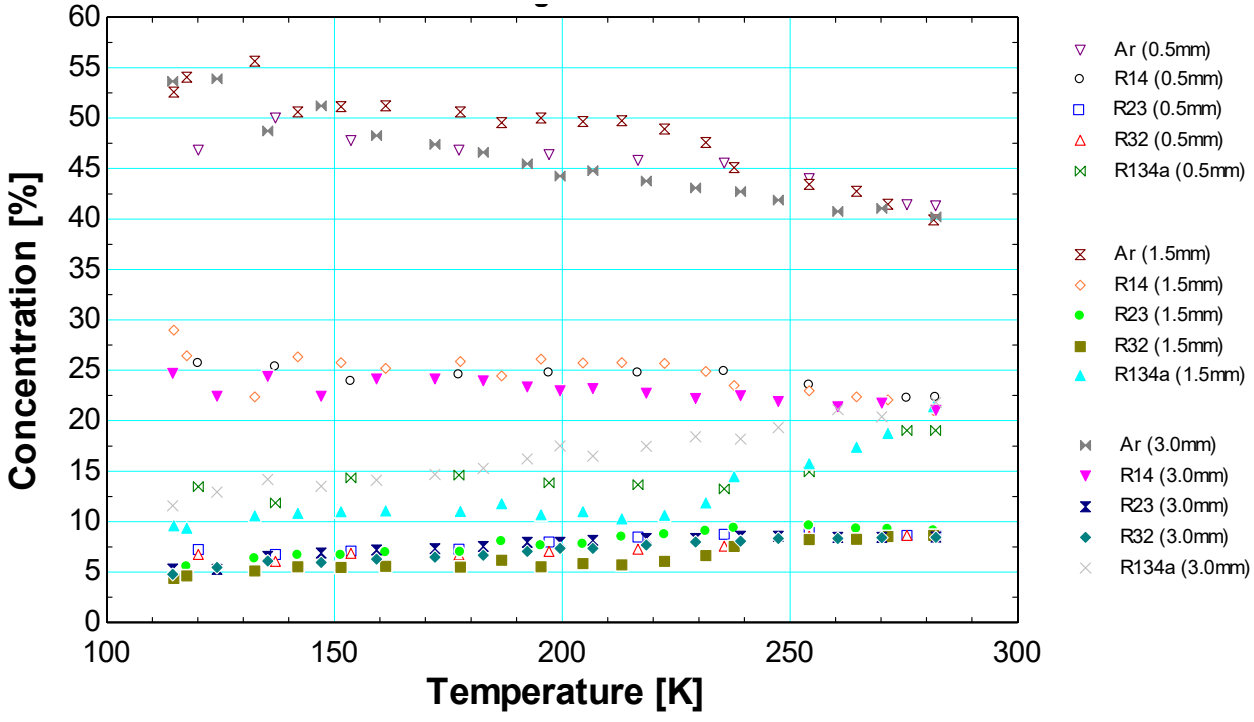

Figure 84. Molar concentration as a function of the average temperature of the fluid flowing through all test section diameters for the fluorocarbon mixture diluted with 40% Argon

6 References

Alfeev, V.N., Brodyanski, V.M., Yagodin, V.M, Nikolsky, V.A., Ivantsov, A.V., 1973, "Refrigerant for a Cryogenic Throttling Unit," UK Patent 1,336,892

Boiarski, M., Khatri, A., Kovalenko, V., 1999, "Design Optimization of the Throttle-Cycle Cooler with Mixed Refrigerant," *Cryocoolers 10*, R.G. Ross, ed., Kluwer Academic/Plenum, pp.789-797.

Gong, M.Q., Wu, J.F., Luo, E.C., Qi, Y.F., Hu, Q.G., Zhou, Y., 2001, "Study on the Overall Heat Transfer Coefficient for the Tube-In-Tube Heat Exchanger used in Mixed-Gases Coolers," Advances in Cryogenic Engineering, Vol. 47A, pp.1483-1490

Hughes, C., "Experimental Measurement of Heat Transfer Coefficients for Mixed Gas Working Fluids in Joule-Thompson Systems", MS Thesis, 2004

Jung, D.S., McLinden, M., Radermacher, R., Didion, D., 1989, "Horizontal flow boiling heat transfer experiments with a mixture of R22/R114," *International Journal of Heat and Mass Transfer*, Vol. 32, No. 1, pp. 131-145.

Kattan, N., Thome, J.R., Favrat, D., 1998, "Flow Boiling in Horizontal Tubes: Part 2 – New Heat Transfer Data for Five Refrigerants," *Journal of Heat Transfer*, Vol. 120, pp.148-155.

Keppler, F, Nellis, G., and Klein, S., 2004, "Optimization of the Composition of a Gas Mixture in a Joule-Thomson Cycle", *International Journal of Heaving, Ventilating, Air-Conditioning, and Refrigerating Research*, Vol. 10, No. 2, pp. 213-230.

Klein, S.A., Nellis, G.F., Thermodynamics, Cambridge, New York, 2012

Appendix

A. Test Section Design Thermal and Fluid Analysis (Barraza)

The parameters used in the CFD model are shown in Table 7**Error! Reference source not found.**.

Table 7. Parameters used in the CFD model

Fluid temperature	200 K
Density (r)	55.5 kg/m^3
Specific heat (c)	1200 J/kg-K
Thermal conductivity (k)	0.0207 W/m-K
Viscosity (m)	2.156×10^{-5} Pa-s
Prandtl number	1.26
Reynolds number	35000

The geometry used in the CFD model is shown in Figure 85.

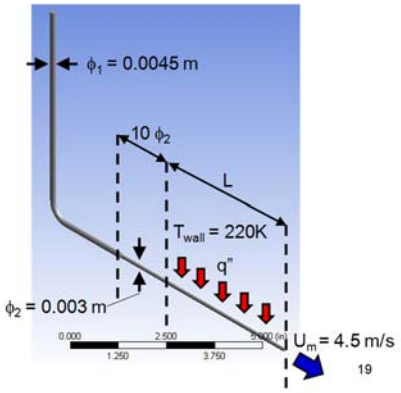

Figure 85. Setup CFD model in Ansys

Hydro dynamic flow is considered fully developed when the wall shear stress is constant. One of the results of the CFD model is shown in Figure 86. This figure shows clearly a constant shear stress, fully developed condition, before a length of ten (10) inner diameters.

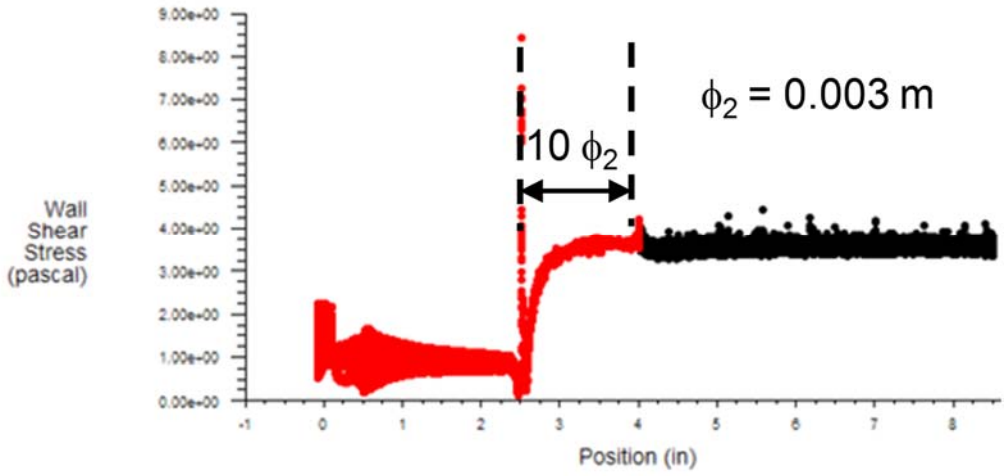

Figure 86. Results of Ansys model, wall shear stress as a function of length

When the flow enters the copper block, it is exposed to a heat load that is applied by a nichrome wire installed on the outer surface of the copper block. The wall temperature is constant due to the high conductivity and large cross-sectional area of the copper. Consequently, a thermal boundary layer appears and grows. When the boundary layer begins to grow, the local Nusselt number is large, and it subsequently decreases as the thermal boundary layer grows. When the local Nusselt number approaching a constant value, it indicates that, the flow has achieved a fully developed thermal condition. This phenomenon is studied using the same CFD model described in Figure 85 and Table 7. The local Nusselt number is shown in Figure 89 as a function of the length of the copper block. The thermal fully developed condition is achieved before 15 inner diameters.

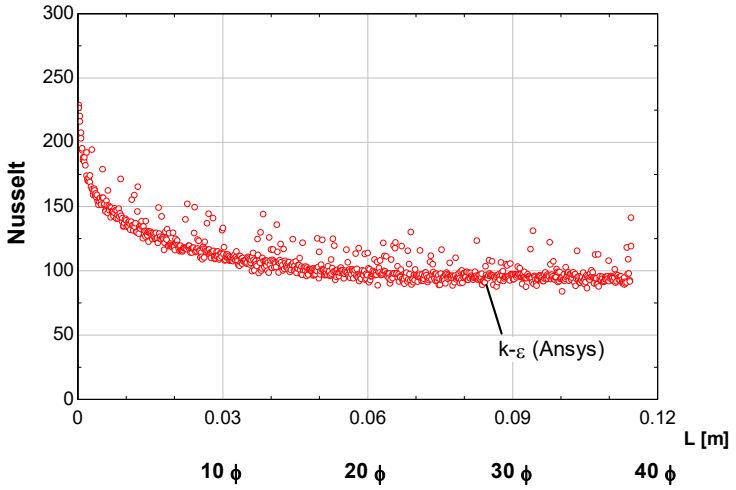

Figure 87. Results of Ansys model, Nusselt as a function of length

The CFD model is validated against a mixing length model and also the Dittus-Boelter correlation. Both the CFD model and the mixing length model describe a hydro dynamically fully developed flow exposed to heating in a constant temperature wall pipe. The mixing length model is a 2D eddy diffusivity of momentum model that uses the Spalding velocity profile as described by Nellis and Klein (2009). The Dittus-Boelter (Incropera et al., 2002) correlation is shown in Equation 2, and it gives the local Nusselt number for a turbulent thermal and hydro dynamically flow.

$$\text{Nusselt} = 0.023\ \text{Re}^{0.8}\ \text{Pr}^{0.4} \qquad (2)$$

Figure 88 shows the comparison of the results between these three approaches. The mixing length model shows good agreement with the CFD model. It has the same trend, but the Nusselt numbers predicted by the mixing length model are greater than CFD model. The Dittus-Boelter correlation matches with the CFD model when the flow is thermal fully developed.

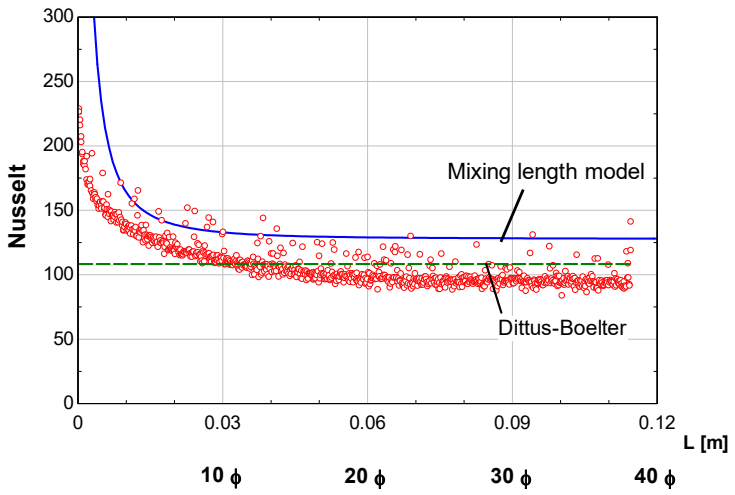

Figure 88. Comparison between CFD model, mixing length model, and Dittus-Boelter

The average heat transfer coefficient is measured in the test facility. However, we are trying to determine the local heat transfer coefficient. The local heat transfer coefficient is large at the beginning of the heating zone, and decreases up to the point where it achieves a thermal fully developed condition. Consequently, there is a difference between the actual average and the local heat transfer coefficient that we are attempted to measure because of the influence of the developing zone. The difference is called an error in this report and is quantified using the following equation.

$$\text{Error} = \frac{\text{Nusselt}_{\text{avg}} - \text{Nusselt}_{\text{local}}}{\text{Nusselt}_{\text{local}}} \qquad (3)$$

The local and average Nusselt number and the difference (error) between them as a function of the length of the copper block is shown in Figure 89. A difference (error) of 10% is observed when the length is 35 inner diameters.

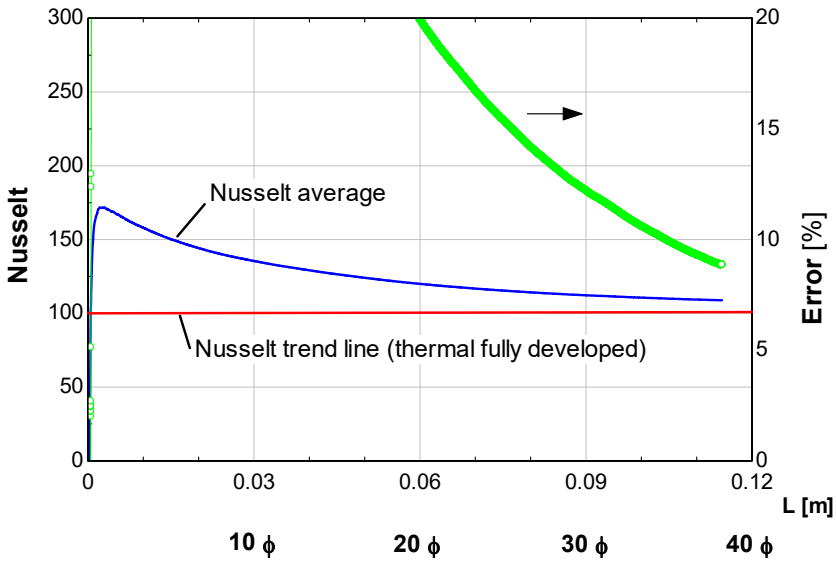

Figure 89. Local and average Nusselt number and error as a function of the length of the heating section

The final design of the test section is shown. This final design takes into account the dimensions that allows both a hydro-dynamic and thermal conditions to be fully developed, and a difference lower than 10% between the local heat transfer coefficient (that we wish to measure) and the average Nusselt number (that we actually measure).

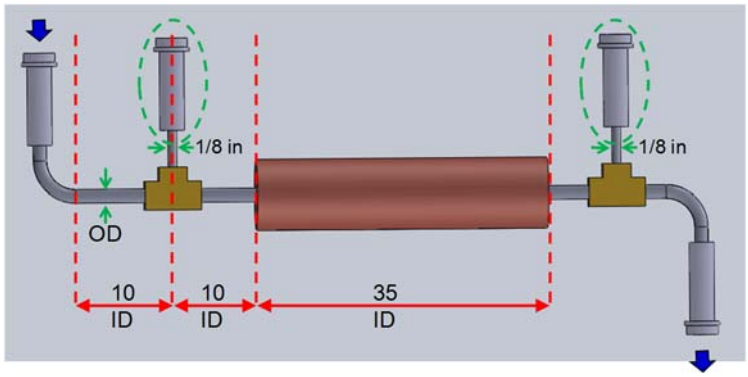

The heat load is limited by the desire to keep nearly constant fluid properties between the inlet and the outlet of the test section in order to measure the local heat transfer coefficient.

B. PRT calibration (Barraza)

PRTs exhibit a known relationship between the resistance across the PRT and their temperature. This relationship is given by the standard curve proposed by Callendar – Van Dusen's (Sostmann and Tavener, 1990).

$$\frac{R_{St}(T)}{R_0} = 1 + 3.9083 \cdot 10^{-3}\ \mathrm{T} - 5.775 \cdot 10^{-7}\ \mathrm{T}^2 \quad (4)$$

(Above 273.15 [K])

$$\frac{R_{St}(T)}{R_0} = 1 + 3.9083 \cdot 10^{-3}\ \mathrm{T} - 5.775 \cdot 10^{-7}\ \mathrm{T}^2 - 4.18301 \cdot 10^{-12}\ \mathrm{T}^3\ (\mathrm{T} - 100\ [\mathrm{C}]) \quad (5)$$

(Below 273.15 [K])

where the reference resistance (R_0) is 100 [ohm], and the temperature (T) is in degrees Celsius. The PRTs are calibrated using a two point calibration. The reference temperatures to carry out the calibration are the saturation temperature of the liquid nitrogen (77.1 K @ 98 kPa), and the freezing point of water (273.15 K). The freezing point is obtained with an ice water bath using distilled water for the water and the ice. Lakeshore, claims an accuracy of 0.25 K using the same calibration technique (Lakeshore, 2013).

The two point calibration takes advantage of the fact that the difference between the voltages measured at two temperatures by an uncalibrated PRT exhibits a linear relationship with the voltage that is provided by the standard curve at the same these two temperatures. Consequently, if we measure the voltage for two known temperatures, we are able to measure a third temperature with accuracy of 0.25 K.

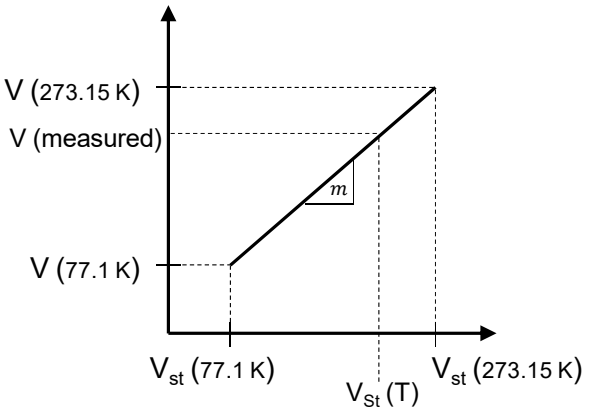

Figure 90. Linearity of voltage difference in PRTs

So, the temperature is obtained from the following expression

$$V_{St}(T) = \frac{V(T) - [V(T_1) - m\, V_{St}(T_1)]}{m} \quad (6)$$

where the slope (m) is defined as

$$m = \frac{V(T_2) - V(T_1)}{V_{St}(T_2) - V_{St}(T_1)} \quad (7)$$

where T_1 is the saturation temperature of nitrogen (77,10 K at an atmospheric pressure of 98.26 kPa (737 mmHg)), T_2 is the freezing point of water (273.15 K), V_{St} is the voltage obtained from the standard curve for PRT, and V is the actual measured voltage. V_{St} is obtained by calculating the standard resistance from the standard curve (equation 5), and using Equation 8

$$V_{St}(T) = I\, R_{St}(T) \quad (8)$$

where the current (I) through PRTs is equal to 0.3 mA.

C. Heat leak (Barraza)

Radiation losses and insulation

The radiation losses related with the cryocooler, the test section, the pipes, and the fittings without any insulation is 18.9 W assuming an operating temperature of 150 K in the test section and an ambient temperature of 300 K. The effect of adding layers of multi-layer insulation (MLI) enclosing these sections is shown in the next Figure. The MLI provides a high radiation resistance due to its low emissivity ($\varepsilon \approx 0.05$). Heat transfer by conduction through the contact between MLI layers is avoided placing dacron netting between them. The installation of five MLI layers reduces the radiation losses by about 95%.

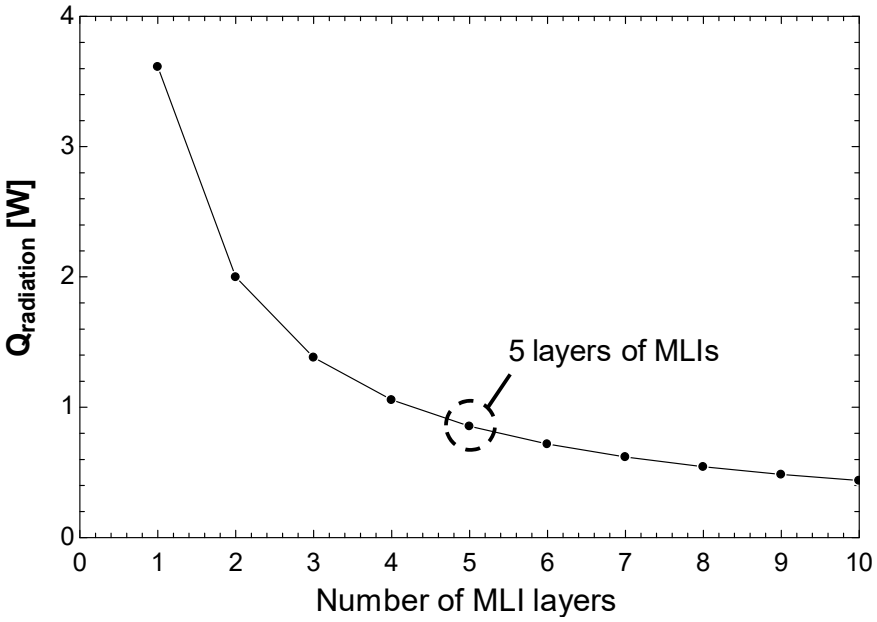

Figure 91. Heat leak by radiation as a function of number of MLI layers

The thermal resistance network used to calculate the radiation losses is shown in the following figure.

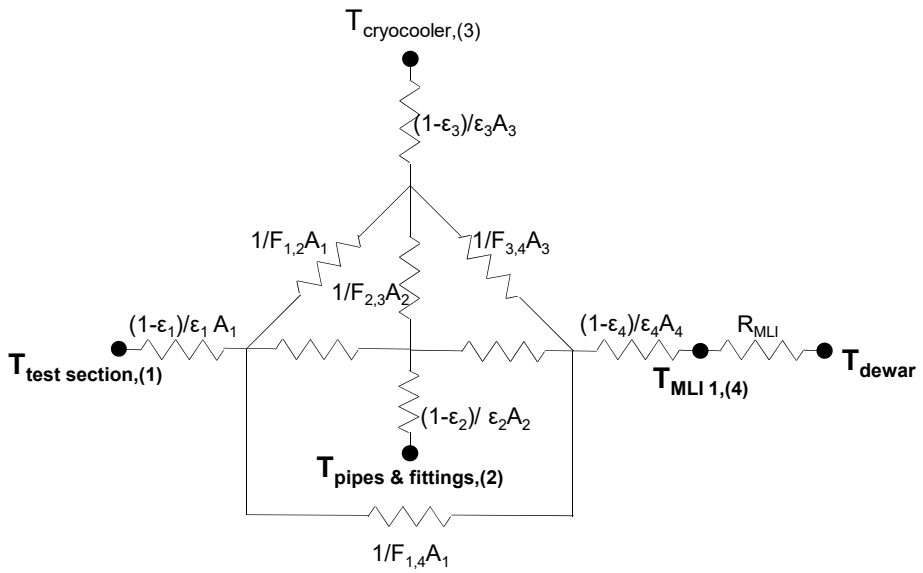

Figure 92. Thermal resistance network

where F are the shape factors, A is the surface area, ε is the emissivity of the surface, and R_{MLI} is the MLI thermal resistance. The MLI thermal resistance is calculated using the following thermal resistance network.

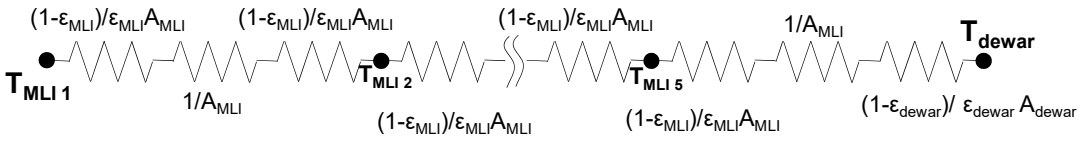

Figure 93. MLI thermal resistance network

The heat leak by radiation is calculated using the following expression

$$Q_{radiation} = \frac{\sigma \left({T_{dewar}}^4 - {T_{test\ section}}^4\right)}{R_{Total}}$$

where σ is the Boltzmann constant, and the R_{Total} is the total resistance. R_{Total} is calculated from the thermal resistance networks. The MLI layers installed in the test facility are shown.

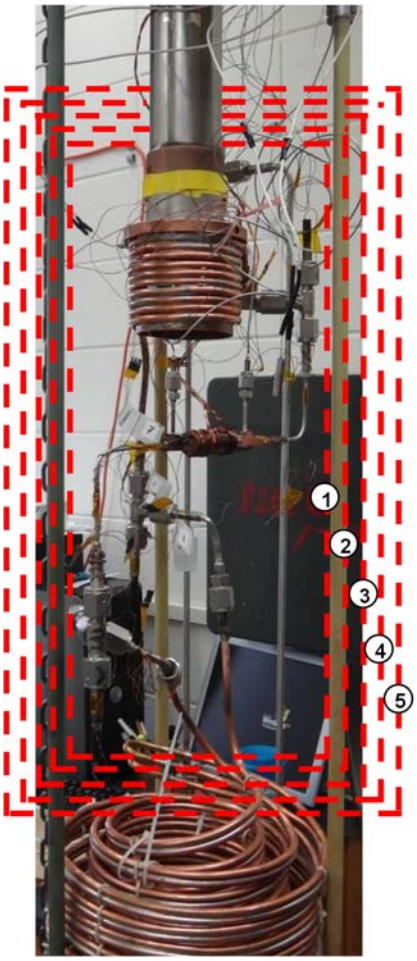

Figure 94. Graphical representation of MLI surrounding test section

Conduction

There is also heat leak (Q_{leak}) by conduction in the stainless steel pipe, heater wires, and PRTs wires. One way to measure this heat leak is to perform a no-flow test. This test is carried out by evacuating the inside (tube side) and outside (Dewar side) of the test section, and applying a small heat load ($Q_{applied}$) in the copper block. When the copper block reaches steady state, the thermal resistance (R_{leak}) between the test section and its surroundings due to conduction is calculated. R_{leak} is defined as:

$$R_{leak} = \frac{(T_{block} - T_{amb})}{Q_{leak}}$$

where T_{block} is the measured copper block temperature, and T_{amb} is the ambient temperature. The heat leak (Q_{leak}) by conduction is found from the energy balance in the copper block.

$$Q_{leak} = Q_{applied} - Q_{radiation} - Q_{transient}$$

The transient heat ($Q_{transient}$) due to the rate of change in the internal energy (U) in the copper block is defined as follow:

$$Q_{transient} = \frac{dU}{dt} = m\,c\,\frac{dT}{dt}$$

where m is the copper block mass, c is the copper specific heat, and dT/dt is the rate of change of the copper block temperature

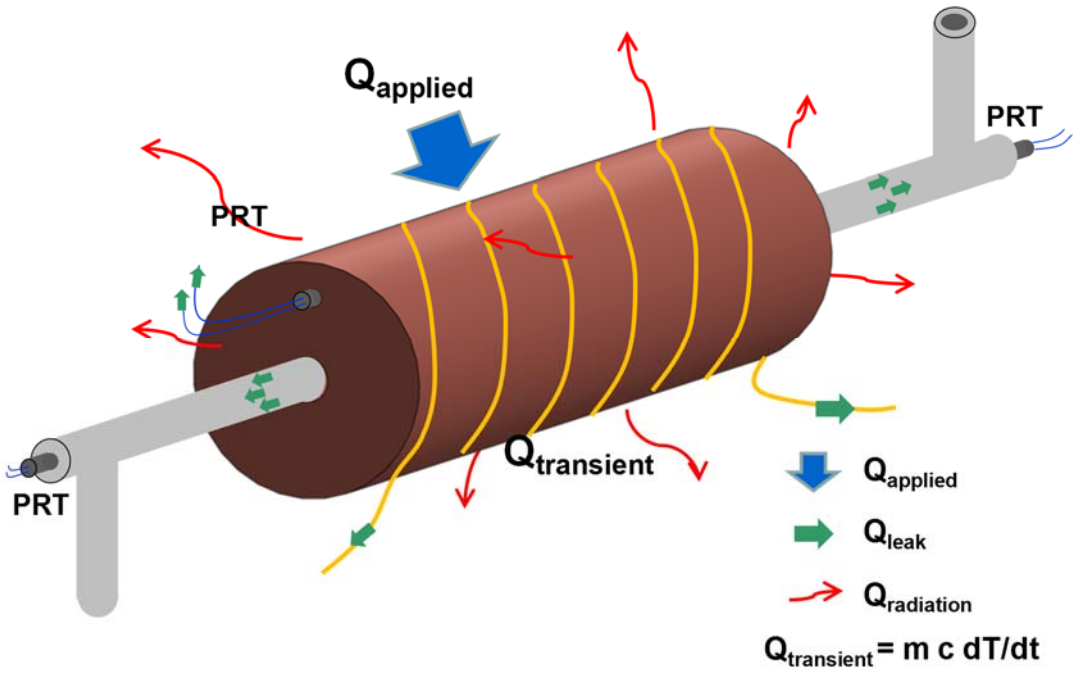

The test was carried out supplying 0.08, 0.16, and 0.24 W of heat load ($Q_{applied}$). The thermal resistance due to the heat leak by conduction (R_{leak}) is determined to be 100 K/W.

D. Equipment List

Table 8. Equipment list of modified test facility

Component ID #	Manufacturer	Part #	Description
CP-1,2	Danfos	SC18CLX.2	Compressor, 1-phase, 60Hz, 120VAC
FT-1	Endress & Hauser	83A02-ASVWAAAABABA	Coriolis mass flow meter
FT-1 (substitute)	Omega	FMA1820	Calorimetric mass flow meter, 0-10 SLPM, 1/4" compression
HX-1	Lytron	6320G3 BD	Heat exchanger, tube-and-fin type
SEP-1,2,3,4	Temprite	Model 320	Coalescing oil separator
V-11,12,13,14,15,20,21	Swagelok	B-1RF4	Needle valve, regulating type, 1/4" FNPT, brass body
V-22	Swagelok	SS-1RF4	Needle valve, regulating type, 1/4" FNPT, stainless steel body
V-18	Swagelok	B-1RF2	Needle valve, regulating type, 1/8" FNPT, brass body
V-1,2,3,4,5,6,7,8,9,10	Swagelok	SS-43GVCR4	Ball valve, 1/4" male VCR, Stainless body
V-23	Swagelok	SS-42VCR4	Ball valve, 1/4" male VCR, Stainless body
V-16,17	Swagelok	SS-MGVR4	Needle valve, regulating type, 1/4" male VCR, medium flow
V-19	Swagelok	SS-4MG-VCR-MH	Needle valve, regulating type, 1/4" male VCR, medium flow, micrometer handle
PCV-1	Swagelok	SS-HFM3B-VCR4-P	Pressure regulator, 0-150 PSIG spring range
PRV-1	Parker	637B-4-1/4-2	Pressure relief valve, brass body, soft seat
PI, Pid, Pis	Wika		Pressure gauge, -30 in Hg to 200 PSIG or 300 PSIG
Pix	Wika		Pressure gauge, 0-200 PSIG, 4.5" dial face, liquid filled
	Manchester Tank		1 US Gallon ASME pressure vessel, carbon steel construction
	Manchester Tank		4.5 US Gallon ASME pressure vessel, carbon steel construction
	Cryomech	AL-125, CP640	Cryocooler coldhead and compressor
T-1,2,3,4,5,6	Lakeshore Cryogenics	PT-103	Platinum resistance thermometer
P2	Setra	204	Pressure sensor, 0-250 PSIA range
dP3	Setra	204D	Differential pressure sensor, 0-25 PSI differential
dP1,dP2	Omega	MMDDU030V5P3B0T3A5CE	Differential pressure sensor, 0-30 PSI differential
	Hewlett Packard	5890 Series II	Gas chromatograph
	Hewlett Packard	HP3396A	Integrator

E. Gas Chromatograph – EES Codes for Concentration

```
"!GC Response/Correction Factors"
"Oven Temp @ 150C, Injector @ 150C, Detector @ 150C"

{date_test$='6/21/13'}

T_avg = (T_in + T_out)/2

A_C2H6_pure = (4125653+4193102+4183974+4225955+4209946)/5
A_CH4_pure = (2651266+2685949+2687589)/3

M_CH4 = area_CH4/A_CH4_pure/(area_CH4/A_CH4_pure + area_C2H6/A_C2H6_pure)
M_C2H6 = area_C2H6/A_C2H6_pure/(area_CH4/A_CH4_pure + area_C2H6/A_C2H6_pure)
```

```
"Mixture Concentration"
"Temperature Program used in GC"
"35C for 7.5 min, ramp 50C/min to 200C, final time of 20 min"
"Oven, Injector, and Detector @ 150C for undiluted hydrocarbons"

dilution$ = 'yes'
"Date of Test"
{date_test$='6/21/13'}

"Pressure and Average Temp of Sample"
{P_abs = (P + 14.7 [psi]) * convert(psi,kPa)}
T_avg = (T_in + T_out)/2

$IF dilution$ = 'yes'
"Pure Nitrogen - with temperature program - February 7, 2015"
A_N2_pure = (2377998+2387365+2386709+2409914+2420878+2432864+2427776+2390126)/8

"Molar Concentration of Hydrocarbon Mixture"
mole%_CH4 = 45
mole%_C2H6 = 35
mole%_C3H8 = 20

"Calculations"
{N2% = A_N2/A_N2_pure*100}                    "used to solve for nitrogen response factor"
N2% = RF_N2*A_N2/A_tot*100
CH4% = RF_CH4*A_CH4/A_tot*100
C2H6% = RF_C2H6*A_C2H6/A_tot*100
C3H8% = RF_C3H8*A_C3H8/A_tot*100

As_CH4 = (972839+901382+964561+921760+914084+909594+948740)/7
As_C2H6 = (1456894+1415092+1414923+1435844+1377532+1411146+1434694)/7
As_C3H8 = (1238283+1261334+1127607+1262492+1137051+1232260+1207409)/7

As_tot = As_CH4 + As_C2H6 + As_C3H8

A_tot_raw = A_N2 + A_CH4 + A_C2H6 + A_C3H8    "uncorrected areas from integrator"
A_tot = A_N2*RF_N2 + A_CH4*RF_CH4 + A_C2H6*RF_C2H6 + A_C3H8*RF_C3H8

RF_N2 = RF_C2H6*(As_C2H6/A_N2_pure)/(mole%_C2H6/100)
RF_CH4 = mole%_CH4*(As_tot/As_CH4)/100        "methane response factor"
RF_C2H6 = mole%_C2H6*(As_tot/As_C2H6)/100     "ethane response factor"
RF_C3H8 = mole%_C3H8*(As_tot/As_C3H8)/100     "propane response factor"

$ELSE

"use known composition to determine response factors"
mole%_CH4=45
mole%_C2H6=35
mole%_C3H8=20

"Injector, Detector, and Oven @ 150"
area%_CH4=(29.70458+29.80934+29.87690+29.69035+30.05186+30.34126+29.11691+29.76278)/8
area%_C2H6=(38.52486+38.63758+38.38291+38.80678+38.47448+38.08838+38.03645+38.23360)/8
area%_C3H8=(31.77055+31.55306+31.74022+31.50288+31.47365+31.57038+32.84662+32.00360)/8

RF_CH4=mole%_CH4/area%_CH4
```

```
RF_C2H6=mole%_C2H6/area%_C2H6
RF_C3H8=mole%_C3H8/area%_C3H8

"compute the corrected areas from GC areas determined for the sample"
AC_CH4=A_CH4*RF_CH4
AC_C2H6=A_C2H6*RF_C2H6
AC_C3H8=A_C3H8*RF_C3H8

"compute the corresponding mole percentages"
CH4%=AC_CH4/(AC_CH4+AC_C2H6+AC_C3H8)
C2H6%=AC_C2H6/(AC_CH4+AC_C2H6+AC_C3H8)
C3H8%=AC_C3H8/(AC_CH4+AC_C2H6+AC_C3H8)

$ENDIF
```

```
"Mixture Concentration"
"Oven, Injector, and Detector @ 130C for undiluted refrigerants"
"Temperature Program used in GC"
"100C for 5 min, ramp 15C/min to 130C, final time of 20 min"

dilution$ = 'no'
{date_test$='6/21/13'}
T_avg = ((T_in + T_out)/2)

$IF dilution$ = 'yes'

"Pure Gas Areas"
A_Ar_Pure = (3272560+3303646+3320758+3369736+3345792)/5
A_R14_Pure = (4572410+4692019+4720317+4754704)/4
A_R23_Pure = (4736973+4835658+4858624+4796173+4899459+4930378)/6
A_R32_Pure = (4451485+4524410+4379290+4710317+4775274+4744541+4869280)/7
A_R134a_Pure = (7003930+6693690+6648403+6798627+6897978+6915488)/6

"Percent Concentration Calculations"
Ar_% =
A_Ar/A_Ar_Pure/(A_Ar/A_Ar_Pure+A_R14/A_R14_Pure+A_R23/A_R23_Pure+A_R32/A_R32_Pure+A_
R134a/A_R134a_Pure)*100[%]
R14_% =
A_R14/A_R14_Pure/(A_Ar/A_Ar_Pure+A_R14/A_R14_Pure+A_R23/A_R23_Pure+A_R32/A_R32_Pure+
A_R134a/A_R134a_Pure)*100[%]
R23_% =
A_R23/A_R23_Pure/(A_Ar/A_Ar_Pure+A_R14/A_R14_Pure+A_R23/A_R23_Pure+A_R32/A_R32_Pure+
A_R134a/A_R134a_Pure)*100[%]
R32_% =
A_R32/A_R32_Pure/(A_Ar/A_Ar_Pure+A_R14/A_R14_Pure+A_R23/A_R23_Pure+A_R32/A_R32_Pure+
A_R134a/A_R134a_Pure)*100[%]
R134a_% =
A_R134a/A_R134a_Pure/(A_Ar/A_Ar_Pure+A_R14/A_R14_Pure+A_R23/A_R23_Pure+A_R32/A_R32_P
ure+A_R134a/A_R134a_Pure)*100[%]

"Argon Pure Areas"
{A_Ar_Pure = (3573672+3781730+3746176+3733429+3741794)/5}

$ELSE

"R14 Pure Areas"
A_R14_Pure = (4544896+4636848+4661821+4657834+4646128)/5

"R23 Pure Areas"
A_R23_Pure = (4446605+4451850+4498976+4492211)/4

"R32 Pure Areas"
A_R32_Pure = (4229757+4265878+4337005+4315642)/4

"R134a Pure Areas"
A_R134a_Pure = (6244458+6179091+6175114)/3

R14_% =
A_R14/A_R14_Pure/(A_R14/A_R14_Pure+A_R23/A_R23_Pure+A_R32/A_R32_Pure+A_R134a/A_R134
a_Pure)*100[%]
```

```
R23_% =
A_R23/A_R23_Pure/(A_R14/A_R14_Pure+A_R23/A_R23_Pure+A_R32/A_R32_Pure+A_R134a/A_R134
a_Pure)*100[%]
R32_% =
A_R32/A_R32_Pure/(A_R14/A_R14_Pure+A_R23/A_R23_Pure+A_R32/A_R32_Pure+A_R134a/A_R134
a_Pure)*100[%]
R134a_% =
A_R134a/A_R134a_Pure/(A_R14/A_R14_Pure+A_R23/A_R23_Pure+A_R32/A_R32_Pure+A_R134a/A_
R134a_Pure)*100[%]

$ENDIF
```